



La Sapienza

Università degli Studi di Roma

Facoltà di Scienze Matematiche, Fisiche e Naturali
Corso di Laurea in Fisica

Optimal Kinematics of Model Cilia

Seduta di Laurea del: 22 Novembre 2012
Anno Accademico 2011/2012

Relatore interno

Dr. Roberto Di Leonardo
CNR-IPCF

Studente

Dario Santi Cortese

Relatore esterno

Prof. Eric Lauga
Applied Mathematics Laboratory
University of California San Diego

-
-
-

Contents

1	Basic concepts	11
1.1	The continuum approximation	11
1.2	Governing equations	13
1.2.1	Continua equations	13
1.2.2	Navier-Stokes equations	14
1.2.3	Energy balance for a Newtonian Perfect incompressible fluid	15
1.3	Scaling and dimensional analysis	15
1.3.1	Scaling of the Navier-Stokes equations	16
1.4	The Reynolds number	18
2	Creeping Flow	19
2.1	The Stokes equations	20
2.2	Properties of solutions of the Stokes equations	21
2.2.1	Uniqueness	21
2.2.2	Reversibility	22
2.2.3	Superposition	22
2.2.4	A minimum in the energy dissipation	22
2.2.5	Lorentz Reciprocal Theorem	22
2.2.6	Total forces and torques balance	23
2.2.7	Swimming at Low Re	23
2.3	Force and Torque on a body	25
2.3.1	Spheres and ellipsoides	27
2.4	Uniform Flow past a Solid Sphere: Stokes' law	28
2.5	Singularity and Boundary integral solutions	31
2.5.1	Fundamental solution: the Stokeslet	31
2.5.2	The boundary integral equation	33
2.5.3	Singularities: multipole expansion for rigid bodies	35
2.6	Faxen's Law for a body in an unbouded fluid	40
3	Hydrodynamic interactions	43
3.1	The method of reflections	44
3.1.1	Resistance problems	45
3.1.2	Mobility problems	46
3.2	Particle-Wall interactions	46
3.2.1	Stokeslet near a wall	47
3.2.2	Stokeslet near a big sphere	47

4	Cilia dynamics	49
4.1	Principal issues	49
4.2	Structure of a cilium	50
4.3	Kinematics and dynamics of the single cilium	51
4.4	Collective cilia dynamics: Metachronal Waves	55
5	Optimal cilia kinematics	
	Numerical results	61
5.1	Ideal cilia: approximations and kinematics	61
5.2	Numerical approach	64
5.3	Interaction among cilia near a rigid plane	64
5.3.1	2 cilia: Linear motion	65
5.3.2	2 cilia: Elliptical motion	67
5.3.3	4 cilia: Linear and elliptical motion	71
5.3.4	Periodic boundary conditions	72
5.4	Interaction among cilia near a rigid sphere	73
5.4.1	2 cilia: angular motion	75
5.4.2	4 cilia: angular and elliptical motion	76
5.5	Infinite array of cilia	77
5.6	Conclusions	79

Introduction

We build too many walls and not enough bridges.

Isaac Newton

Nature has devised many different ways of creating fluid flow, most of them for animal propulsion, that is, for flying or swimming. At larger scales, examples are the flapping wings of birds, and the waving tails of fishes. Flapping wings are also found at smaller scales in insects. At really small scales, typically for sub-*mm* sizes, a fluid manipulation mechanism used by nature is that by cilia or flagella.

In a way we all owe our existence to the beating of cilia and flagella, since not only the swimming of sperm but also the transport of the fertilised egg to the uterus is a result of the activity of these organelles. Cilia and flagella are actively bending hair-like appendages that act as sensing and motility generating organelles of eukaryotic cells. Their evolutionary highly conserved [1] working mechanism as well as their widespread occurrence in a great variety of systems demonstrate the power and importance of physical interactions as a means of achieving biological function.

A prominent example of the many different circumstances, where the ability of cilia and flagella to generate regular beat patterns plays a vital role to create motion on a cellular level, is the propulsion of single cells such as the swimming of protozoa and spermatozoa. Fig.1 gives an idea of how many other different micro-organisms make use of ciliary propulsion or fluid manipulation.

Also the transport of fluid along a stationary layer of cells as for example in the trachea and oviduct is achieved through the beating of cilia covering epithelial cells. Another most striking display of the importance of ciliary beats is the recently discovered vortical motion of nodal cilia that leads to an external fluid flow during embryological development [2]. This flow has been shown to be responsible for the establishment of the left-right axis across many vertebrate species [3], a spectacular finding which has answered a long standing medical puzzle: why approximately half of the people whose cilia are immotile due to a genetic defect (primary ciliary dyskinesia [2]) exhibit an inversion of the usual left-right asymmetry of their internal organs (situs inversus).

In this work, we focus on the ciliary kinematics, with particular attention at array of a certain number of cilia in different geometric configuration. This problem is strictly related, for instance, in the case of a spheric surface covered by cilia, to the propulsion of microswimmers as *Paramecium* (Fig. 2), for which two levels of symmetry-breaking and two types of waves are observed. [4] At the level of

an individual cilium, a deformation wave propagates along the cilium length as for flagellar motion.

The beating pattern is however different from that of individual flagella, and the individual stroke of a cilium can be decomposed into two parts: an effective stroke, during which the cilium is extended and offers the most resistance to the fluid, and a recovery stroke, in which the cilium is bent in such a way as to reduce the viscous drag. In addition to such asymmetric beating at the level of an individual cilium, the beating coordination of neighboring cilia at the organism level results in a collective behavior known as metachronal waves.

All cilia on the surface of a microorganism perform similar beating patterns, but they deform in time with a small phase difference with respect to their neighbors, and these phase differences are spatially distributed in a way that leads to symmetry-breaking at the level of the whole cell and the formation of a wave pattern of surface deformation [4, 5] (see Fig.3). The origin of the synchronization responsible for the metachronal waves in ciliary propulsion is still debated, but several recent studies have suggested that it results from hydrodynamic interactions between neighboring cilia. [6].

Even more debated, and not yet investigated, is the possibility that the metachronal waves are the most efficient solution for the propulsion of the surrounding fluid, i.e., given the kinematics of the cilia, the metachronal waves allow the force exerted by means of their motion to the fluid (and so to the object they are attached to) to have the strongest possible value. This point is controversial because is not at all sure that the energy balance of a cell or microorganism is mostly dominated by the propulsion and mechanic contribute, instead, for instance, by the feeding or chemical ones.

In this thesis, we consider the physical background on which the mechanics of cilia and flagella can be extensively studied, starting from a brief review of the basic concepts of Fluid mechanics in the first chapter, passing through the Creeping flow approximation, necessary because of the scale at issue in our case, in the second chapter. The third chapter is devoted to an overview of the typical techniques in the study of hydrodynamic interactions between particles. The last two chapter represent the core of this work, giving for the first time a systematic description of the different modeling approaches proposed in the past to address the problem of cilia dynamics, and finally presenting our original contribute. We focused our attention on the optimal kinematics of an array of cilia, proposing and developing an original approach to study two cases: near a spherical rigid surface and near a plane wall. In this systems, we ask the fundamental question of why metachronal waves arise, and if this can be related to an optimal force exerted on the fluid.

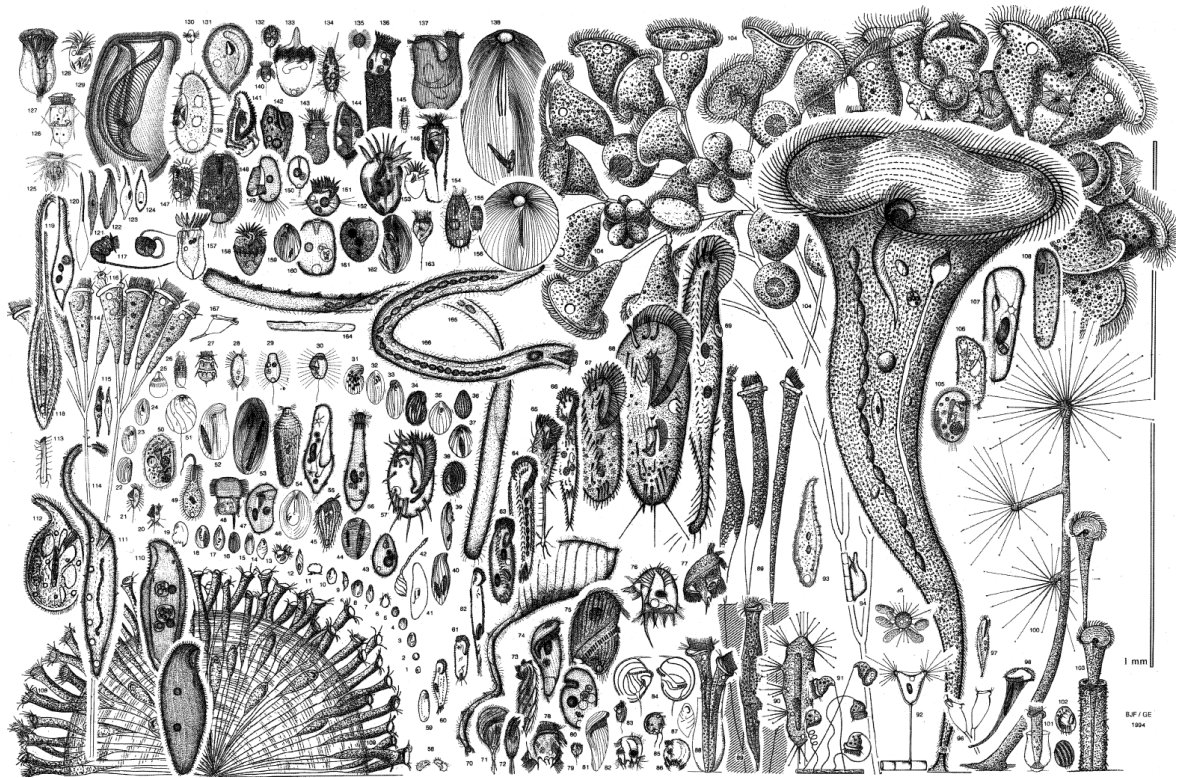


Figure 1: Ciliated micro-organisms, living in lakes and rivers. The bar on the right indicates the scale (1 mm). B.J Finlay et G.F. Esteban : The Ciliate Diversity Chart. Drawing, Institute of Freshwater Ecology, Windermere Laboratory, UK.

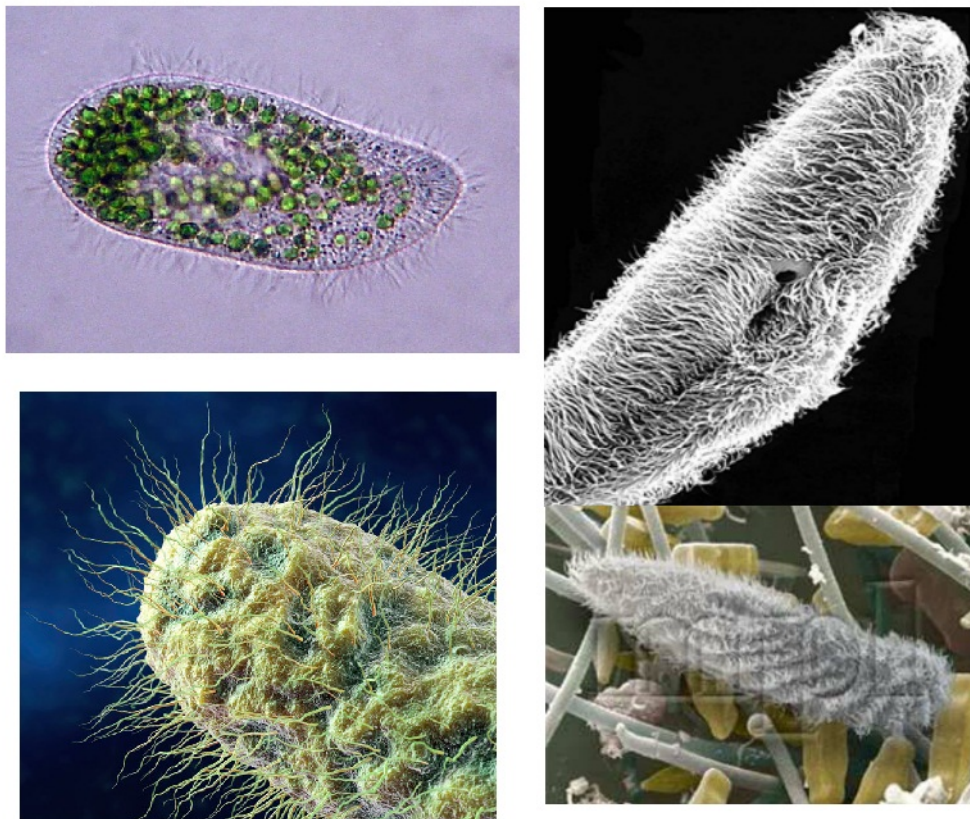


Figure 2: Different species of Paramecium, edited from [16]

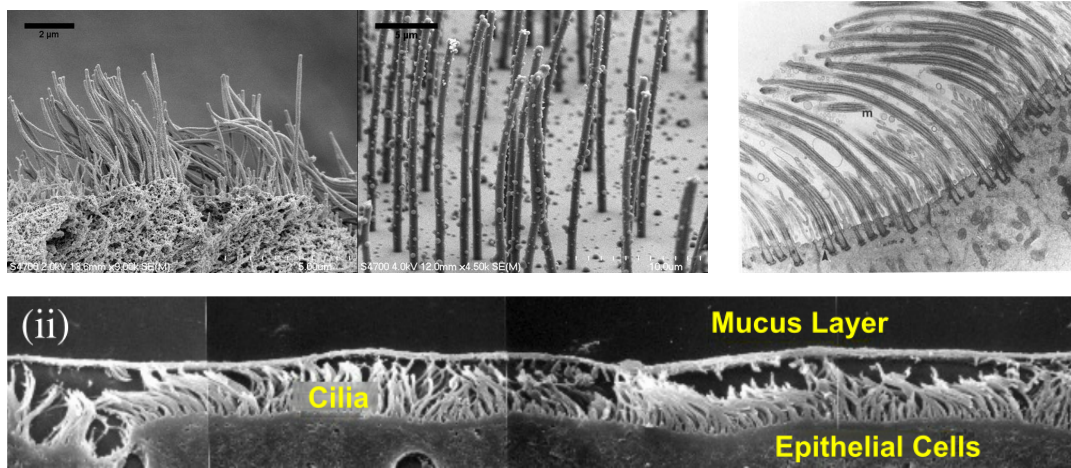


Figure 3: Cilia and flagella at work in different circumstances. In the respiratory tract the concerted action of beating cilia transports mucus up the trachea (wind pipe) which works as an important cleaning and defence mechanism, sometimes instructively called “mucociliary escalator”.

Notation

v Bold type signifies vector character.

\mathbf{e}_i , $i = 1, 2, 3$ Canonical base of \mathbb{R}^3

A Underline bold type indicates a second order tensor, such that: **A** : $\mathbb{R}^3 \times \mathbb{R}^3 \rightarrow \mathbb{R}$. **A** = $A_{ij}\mathbf{e}_i \otimes \mathbf{e}_j$

A Double underline bold type indicates a third order tensor, such that: **A** : $\mathbb{R}^3 \times \mathbb{R}^3 \times \mathbb{R}^3 \rightarrow \mathbb{R}$. **A** = $B_{ijk}\mathbf{e}_i \otimes \mathbf{e}_j \otimes \mathbf{e}_k$

A · **b**, **a** · **b** Inner and scalar product $A_{ij}b_j$ or $a_i b_i$

a × **b** Edge vector product $\epsilon_{ijk}a_j b_k$ where $\epsilon_{ijk} = +1$ if (i, j, k) even permutation of $(1, 2, 3)$, $\epsilon_{ijk} = 0$ if at least two of the three index are equal, $\epsilon_{ijk} = -1$ otherwise.

AB Tensor product **A** ⊗ **B** = $A_{ij}B_{lm}$

x = (x, y, z) Position vectors; $|\mathbf{x}| = r$

v = $(v_x, v_y, v_z) \equiv \mathbf{v}(\mathbf{x}, t)$ Velocity at a specified time and position in space; $|\mathbf{v}| = v$

σ, **e** Stress and deformation tensors

p , ρ , μ , $\nu = \frac{\mu}{\rho}$ pressure, density, kinematic and dynamic viscosity

$\partial_x \equiv \frac{\partial}{\partial x}$ Partial differentiation respect to the variable x

$\nabla \equiv (\partial_x, \partial_y, \partial_z)$ Gradient vector

$\nabla^2 \equiv \partial_x^2 + \partial_y^2 + \partial_z^2$ Laplacian operator

$D_t = \partial_t + \mathbf{v} \cdot \nabla$ operator giving the material derivative, or rate of change at a point moving with the fluid locally; applies only to functions of **x** and **t**

Chapter 1

Basic concepts

I am rooted, but I flow.
Virginia Woolf

It is assumed that the reader is familiar with the basic principles and equations that describe the Fluid dynamics processes from a continuum mechanics point of view. Nevertheless, we begin our discussion with a review of these principles and the governing equations, following some classical book treatment [9, 10, 11, 12, 13].

1.1 The continuum approximation

One possible approach to the description of a fluid in motion at small scales is to examine what occurs at the microscopic level where the stochastic motions of individual molecules can be distinguished. However, the resulting many-body problem of molecular dynamics is impossibly complex under normal circumstances because the fluid domain contains an enormous number of molecules. Thus efforts to provide a mathematical description of fluids in motion could not have succeeded without the introduction of sweeping approximations. The most important among these is the so-called continuum hypothesis. According to this hypothesis, the fluid is modeled as infinitely divisible without change of character. This implies that all quantities, including the material properties such as density, viscosity, or thermal conductivity, as well as variables such as pressure, velocity, and temperature, can be defined at a mathematical point in an unambiguous way as the limit of the mean of the appropriate quantity over the (inevitable) molecular fluctuations.

The desired description of fluid motion is then at this larger, macroscopic level where, for example, an average of the forces of interaction between the fluid and the bounding surface may be needed, but not the instantaneous forces of interaction between this surface and individual molecules of the fluid. Once the continuum hypothesis has been adopted, the usual macroscopic laws of classical continuum physics are invoked to provide a mathematical description of fluid motion, namely, conservation of mass, conservation of linear and angular momentum (the basic principles of Newtonian mechanics), and conservation of energy (the first law of thermodynamics).

In adopting the continuum hypothesis, we assume that it is possible to develop a description of fluid motion on a much coarser scale of resolution than on the molecular

scale that is still physically equivalent to the molecular description in the sense that the former could be derived, in principle, from the latter by an appropriate averaging process. Thus it must be possible to define any dependent macroscopic variable as an average of a corresponding molecular variable. A convenient average for this purpose is suggested by the utility of having macroscopic variables that are readily accessible to experimental observation. Now, from an experimentalist's point of view, any probe to measure velocity, say, whose dimensions were much larger than molecular, would automatically measure a spatial average of the molecular velocities. At the same time, if the probe were sufficiently small compared with the dimensions of the flow domain, we would say that the velocity was measured "at a point," in spite of the fact that the measured quantity was an average value from the molecular point of view. This simple example suggests a convenient definition of the macroscopic variables in terms of molecular variables, namely as volume averages, for example,

$$\mathbf{v} \equiv \langle \mathbf{u} \rangle \equiv \frac{1}{V} \int_V \mathbf{u} dV \quad (1.1)$$

where V is the averaging volume.

If $\langle \mathbf{w} \rangle$ is to represent a statistically significant average, the typical linear dimension of the averaging volume $V^{1/3}$ must be large compared with the scale δ that is typical of the microstructure of the fluid. Most frequently δ represents a molecular length scale. If at the same time $\langle \mathbf{w} \rangle$ is to provide a meaningful point variable in the macroscopic description, it must have a unique value at each point in space at any particular instant, and this implies that the linear dimension $V^{1/3}$ must be arbitrarily small compared with the macroscopic scale L that is characteristic of spatial gradients in the averaged variables (frequently this scale will be determined by the size of the flow domain). Thus, with macroscopic variables defined as volume averages of corresponding microscopic variables, the existence of an equivalent continuum description of fluid motions or heat transfer processes (that is, the validity of the continuum hypothesis) requires

$$\delta \ll V^{1/3} \ll L \quad (1.2)$$

In other words, it must be possible to choose an averaging volume that is arbitrarily small compared with the macroscale L while still remaining very much larger than the microscale δ .

One consequence of the continuum approximation is the necessity to hypothesize two independent mechanisms for heat or momentum transfer: one associated with the transport of heat or momentum by means of the continuum or macroscopic velocity field \mathbf{v} , and the other described as a "molecular" mechanism for heat or momentum transfer that will appear as a surface contribution to the macroscopic momentum and energy conservation equations. This split into two independent transport mechanisms is a direct consequence of the coarse resolution that is inherent in the continuum description of the fluid system.

Obviously, the sum of the convective and molecular flux contributions in the continuum description must be identical to the total flux of heat due to molecular motions if the continuum description of the system is to have any value.

1.2 Governing equations

We indicate with $\mathbf{v}(\mathbf{x}, t)$ the Eulerian velocity, evaluated instantaneously at time t and at the point \mathbf{x} fixed with respect to the laboratory.

In the continuum approximation, any scalar quantity B associated with a fixed material point and the partial derivatives of B with respect to time and spatial position in a fixed (inertial) reference frame, changes for a moving material point both because B may vary with respect to time at each fixed point at a rate $\partial B/\partial t$ and because the material point moves through space and B may be a function of spatial position in the direction of motion. The rate of change of B with respect to spatial position is just ∇B . The rate at which B changes with time for a material point with velocity \mathbf{v} is then just the projection of ∇B onto the direction of motion multiplied by the speed, which is $\mathbf{v} \cdot \nabla B$. It follows that the convected time derivative of any scalar B can be expressed in terms of the partial derivatives of B with respect to time and spatial position, in this Eulerian (also called *material* picture), with the *material derivative* notation:

$$D_t B \equiv \partial_t B + \mathbf{v} \cdot \nabla B$$

Moreover, the Reynolds transport theorem states

$$D_t \int_{V_m(t)} B(\mathbf{x}, t) dV = \int_{V_m(t)} (\partial_t B + \mathbf{v} \cdot \nabla B) dV \quad (1.3)$$

This is essentially a generalization of Leibnitz rule for differentiation of a one-dimensional integral with respect to some variable when both the integrand and the limits of integration depend on that variable. And this relation can be used to impose the total mass, momentum, energy conservation laws.

1.2.1 Continua equations

Starting from the assumption that the mass is conserved along the particles' paths, and using the (1.3), the so-called equation of continuity can be established for a generic continuum:

$$\boxed{\partial_t \rho + \nabla \cdot (\rho \mathbf{v}) = 0} \quad (1.4)$$

where $\rho(\mathbf{x}, t)$ is the fluid density.

From the Newton's second Law, stating the balance between the variation of total momentum $\int_V \rho \mathbf{v}$ and the external body and stress forces, we can derive the fundamental equation:

$$\rho D_t \mathbf{v} = \rho \mathbf{f} + \nabla \cdot \underline{\boldsymbol{\sigma}} \quad (1.5)$$

where $\boldsymbol{\sigma}$ is the *stress tensor* of the continuum, taking into account the surface forces on each material particle, and \mathbf{f} the *external body force* per unit mass. From the Energy Balance, an analogous relation can be derived:

$$\boxed{D_t \left(\frac{1}{2} \rho v^2 + \rho \mathcal{E} \right) = \rho \mathbf{v} \cdot \mathbf{f} + \nabla \cdot (\underline{\boldsymbol{\sigma}} \cdot \mathbf{v}) + \nabla \cdot \mathbf{q}} \quad (1.6)$$

where \mathcal{E} is the internal energy per unit mass, and \mathbf{q} is the heat flux.

If the continuum is nonpolar, such that the torques within it arise only as the moments of direct forces, the conservation of the angular momentum implies the symmetry of the stress tensor. The equations (1.6)(1.5)(1.4) describe the dynamics of a generic continuum.

1.2.2 Navier-Stokes equations

To write down the equations in the case of a fluid flow, we must have a model for the relation between the stress and the state of the fluid. Let us consider an incompressible fluid, for which the continuity equation (1.4) states that $\nabla \cdot \mathbf{v} = 0$. In practice we shall restrict to fluids with uniform density, that is a more restrictive assumption than the incompressibility. The conditions under which a fluid can be considered as incompressible can in most cases be described by the inequality $U \ll c$ where U represents a characteristic velocity for the flow and c is the speed of pressure waves in the given fluid (for example, the speed of sound) [13].

Naturally, we would expect this relation to vary from one material to another. If any element of area experiences a stress normal to itself and this stress is independent of the orientation, the stress is called *hydrostatic*. All the fluid at rest exhibit this stress behaviour. It implies that the stress tensor can be write as $\sigma_{ij} = -p\delta_{ij}$ for a state of hydrostatic stress.

Now we consider deformation. The intuitive distinction between a solid and a fluid is that the stress in solids depends on the amount of deformation, while in fluid is that the stress in solids depends on the amount of deformation, while in fluids it depende on the rate of deformation. The istantaneous rate of deformation of a small material filament is characterized by the rate of strain tensor

$$e_{ij} = \frac{1}{2}(\partial_i v_j + \partial_j v_i) - \frac{1}{3}(\nabla \cdot \mathbf{v})\delta_{ij}$$

The simplest theory for a fluid is based on the hypothesis that the stress is linear with respect to \mathbf{e} , so that

$$\sigma_{ij} = -p\delta_{ij} + 2\mu e_{ij}$$

and this equation is known as the *Newtonian constitutive equation*. Real fluids satisfying this relation to the limits of the purpose at hand are called *Newtonian fluids*. The material property μ is called the *dynamic viscosity*. The factor two is due to historical reasons. Combining this constitutive relation with the momentum equation leads to the Navier-Stokes equations for an incompressible Newtonian fluid:

$$\boxed{\begin{aligned} \rho(\partial_t \mathbf{v} + \mathbf{v} \cdot \nabla \mathbf{v}) &= -\nabla p + \mu \nabla^2 \mathbf{v} + \rho \mathbf{f} \\ \nabla \cdot \mathbf{v} &= 0 \end{aligned}} \quad (1.7)$$

where rigorously $\mathbf{v} : D \times \mathbb{R} \rightarrow D \subset \mathbb{R}^3$ is a function usually taken differentiable at least three times.

Requiring that on the surface of any solid obstacle in the domain of the flow there is no slip, we must also have:

$$\boxed{\mathbf{v}|_{\partial D} = \mathbf{0}}$$

1.2.3 Energy balance for a Newtonian Perfect incompressible fluid

In the case of an incompressible perfect fluid, without heat transfer, equation (1.6) can be written in the form:

$$D_t \left(\frac{1}{2} \rho v^2 \right) = \rho \mathbf{v} \cdot \mathbf{f} - \nabla p \cdot \mathbf{v} + 2\mu (\nabla \cdot \underline{\mathbf{e}}) \cdot \mathbf{v} - 2\mu \underline{\mathbf{e}} : \underline{\nabla \mathbf{v}} \quad (1.8)$$

and can be integrated by use of the divergence theorem to obtain:

$$\int_V D_t \left(\frac{1}{2} \rho v^2 \right) dV = \int_V \rho \mathbf{v} \cdot \mathbf{f} dV - \int_{\partial V} p \mathbf{v} \cdot \mathbf{n} dS + 2\mu \int_{\partial V} (\underline{\mathbf{e}} \cdot \mathbf{n}) \cdot \mathbf{v} dS - 2\mu \int_V e_{ij} \partial_i v_j dV$$

- The first term corresponds to the increase in energy resulting from external forces. This term is positive when $\rho \mathbf{f}$ and \mathbf{v} are in the same direction, as would be the case for a fluid flowing downwards within the Earth's gravitational field ($\mathbf{f} = \mathbf{g}$), leading to an increase in the kinetic energy;
- The second and third terms give, respectively, the work done by the pressure forces and by the components of the viscous stresses which act normal to the surface ∂V ;

These first four terms represent, then, the complete set of possible changes in the energy due to convective effects resulting from the work done by the forces exerted on the surface ∂V , or from an external force field. (In this last case, if the field is conservative, we have an exchange of kinetic and potential energy).

- Finally, the last term represents the irreversible transformation of kinetic energy, by viscous dissipation, into internal energy of the fluid in the form of heat. This can be made explicit, using the symmetry of $e_{ij} = \partial_i v_j + \partial_j v_i$:

$$2e_{ij} \partial_i v_j = \frac{1}{2} (\partial_j v_i + \partial_i v_j) (\partial_j v_i + \partial_i v_j) = 2 \|\underline{\mathbf{e}}\|$$

Therefore, the rate of kinetic energy dissipation through viscous mechanism is:

$$\epsilon := (D_t E_c)_{visc} = 2\mu \int_V \|\underline{\mathbf{e}}\| dV = \frac{\mu}{2} \int_V (\partial_j v_i + \partial_i v_j) (\partial_j v_i + \partial_i v_j) dV$$

1.3 Scaling and dimensional analysis

The equations of fluid motion presented in the preceding section are, in general, difficult to solve. They comprise a nonlinear system of partial differential equations, and in many situations it is not yet possible even to rigorously prove that solutions exist.

At least in part because of these difficulties, until only very recently much of the practical work in fluid dynamics required laboratory experiments. Clearly, in any of these cases it could be prohibitively expensive to build a succession of full-scale models (often termed “prototypes”) for testing and subsequent modification until a

proper configuration was found. Under what circumstances will the flow field about a scale model be the same as that about the actual full-size object? It is this question, that will be addressed in the present section, following the reasoning of McDonough [8], and showing that the basic answer is: geometric and dynamic similarity must be maintained between scale model and prototype if data obtained from a model are to be applicable to the full-size object.

The requirement of geometric similarity can be expressed as following: two objects are said to be geometrically similar if all linear length scales of one object are a fixed ratio of all corresponding length scales of the second object. Here, “linear” length scale simply means any length that can be associated with a straight line extending from a chosen coordinate origin to an appropriate part of the object being considered. The definition immediately implies that the two objects are of the same general shape, for otherwise there could be no “corresponding” linear length scales.

A more complex concept is that of Dynamic similarity: two geometrically similar objects are said to be dynamically similar if the forces acting at corresponding locations on the two objects are everywhere in the same ratio. The specific requirements of the above definition are not easily checked, and we will subsequently demonstrate that all that is actually needed is equality of all dimensionless parameters associated with the flow in, or around, the two objects.

There are two ways by means of which we can determine the dimensionless parameters, and thus requirements for dynamic similarity, in any given physical situation. In cases for which governing equations are known, straightforward scaling of these equations will lead to the requirements needed to satisfy the above definition. On the other hand, when the governing equations are not known, the standard procedure is to employ the Buckingham theorem. In the case of fluid dynamics the governing equations are known - they are the Navier–Stokes equations derived in preceding sections. Thus, we would expect to usually make direct application of scaling procedures.

1.3.1 Scaling of the Navier-Stokes equations

From the definition of dynamic similarity we see that it is the ratios of forces at various corresponding locations in two (or more) flow fields that are of interest. Now if one could somehow arrange the equations of motion (via scaling) so that their solutions would be the same in each of the flow fields of interest, then obviously the ratios of forces would be the same everywhere in the two flow fields—trivially.

In light of this, the goal should be to attempt to cast the Navier–Stokes equations in a form that would yield exactly the same solution for two geometrically similar objects, via scaling. Then, although the “unscaled” solutions would be different (as would be their solutions), they would differ in a systematic way related to geometric similarity of the objects under consideration. It is important to note that the form of the N.S. equations given in (1.7) does not possess this property because we could change either ρ or ν (or both) in these equations thus producing different coefficients on pressure and viscous force terms, and the equations would have different solutions for the two flow fields, even for flows about geometrically similar objects.

The method we usually employed to achieve the desired form of the equations of motion is called scaling, or sometimes dimensional analysis. The goal of such an

analysis is to identify the set of dimensionless parameters associated with a given physical situation (in the present case, fluid flow represented by the N.S. equations) which completely characterizes behavior of the system (i.e., solutions to the equations). The first step in this process is identification of independent and dependent variables, and parameters, that fully describe the system. Once this has been done, we introduce “typical values” of independent and dependent variables in such a way as to render the system dimensionless. Then, usually after some rearrangement of the equations, the dimensionless parameters that characterize solutions will be evident, and it is these that must be matched between flows about two geometrically similar objects to guarantee dynamic similarity. In our case the independent variables of the system are $\mathbf{x} = (x, y, z)$ and t , the dependent variables $\mathbf{v} = (u, v, z)$ and p , and the parameters ρ and ν , if we take $\mathbf{f} = \mathbf{0}$. In general, the boundary and initial conditions associated with (1.7) don’t introduce new independent or dependent variables, and usually don’t lead to additional parameters. Thus, in the present analysis we will not consider these. Introducing the typical scale for the values of independent and dependent variables, we make the scaling:

$$\mathbf{x}' = \mathbf{x}/L \quad , \quad t' = t/T \quad , \quad \mathbf{v}' = \mathbf{v}/U \quad , \quad p' = pL/(\mu U)$$

and substituting in the equations:

$$\frac{L}{UT} \partial_t \mathbf{v} + \mathbf{v} \cdot \nabla \mathbf{v} = \frac{\nu}{UL} \left(-\nabla p + \nabla^2 \mathbf{v} \right) \quad , \quad \nabla \cdot \mathbf{v} = 0 \quad (1.9)$$

The final quantities in (1.9) with which we must deal are UL/ν and TU/L . The first dimensionless group, is probably the single most important parameter in all of fluid dynamics. It is called the Reynolds number after Osbourne Reynolds who identified it as a key parameter in his early studies of transition to turbulence. In general we express the Reynolds number as

$$\boxed{Re = \frac{UL}{\nu} = \frac{UL\rho}{\mu}} \quad (1.10)$$

where U and L are, respectively, velocity and length scales; ν , as usual, denotes kinematic viscosity. It is interesting to note that this single dimensionless parameter contains two fluid property parameters, ρ and μ , a characteristic flow speed, and a characteristic geometric parameter, the length scale. Since time and pressure scales can be readily derived from these, it is seen that this single parameter completely characterizes many fluid flows.

The second dimensionless group, is only relevant when the problem is not stationary, and is the so-called *Strouhal number*

$$\boxed{S = \frac{TU}{L}}$$

Equations (1.9) are dimensionless, and their solutions now depend only on the parameter Re . In particular, if flow fields associated with two geometrically similar objects have the same Reynolds number, then they have the same scaled velocity

and pressure fields. In turn, it is easily seen from the equations of motion that this implies that they will exhibit the same scaled forces at all locations in the flow. Then, in light of geometric similarity, the unscaled forces will be in a constant ratio at all corresponding points of the two flow fields, and dynamic similarity will have been achieved. Hence, for flows in, or around, geometrically similar objects, dynamic similarity is achieved if all dimensionless parameters associated with these flows are the same.

1.4 The Reynolds number

As we saw in the former section, the Reynolds number is a dimensionless quantity which qualitatively captures the characteristics of the flow regime, and it has several different physical interpretations. Let us consider the flow around an obstacle, or a moving body [15]. It is classically defined as the ratio of the typical inertial terms in the Navier-Stokes equation, to the viscous forces per unit volume.

$$Re \sim \frac{|\mathbf{v} \cdot \nabla \mathbf{v}|}{|\nu \nabla^2 \mathbf{v}|} \quad (\text{steady}) \quad , \quad Re \sim \frac{|\partial_t \mathbf{v}|}{|\nu \nabla^2 \mathbf{v}|}$$

A low Reynolds number flow is one for which viscous forces dominate in the fluid.

A second interpretation can be given as the ratio of time scales. The typical time scale for a local velocity perturbation to be transported convectively by the flow along the body is $t_{adv} \sim L/U$, whereas the typical time scale for this perturbation to diffuse away from the body due to viscosity is $t_{diff} \sim \rho L^2/\mu$. We see therefore that

$$Re = \frac{\rho L^2/\mu}{L/U} \sim \frac{t_{diff}}{t_{adv}}$$

and a low Reynolds number flow is one for which fluid transport is dominated by viscous diffusion.

We can also interpret Re as a ratio of forces on the body. A typical viscous stress on a bluff body is given by $\sigma_{visc} \sim \mu U/L$, leading to a typical viscous force on the body of the form $f_{visc} \sim \mu U L$. A typical inertial stress is given by a Bernoulli-like dynamic pressure, $\sigma_{in} \sim \rho U^2$, leading to an inertial force $f_{in} \sim \rho U^2 L^2$. We see that the Reynolds number is given by

$$Re = \frac{\rho U^2 L^2}{\mu U L} \sim \frac{f_{in}}{f_{visc}}$$

and therefore in a low Reynolds number flow the forces come primarily from viscous drag.

A fourth interpretation, more subtle, was offered by Purcell [14]. He noted that, for a given fluid, $\mathcal{F} = \mu^2/\rho$ has units of force, and that any body acted upon by the force \mathcal{F} will experience a Reynolds number of unity, independent of its size. Indeed, it is easy to see that

$$Re = \frac{\mu U L}{\mu^2/\rho} \sim \frac{f_{visc}}{\mathcal{F}}$$

and $Re = (f_{in}/\mathcal{F})^{1/2}$, and therefore a body with a Reynolds number of one will have $f_{in} = f_{visc} = \mathcal{F}$. A body moving at low Reynolds number therefore experiences forces smaller than \mathcal{F} , where $\mathcal{F} \sim 1$ nN for water.

Chapter 2

Creeping Flow

You can't trust water: Even a straight stick turns crooked in it.
William Claude Fields

It was shown in the previous chapter that non-dimensionalization reveals the dimensionless combination(s) of independent parameters that control the form of the solution of the set of equations that describes the motion of a fluid. In general, for isothermal flow of an incompressible, Newtonian fluid in a domain with solid, fixed boundaries, we saw that there is a single dimensionless group, called the Reynolds number, that determines the form of solutions to the Navier–Stokes and continuity equations. When this parameter is very small, the (linear) viscous terms in the equation are dominant over the (nonlinear) inertial or acceleration terms, and a linear approximation of the equations is thus possible in the asymptotic limit as the Reynolds number approaches zero. The class of fluid motions where this approximation can be used is known as *creeping flow*, and this chapter focuses on general analysis of motion of this type.

Since the Reynolds number $Re = UL/\nu$ is obtained by the combination of three, quite disparate, physical quantities, flow at low Reynolds numbers can be observed in a wide variety of physical phenomena.

- The motion of microscopic objects (here the low value of Re is associated with a small L), as the movement of bacteria (with typical sizes in the range of a few microns). Typically, in water ($\nu \sim 10^{-6} \text{ m}^2/\text{s}$), for bacteria of approximate length $3\mu\text{m}$, moving at a velocity of $10\mu/\text{s}$, we find that $Re \sim 3 \cdot 10^{-5}$. For such motion, the role of inertia is totally negligible: when a bacterium stops its propulsion, the velocity decreases to zero in a time of the order of microseconds. Another microscopic domain is the dynamics of suspensions of small-diameter particles.
- Also low-velocity motion of geological features (here, the huge linear dimensions of the flow are more than compensated by the small value of the ratio U/ν). Two examples can be cited: the motion of glaciers and the motion of the Earth's mantle.

- Finally, the flow of highly viscous fluids, such as petroleum tars, alimentary pasta, plastics, or honey. A number of heavy crude oils have, at ordinary temperatures, viscosities more than a million times greater than that of water.

2.1 The Stokes equations

In every case that we have just listed, the fluid can be considered to be incompressible. In fact, the velocity of the fluid remains very small relative to the velocity of sound, and we can therefore make use of the Navier-Stokes equations, which are applicable to incompressible Newtonian fluids:

$$\partial_t \mathbf{v} + \mathbf{v} \cdot \nabla \mathbf{v} = -\frac{\nabla(p - p_0)}{\rho} + \nu \nabla^2 \mathbf{v} \quad , \quad \nabla \cdot \mathbf{v} = 0 \quad , \quad \nabla p_0 = \rho \mathbf{f}$$

where we assumed a potential force field. In their non-dimensionalized form they can be written:

$$Re \left(\frac{\partial_t \mathbf{v}}{S} + \mathbf{v} \cdot \nabla \mathbf{v} \right) = -\nabla p + \nabla^2 \mathbf{v} \quad , \quad \nabla \cdot \mathbf{v} = 0 \quad (2.1)$$

As we saw in the last section of the former chapter, the fundamental assumption, in the discussion of flow at low Reynolds numbers, is that the magnitude of the terms $\mathbf{v} \cdot \nabla \mathbf{v}$, corresponding to inertial forces, is small relative to that of the viscous friction per unit volume $\nu \nabla^2 \mathbf{v}$.

Actually, in the most general case, when the motion is non-steady, the relative magnitude of the the Eulerian acceleration is determined by the ratio of the Reynolds number to the Strouhal number, Re/S (note that for steady flows the characteristic time $T = L/U$ and $S = 1$). In particular, inertia terms become small compared with viscous and pressure-gradient terms as the Reynolds number becomes small:

$$\boxed{Re \ll 1 \quad \text{or} \quad Re/S \ll 1.} \quad (2.2)$$

Thus, under this combination of assumptions, the Navier-Stokes equation reduces to

$$\boxed{\nabla p = \mu \nabla^2 \mathbf{v} \quad , \quad \nabla \cdot \mathbf{v} = 0} \quad (2.3)$$

where for the general case we substituted $p \rightarrow p - p_0$ to take into account the volume forces. These equations are known as the *creeping-flow or Stokes equations*. The most important feature of the (2.3) is that they are **linear** and thus can be solved by a number of well-known methods for linear differential equations. Moreover, as we see, the double limit (2.2) implies that the time derivative in the equations of motion is also neglected. For this reason, creeping flows are sometimes called **quasi-steady**. Thus time appears in a creeping-flow solution only as a parameter that characterizes the instantaneous boundary velocity, or boundary geometry, either of which may depend on time.

Other forms of the Stokes equations

Recalling the definition of the stress tensor $\sigma_{ij} = -p\delta_{ij} + 2\mu e_{ij}$, and that $2\nabla \cdot e_{ij} = \nabla^2 \mathbf{v}$, we can write the first of the Stokes equations:

$$\boxed{\nabla \cdot \underline{\sigma} = 0}$$

Low-Reynolds-number flow can also be described (just like any other flow) in terms of the vorticity vector $\boldsymbol{\omega} = \nabla \times \mathbf{v}$ instead of the velocity itself. Therefore, using the incompressibility condition, we obtain also the form:

$$\nabla p = -\mu \nabla \times \boldsymbol{\omega} \quad \Longrightarrow \quad \boxed{\nabla^2 p = 0} \quad (2.4)$$

At last, taking the curl of (2.4) :

$$\boxed{\nabla^2 \boldsymbol{\omega} = 0} \quad (2.5)$$

This last equation is a specific form of the equation of evolution of vorticity for stationary flow at low Reynolds number. The transport of vorticity by viscous diffusion is then represented there by the term $\mu \nabla^2 \boldsymbol{\omega}$. Thus, a physical interpretation the Stokes equation is that, in stationary flow at low Reynolds number, the velocity gradients reach an equilibrium state: no transport of vorticity occurs within stationary flow of such a type.

In the specific case of two-dimensional or axisymmetric flows, we know from the classical mathematical theory of fluid mechanics that we can represent the velocity field in terms of a streamfunction, such that:

$$\mathbf{v} = \nabla \times \hat{\mathbf{n}}\psi \quad , \quad \hat{\mathbf{n}} \perp \text{plane of the motion (2D) or azimuthal (axisymmetric)}$$

and thus taking the divergence of the Stokes equation we obtain, in Cartesian coordinate, the classical *biharmonic equation*:

$$\nabla \cdot \nabla^2 \mathbf{v} = \nabla \cdot \nabla^2 \nabla \times \psi \hat{\mathbf{n}} = \frac{\nabla^2 p}{\mu} \quad \Longrightarrow \quad \boxed{\nabla^4 \psi = 0}$$

or in spherical coordinates, the equation [9]:

$$\left[\frac{\partial^2}{\partial r^2} + \frac{\sin \theta}{r^2} \frac{\partial}{\partial \theta} \left(\frac{1}{\sin \theta} \frac{\partial}{\partial \theta} \right) \right]^2 \psi = 0$$

2.2 Properties of solutions of the Stokes equations

2.2.1 Uniqueness

For a given flow geometry, and specific boundary conditions (both at infinity and at all solid walls), the Stokes equation has a unique solution. This crucial property follows from the linearity of the equation. In contrast, for the flow of real fluids at sufficiently large Reynolds numbers, there exists a multiplicity of non-stationary solutions of the Navier-Stokes equation, resulting from the non-linear convective terms, and the presence of vorticity. For a proof see [13, 10].

2.2.2 Reversibility

Reversibility is also a direct result of the linearity of the Stokes equation. Indeed, if we assume that we know a velocity field $\mathbf{v}(x, y, z)$ which is solution of the equation, with a corresponding pressure field $p(x, y, z)$, $-\mathbf{v}(x, y, z)$ will also be a solution provided only that we reverse the sign of the pressure gradients, as well as that of the velocities, at every solid boundary. Equation (2.3) is then again satisfied, since its two terms are replaced by their negatives and the boundary conditions are appropriately changed. As a consequence of the reversibility of the solutions, when an object has a plane of symmetry, and the flow velocity far away is normal to this plane, $x = 0$, the streamlines upstream and downstream of the object are symmetrical.

This result is a very sensitive test for small values of the Reynolds number. For the case of the flow around a cylinder, as soon as Re becomes of order unity, recirculation zones appear on the downstream face of the obstacle. For rapid flow, a large turbulent wake is observed downstream, while, upstream, the streamlines remain perfectly stable. If the obstacle lacks a plane of symmetry, low-Reynolds-number flow is no longer symmetric between the upstream and the downstream sides.

2.2.3 Superposition

This property is again an immediate consequence of the linearity of the Stokes equation: if $\mathbf{v}_1(\mathbf{r}, t)$ and $\mathbf{v}_2(\mathbf{r}, t)$ are two solutions of this equation, then $\lambda_1\mathbf{v}_1 + \lambda_2\mathbf{v}_2$ is also a solution with a corresponding pressure gradient, which can be written $\nabla p = \lambda_1\nabla p_1 + \lambda_2\nabla p_2$.

The velocity at the walls is the linear combination of the velocities for solutions 1 and 2 with the same coefficients λ_1 and λ_2 . Since there exists a unique velocity field corresponding to given boundary conditions, it is the solution $\lambda_1\mathbf{v}_1 + \lambda_2\mathbf{v}_2$ that is observed experimentally. We can therefore superimpose linearly the velocity fields corresponding to different flows, in configurations with identical geometry, provided that we combine linearly, with the same coefficients, the values of the velocities at the walls.

2.2.4 A minimum in the energy dissipation

For given boundary conditions at the walls and at infinity, a flow which obeys the Stokes equation (2.3) corresponds to a minimum in the rate of dissipation of energy ϵ due to the viscous mechanism. For a proof see [13, 10].

This property applies only when the Reynolds number is low: at high Reynolds numbers, turbulent solutions are allowed and dissipate a greater amount of energy than laminar ones for identical boundary conditions.

2.2.5 Lorentz Reciprocal Theorem

An important property of Stokes flows is the so-called reciprocal theorem. Let us consider a closed region of fluid V bounded by a surface S . If we suppose the velocity fields \mathbf{v} and \mathbf{v}' both satisfy the Stokes equations, and denoting their respective stress fields by $\underline{\sigma}$ and $\underline{\sigma}'$, the Lorentz reciprocal theorem states, in the integral and local

form:

$$\oint_S \mathbf{v} \cdot (\underline{\boldsymbol{\sigma}}' \cdot \mathbf{n}) dS = \oint_S \mathbf{v}' \cdot (\underline{\boldsymbol{\sigma}} \cdot \mathbf{n}) dS \quad \text{or, equivalently} \quad \nabla \cdot (\mathbf{v} \cdot \underline{\boldsymbol{\sigma}}') = \nabla \cdot (\mathbf{v}' \cdot \underline{\boldsymbol{\sigma}}) \quad (2.6)$$

The proof is easily computed passing through the products $\underline{\boldsymbol{\sigma}}' \underline{\mathbf{e}}$ and $\underline{\boldsymbol{\sigma}} \underline{\mathbf{e}}$ and remembering that $p' \delta_{ij} e_{ij} = p' e_{ii} = p' \nabla \cdot \mathbf{v} = 0$, the symmetry of $\underline{\boldsymbol{\sigma}}$ and $\nabla \cdot \underline{\boldsymbol{\sigma}} = \mathbf{0}$:

$$\underline{\boldsymbol{\sigma}}' \underline{\mathbf{e}} = (-p' \delta_{ij} + 2\mu e'_{ij}) e_{ij} = -p' \delta_{ij} e_{ij} + 2\mu e'_{ij} e_{ij} = 2\mu e'_{ij} e_{ij} = \underline{\boldsymbol{\sigma}} \underline{\mathbf{e}}'$$

$$\sigma'_{ij} e_{ij} = \frac{1}{2} \sigma'_{ij} (\partial_j v_i + \partial_i v_j) = \sigma'_{ij} \partial_j v_i = \partial_j (\sigma'_{ij} v_i) - v_i (\partial_j \sigma'_{ij}) = \partial_j (\sigma'_{ij} v_i) = \nabla \cdot (\mathbf{v} \cdot \underline{\boldsymbol{\sigma}}')$$

$$\sigma_{ij} e'_{ij} = (\text{same steps}) = \nabla \cdot (\mathbf{v}' \cdot \underline{\boldsymbol{\sigma}}) = \sigma'_{ij} e_{ij} = \nabla \cdot (\mathbf{v} \cdot \underline{\boldsymbol{\sigma}}')$$

The major strength of the reciprocal identity is that it allows us to obtain information about a flow without having to solve the equations of motion explicitly, but merely by using information about another flow. We will see an application of this in Section 2.6. It is worth noting, moreover, that if the assumptions $\nabla \cdot \underline{\boldsymbol{\sigma}} = \mathbf{0}$ and $\nabla \cdot \underline{\boldsymbol{\sigma}}' = \mathbf{0}$ are “relaxed”, we must retain one more term in the previous steps, obtaining:

$$\oint_S \mathbf{v} \cdot (\underline{\boldsymbol{\sigma}}' \cdot \mathbf{n}) dS - \int_V \mathbf{v} \cdot (\nabla \cdot \underline{\boldsymbol{\sigma}}') dV = \oint_S \mathbf{v}' \cdot (\underline{\boldsymbol{\sigma}} \cdot \mathbf{n}) dS - \int_V \mathbf{v}' \cdot (\nabla \cdot \underline{\boldsymbol{\sigma}}) dV \quad (2.7)$$

2.2.6 Total forces and torques balance

As we saw in Section 1.4, the absence of the inertial terms in the equation of motion of the fluid can be interpreted as an instantaneously quick diffusion and a infinitely slow advection of momentum. Thus in the limit of very low Re , velocity perturbations diffuse rapidly relative to the rate at which fluid particles are carried along by the flow.

A consequence of this analysis is that in a world of low Reynolds number, the response of the fluid to the motion of boundaries is instantaneous. Therefore, the rate at which the momentum of a low- Re flow is changing is completely negligible when compared with the typical magnitude of the forces from the surrounding viscous fluid. As a result, Newton’s law becomes a simple statement of instantaneous balance between external and fluid forces and torques

$$\boxed{\mathbf{F}(t) + \mathbf{F}_{fluid}(t) = \mathbf{0}} \quad \boxed{\mathbf{T}(t) + \mathbf{T}_{fluid}(t) = \mathbf{0}} \quad (2.8)$$

This result is hugely useful. Indeed, we can use it to calculate directly the force exerted by the fluid on an obstacle or a wall, due to his motion.

2.2.7 Swimming at Low Re

When applied to low Reynolds number locomotion, the linearity and time-independence of Stokes equation of motion lead to two important properties for what we shall call *swimmers*. We call a body a ‘swimmer’ if by deforming its surface it is able to sustain movement through fluid in the absence of external (non-hydrodynamic) forces and torques. Note that the ‘body’ includes appendages such as the cilia covering a Paramecium or the helical flagella of E. coli.

Mathematically, the swimming problem is stated as follows. Consider a body submerged in a viscous fluid. In a reference frame fixed with respect to some arbitrary reference point in its body, the swimmer deforms its surface in a prescribed time-varying fashion given by a velocity field on its surface, $u_S(t)$. A swimmer is a deformable body by definition, but it may be viewed at every instant as a solid body with unknown velocity $\mathbf{U}(t)$ and rotation rate $\boldsymbol{\Omega}(t)$. The instantaneous velocity on the swimmer's surface is therefore given by $\mathbf{u} = \mathbf{U} + \boldsymbol{\Omega} \times \mathbf{x} + \mathbf{u}_S$, which, due to the no-slip boundary condition, provides the boundary conditions needed to solve equation 2.3. The unknown values of $\mathbf{U}(t)$ and $\boldsymbol{\Omega}(t)$ are determined by satisfying equation (2.8). Applying the reciprocal theorem to the swimming problem, we can subject the shape $S(t)$ to an external force \mathbf{F}' and torque \mathbf{T}' , and obtaining from equation (2.8):

$$\mathbf{F} \cdot \mathbf{U} + \mathbf{T} \cdot \boldsymbol{\Omega} = - \int_{S(t)} \mathbf{u}_S \cdot \underline{\boldsymbol{\sigma}}' \cdot \mathbf{n} \, dS \quad (2.9)$$

The first property deriving from the reversibility and the linearity of the Stokes flow is rate independence: *if a body undergoes surface deformation, the distance travelled by the swimmer between two different surface configurations does not depend on the rate at which the surface deformation occurs but only on its geometry* (i.e. the sequence of shapes the swimmer passes through between these two configurations). A mathematical proof of this statement can be derived from (2.9), showing that the net distance traveled by the swimmer does not depend on the rate at which it is being deformed, but only on the geometrical sequence of shape, and is outlined in [15].

The second important property of swimming without inertia is the so-called **scallop theorem**: *if the sequence of shapes displayed by a swimmer deforming in a time-periodic fashion is identical when viewed after a time-reversal transformation, then the swimmer cannot move on average.*

Note that the condition is not that the motion be strictly time-reversal invariant, with the same forward and backwards rate, but only that the sequence of shapes is the same when viewed forward or backward in time. This class of surface deformations is termed *reciprocal deformation*. The scallop theorem puts a strong geometrical constraint on the type of swimming motion which is effective at low Reynolds numbers. An outline of the proof can be again derived from (2.9), and can be found in [15].

Reciprocal motion cannot be used for locomotion at low Reynolds numbers. Note that we did not need to assume anything about the geometry of the fluid surrounding the swimmer; the scallop theorem remains valid near solid walls, and more generally in confined environments. However, the scallop theorem does not hold for a body making reciprocal motions near a flexible object, such as a wall or another swimmer, since in that case equation (2.9) must be modified to include u_S at the surface of the flexible object.

In his original article [14], Purcell illustrated the futility of reciprocal motion with the example of a scallop, a mollusk that opens and closes its shell periodically. Independent of the rate of opening and closing, a low-Reynolds number scallop cannot swim. Another example of a reciprocal deformation is a dumbbell, made of two solid spheres separated by time-periodic distance. More generally, bodies with a single degree of freedom deform in a reciprocal fashion, and cannot move on average.

Finally, it is worth emphasizing that the scallop theorem is strictly valid in the limit where all the relevant Reynolds numbers in the swimming problem are set to zero.

2.3 Force and Torque on a body

Another of the consequences of the Stokes equation is the direct proportionality between the forces on solid walls and the characteristic velocity of the fluid. We consider the case of arbitrary motion of a solid, in a fluid which is at rest at infinity. We shall thus be able to predict relationships between the forces and rotational and translational velocities, on the basis of the symmetry properties of the solid object.

To illustrate this assertion, we consider a solid particle of arbitrary shape moving with translational velocity $\mathbf{V}(t)$ and angular velocity $\mathbf{\Omega}(t)$ through an unbounded, quiescent viscous fluid in the creeping-flow limit $Re \ll 1$ and $Re/S \ll 1$. The problem of calculating the force or torque on the particle requires a solution of the creeping-flow equations, subject to boundary conditions. In dimensional terms, the problem is given by the equations (2.3), with

$$\boxed{\begin{aligned} \mathbf{v} &= \mathbf{V} + \mathbf{\Omega} \times \mathbf{x} && \text{on the particle surface } S \\ \mathbf{v} &\rightarrow \mathbf{0} && \text{as } |\mathbf{x}| \rightarrow \infty \end{aligned}} \quad (2.10)$$

where \mathbf{x} is a position vector measured from the center of gravity of the particle. The force and the torque on the particle are

$$\boxed{\mathbf{F} = \int_S (\underline{\boldsymbol{\sigma}} \cdot \mathbf{n}) dS \quad , \quad \mathbf{T} = \int_S (\mathbf{x} \times \underline{\boldsymbol{\sigma}} \cdot \mathbf{n}) dS} \quad (2.11)$$

The critical difficulty with this problem is that the solution depends on the orientations of \mathbf{V} and $\mathbf{\Omega}$ relative to axes fixed in the particle, as well as on the relative magnitudes of \mathbf{V} and $\mathbf{\Omega}$. Thus, for every possible orientation of \mathbf{V} and/or $\mathbf{\Omega}$, a new solution appears to be required to calculate \mathbf{v} , p , \mathbf{F} , or \mathbf{T} . Fortunately, however, the possibility of constructing solutions of a problem as a sum (or superposition) of solutions to a set of simpler problems means that this is not actually necessary in the creeping-flow limit. Rather, to evaluate \mathbf{v} , p , \mathbf{F} , or \mathbf{T} for any arbitrary choice of \mathbf{V} and $\mathbf{\Omega}$, we will show that it is sufficient to obtain detailed solutions for translation in three mutually orthogonal directions (relative to axes fixed in the particle) with unit velocity $\mathbf{V} = \mathbf{e}_i$ and $\mathbf{\Omega} \equiv \mathbf{0}$, and for rotation about three mutually orthogonal axes with unit angular velocity $\mathbf{\Omega} = \mathbf{e}_i$ and $\mathbf{V} \equiv \mathbf{0}$.

To prove this assertion, we return to the full problem (2.3),(2.10),(2.11). For convenience, we can consider the solution as a superposition of two problems: the first is pure translation with arbitrary velocity \mathbf{V} , and the second is pure rotation with arbitrary angular velocity $\mathbf{\Omega}$. We can denote the solutions of these two problems as $(\mathbf{v}_{tr}, p_{tr})$ and $(\mathbf{v}_{rot}, p_{rot})$, respectively, with the corresponding force and torque being $(\mathbf{F}_{tr}, \mathbf{T}_{tr})$ and $(\mathbf{F}_{rot}, \mathbf{T}_{rot})$. The full solution is then $\mathbf{v} = \mathbf{v}_{tr} + \mathbf{v}_{rot}$ and $p = p_{tr} + p_{rot}$, and the force and torque are $\mathbf{F} = \mathbf{F}_{tr} + \mathbf{F}_{rot}$ and $\mathbf{T} = \mathbf{T}_{tr} + \mathbf{T}_{rot}$.

Now, let us consider the translation problem:

$$\mu \nabla^2 \mathbf{v}_{tr} - \nabla p_{tr} = 0 \quad , \quad \nabla \cdot \mathbf{v}_{tr} = 0$$

$$\mathbf{v}_{tr} = \mathbf{V} \text{ on } S \quad , \quad \mathbf{v}_{tr} \rightarrow \mathbf{0} \text{ at } \infty$$

We see that the problem is linear in \mathbf{V} . Thus the solution $(\mathbf{v}_{tr}, p_{tr})$ can depend only linearly on \mathbf{V} , and by the (2.11) this means that the force and the torque must also be linear functions of \mathbf{V} :

$$\mathbf{F}_{tr} = \underline{\mathbf{A}}' \cdot \mathbf{V} \quad , \quad \mathbf{T}_{tr} = \underline{\mathbf{C}}' \cdot \mathbf{V} \quad (2.12)$$

where $\underline{\mathbf{A}}'$ and $\underline{\mathbf{C}}'$ are respectively a second order tensor and a second order pseudo-tensor. The components of these tensors have a simple interpretation: A'_{ij} and C'_{ij} are the i -components of the force and the torque on the body for traslation with unit velocity in the \mathbf{e}_j direction.

An identical analysis also can be applied to the rotation problem and the result for the force and torque in this case is

$$\mathbf{F}_{rot} = \underline{\mathbf{B}}' \cdot \boldsymbol{\Omega} \quad , \quad \mathbf{T}_{rot} = \underline{\mathbf{D}}' \cdot \boldsymbol{\Omega} \quad (2.13)$$

Thus, a propeller rotating at low velocity around its axis in a very viscous fluid is subjected to a force parallel to its axis: this corkscrew-type effect is due to the lack of a plane of symmetry normal to the axis of rotation; it is very different from inertial phenomena, like the Magnus force, which accounts for the motion of ships or airplanes, propeller- driven through water or air (low-viscosity fluids). Now, combining (2.12) and (2.13), as allowed by the linearity of the governing equations, we find that the force and torque on a particle that moves with arbitrary velocities \mathbf{V} and $\boldsymbol{\Omega}$ through an otherwise quiescent fluid is

$$\boxed{\mathbf{F} = \mu(\underline{\mathbf{A}} \cdot \mathbf{V} + \underline{\mathbf{B}} \cdot \boldsymbol{\Omega}) \quad , \quad \mathbf{T} = \mu(\underline{\mathbf{C}} \cdot \mathbf{V} + \underline{\mathbf{D}} \cdot \boldsymbol{\Omega})} \quad (2.14)$$

Note that the viscosity will appear linearly in each of the second-order tensor coefficients in (2.12) and (2.13), and thus has been factored out, that is $\underline{\mathbf{A}}' = \mu \underline{\mathbf{A}}$ and so on. $\underline{\mathbf{A}}$, $\underline{\mathbf{B}}$, $\underline{\mathbf{C}}$, $\underline{\mathbf{D}}$ are called *resistance tensors* and their most important property is that they depend on only the geometry of the particle and are independent of all other parameters of the problem including, of course, \mathbf{V} and $\boldsymbol{\Omega}$.

In the absence of resistance tensors, we could calculate the force or torque on an arbitrary body that translates and/or rotates with arbitrary velocities \mathbf{V} and $\boldsymbol{\Omega}$ only by completely resolving the equations of motion for each change in the relative magnitudes of \mathbf{V} and $\boldsymbol{\Omega}$ or in their orientation relative to axes that are fixed in the body. Indeed, for nonzero Reynolds number, for which the governing equations are the full, nonlinear Navier–Stokes equations, this is precisely what must be done. Once the existence of the resistance tensors is recognized, however, we see that the force and torque for arbitrary \mathbf{V} and $\boldsymbol{\Omega}$ can be specified completely by solving a maximum of six fundamental problems, corresponding, respectively, to translation in three orthogonal directions with no rotation, and rotation about three orthogonal axes with no translation. These six problems can be solved, once and for all, to determine the components of the tensors $\underline{\mathbf{A}}$, $\underline{\mathbf{B}}$, $\underline{\mathbf{C}}$, $\underline{\mathbf{D}}$, and these results can then be used for all possible combinations of \mathbf{V} and $\boldsymbol{\Omega}$.

It must be noticed that many physical problems in microhydrodynamics require the solution of the motion of a particle in response to prescribed forces and torques in a known ambient flow. Such situations can be called *mobility* problems, in opposition

to the *resistance* problem previously described. The linearity can be invoked again to write:

$$\begin{array}{l} \mu \mathbf{V} = \underline{\mathbf{a}} \cdot \mathbf{F} + \underline{\mathbf{b}} \cdot \mathbf{T} \\ \mu \boldsymbol{\Omega} = \underline{\mathbf{c}} \cdot \mathbf{F} + \underline{\mathbf{d}} \cdot \mathbf{T} \end{array}$$

where $\underline{\mathbf{a}}$, $\underline{\mathbf{b}}$, $\underline{\mathbf{c}}$, $\underline{\mathbf{d}}$ are the *mobility tensors*. Clearly, the resistance and mobility formulation are related and are formal inverses of each other. Indeed, can be shown [10] that:

$$\begin{pmatrix} \underline{\mathbf{A}} & \underline{\mathbf{B}} \\ \underline{\mathbf{C}} & \underline{\mathbf{D}} \end{pmatrix} = \begin{pmatrix} \underline{\mathbf{a}} & \underline{\mathbf{b}} \\ \underline{\mathbf{c}} & \underline{\mathbf{d}} \end{pmatrix}^{-1}$$

An extremely important and general result [13] states the simmetry condition:

$$\underline{\mathbf{A}} = \underline{\mathbf{A}}^T \quad , \quad \underline{\mathbf{B}} = \underline{\mathbf{C}}^T \quad , \quad \underline{\mathbf{D}} = \underline{\mathbf{D}}^T \quad (2.15)$$

Since the matrix A_{ij} , which relates F_i and U_j , is symmetric, it can be diagonalized. There thus exists, for a body of arbitrary shape, a set of orthogonal coordinate axes, along which each component of the force is directly proportional to the corresponding component of the velocity:

$$F_i = \mu \lambda_i V_i$$

(contrary to our usual notation, there is no implied summation on the index i , in the above equation). The scalar product $\mathbf{F} \cdot \mathbf{V}$ representing the energy loss through viscous dissipation, must therefore be negative for any value of \mathbf{V} , implying that the three eigenvalues λ_i are all negative. From a geometrical point of view, the $\mathbf{F} \cdot \mathbf{V} < 0$ relation indicates that the angle between the force \mathbf{F} and the direction of motion must always be greater than a right angle.

2.3.1 Spheres and ellipsoides

In addition to general symmetry properties (2.15), considerable effort has been made to understand the relationships between symmetries in the geometry of the problem and the forms of the resistance tensors [17]. For example, if we consider the motion of a body with spherical symmetry in an unbounded fluid, with the origin of coordinates at the geometric center of the body, it can be shown that:

$$\underline{\mathbf{A}} = c_A \mathbf{1} \quad , \quad \underline{\mathbf{D}} = c_D \underline{\mathbf{A}} \quad , \quad \underline{\mathbf{C}} = \underline{\mathbf{B}} = \mathbf{0}$$

In particular, as we will see in the next section, the Stokes' law implies that $c_A = 6\pi a$ where a is the radius of the sphere.

On the other hand, for an ellipsoid of revolution with the origin of the coordinate system at the geometric center and coordinate axes parallel and perpendicular to the principal axes of the ellipse, it can be shown that

$$\underline{\mathbf{A}} = \text{diag}(a_{||}, a_{\perp}, a_{\perp}) \quad , \quad \underline{\mathbf{D}} = \text{diag}(d_{||}, d_{\perp}, d_{\perp}) \quad , \quad \underline{\mathbf{B}} = \underline{\mathbf{C}}^T = \mathbf{0}$$

2.4 Uniform Flow past a Solid Sphere: Stokes' law

In the previous section we showed that the linearity of the creeping flow equations implies a linear relation between forces and velocities. A particular case, where the expression of the force acting on the particle is simple and well-known, is the classical Stokes' problem (first solved by Stokes in 1851) of the uniform streaming motion in the positive x direction, past a stationary solid sphere. This problem can also be viewed as that of a solid spherical particle that is translating in the negative x direction through an unbounded stationary fluid under the action of some external force.

We choose a frame of reference whose origin is instantaneously fixed at the center of the sphere, with the natural spherical coordinates suggested by the symmetry of the problem. In this coordinate system, with base vectors \mathbf{e}_r , \mathbf{e}_θ , \mathbf{e}_φ , the velocity can be written:

$$\mathbf{v} = (v_r, v_\theta, v_\varphi) = \left(\frac{\partial_\theta \psi}{r^2 \sin \theta}, -\frac{\partial_r \psi}{r \sin \theta}, 0 \right), \quad \mathbf{v}(\infty) = \mathbf{U} = U \mathbf{e}_x \quad (2.16)$$

and we must just solve the biharmonic-like equation, with the boundary conditions:

$$\left[\frac{\partial^2}{\partial r^2} + \frac{\sin \theta}{r^2} \frac{\partial}{\partial \theta} \left(\frac{1}{\sin \theta} \frac{\partial}{\partial \theta} \right) \right]^2 \psi = 0 \quad (2.17)$$

$$\begin{cases} \psi(a, \theta) = 0 & [v_r = 0 \text{ at surface}] \\ \partial_r \psi(a, \theta) = 0 & [v_\theta = 0 \text{ at surface}] \\ \psi(\infty, \theta) = \frac{1}{2} U r^2 \sin^2 \theta & [\text{uniform flow at } \infty] \end{cases} \quad (2.18)$$

where the last condition follows from the fact that the stream function for a uniform flow is $(1/2)U r^2 \sin^2 \theta$ in spherical coordinates. The last upstream condition (2.18) suggests a separable solution of the form $\psi = f(r) \sin^2 \theta$, and substitution of this into (2.17) gives:

$$f'''' - \frac{4f''}{r^2} + \frac{8f'}{r^3} - \frac{8f}{r^4} = 0 \quad \implies \quad f = Ar^4 + Br^2 + Cr + \frac{D}{r}$$

Imposing the last of (2.18) we have $A = 0$ and $B = U/2$, whereas the first two give $C = -3U/a$ and $D = Ua^3/4$. Therefore, the solution reduces to:

$$\psi = U r^2 \sin^2 \theta \left[\frac{1}{2} - \frac{3a}{4r} + \frac{a^3}{4r^3} \right] \quad (2.19)$$

and the velocity components are, from the (2.16):

$$\mathbf{v} = U \left(\cos \theta \left(1 - \frac{3a}{2r} + \frac{a^3}{2r^3} \right), -\sin \theta \left(1 - \frac{3a}{4r} + \frac{a^3}{4r^3} \right), 0 \right) \quad (2.20)$$

The pressure can be found by integrating the Stokes equation $\nabla p = \mu \nabla^2 \mathbf{v}$, and the vorticity taking the curl of \mathbf{v} :

$$p = -\frac{3a\mu U \cos \theta}{2r^2} + p_\infty, \quad \boldsymbol{\omega} = -\frac{1}{2r^2} \sqrt{1 - \cos^2 \theta} \mathbf{e}_\varphi$$

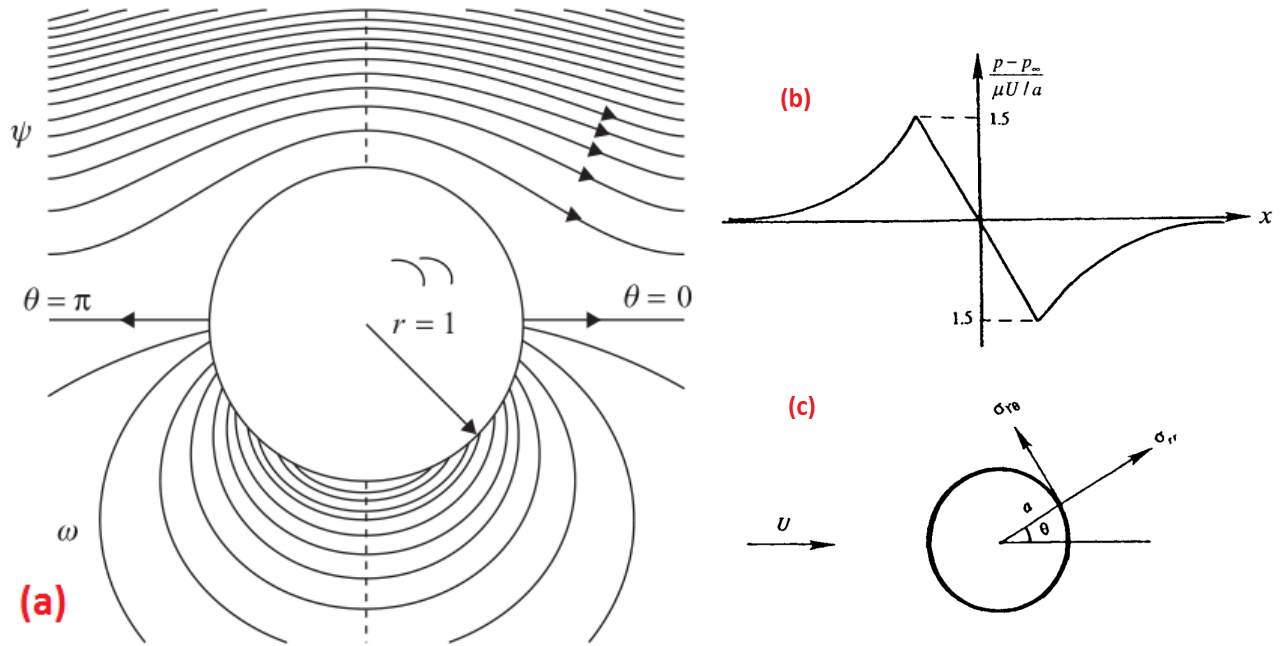


Figure 2.1: (a) streamlines and contours of constant vorticity for uniform streaming flow past a solid sphere. (b) pressure distribution in an axial ($\varphi = \text{const.}$) plane. (c) Viscous stress components at the surface.

The streamlines, and contours of constant vorticity, together with the pressure distribution are sketched in Figure 2.1. The streamlines are symmetrical about a plane normal to \mathbf{U} , as is of course implied by the linearity of \mathbf{v} in \mathbf{U} ; reversing the direction of \mathbf{U} merely leads to a change of the sign of \mathbf{v} everywhere. It will also be noticed that the disturbance due to the sphere extends to a considerable distance from the sphere, the velocity approaching zero as r^{-1} at large values of r . As a consequence, the presence of an outer rigid boundary, for example in the form of a cylinder with generators parallel to \mathbf{U} , can modify the fluid motion appreciably, even when it is at a distance of many diameters from the sphere; likewise the interaction between two moving spheres many diameters apart can be appreciable.

Clearly, these features of the solution reflect the absence of the inertia term in the equation of motion. The equation for vorticity $\nabla^2 \omega = 0$ shows that the flow is effectively due solely to steady molecular diffusion of vorticity to infinity in all directions, the sphere being a source of vorticity as a consequence of the no-slip condition. There is, in fact, a strong similarity between the transport of vorticity in 2D in axisymmetric flows and the transport of heat from a heated body. Not surprisingly, constant-vorticity lines are often similar in appearance to isotherms in the thermal problem. In the simplest thermal problem, however, the surface of the body would be assumed to be at constant temperature so that the temperature field in the case of pure conduction from a sphere would be spherically symmetric. The sphere surface is not a uniform source of vorticity. In regions where the velocity gradients are largest, the surface vorticity is highest. As a consequence, even for creeping flow with a spherical body, the vorticity distribution is not spherically symmetric.

In order to find the force exerted by the fluid on the sphere, we must evaluate

the stress tensor at $r = a$, and integrate it over all the surface. Indicating with \mathbf{n} the outward unit normal vector, the force per unit area normal to a surface is:

$$\begin{aligned} \mathbf{t} &= \sigma_{ij}n_j = \begin{pmatrix} \sigma_{rr} & \sigma_{r\theta} & 0 \\ \sigma_{\theta r} & \sigma_{\theta\theta} & 0 \\ 0 & 0 & 0 \end{pmatrix} \begin{pmatrix} -1 \\ 0 \\ 0 \end{pmatrix} = \begin{pmatrix} \sigma_{rr} \\ \sigma_{r\theta} \\ 0 \end{pmatrix} \\ &= -\sigma_{rr}\mathbf{e}_r - \sigma_{r\theta}\mathbf{e}_\theta = (\sigma_{rr}\cos\theta - \sigma_{r\theta}\sin\theta)\mathbf{e}_x + (\sigma_{rr}\sin\theta - \sigma_{r\theta}\cos\theta)\mathbf{e}_y \end{aligned} \quad (2.21)$$

and calculating the stress from the definition $\sigma_{ij} = -p\delta_{ij} + \mu(\partial_i v_j + \partial_j v_i)$

$$\sigma_{rr} = -p + 2\mu\partial_r v_r = 2\mu U \cos\theta \left(\frac{3a}{r^2} - \frac{3a^3}{2r^4} \right), \quad \sigma_{r\theta} = \mu \left(r\partial_r \left(\frac{v_\theta}{r} \right) + \frac{\partial_\theta u_r}{r} \right) = -\frac{3\mu U a^3}{2r^4} \sin\theta$$

and on the surface of the sphere ($r = a$) we obtain from (2.21):

$$\mathbf{t}(r = a, \theta) = \left(\frac{3\mu\mathbf{U}}{2a} \cos^2\theta + \frac{3\mu\mathbf{U}}{2a} \sin^2\theta, 0 \right) \quad (2.22)$$

$$\mathbf{F}(a) = \oint_S \sigma_{ij}n_j dS = \int_0^{2\pi} \int_0^\pi \mathbf{t}(a, \theta) 2r dr d\theta = \left(4\pi a^2 \frac{3\mu\mathbf{U}}{2a}, 0 \right)$$

$$\boxed{\mathbf{F}_D = 6\pi\mu a\mathbf{U}} \quad \text{Stokes' Law}$$

that is the classical result called the *Stokes' law of resistance*.

It remains to verify the limit of the approximation made using the Stokes' equation to estimate the flow field. According to the solution (2.20), an estimate of the magnitude of the viscous force is $\mu\nabla^2\mathbf{v}$ is $\mu U a/r^3$. If the sphere velocity is exactly steady, and the rate of change of \mathbf{v} at a fixed point is due simply to the sphere changing its position relative to the point concerned, the operator ∂_t is equivalent to $-\mathbf{U} \cdot \nabla$. Resuming, and using again the (2.20):

$$f_{in} \sim |\rho(-\mathbf{U} \cdot \nabla\mathbf{v} + \mathbf{v} \cdot \nabla\mathbf{v})| \sim 2\frac{\rho U^2 a}{r^2} + \frac{\rho U^2 a}{r^3}, \quad f_{visc} \sim |\mu\nabla^2\mathbf{v}| \sim \mu U a/r^3$$

$$\frac{f_{in}}{f_{visc}} \sim \frac{\rho a U}{\mu} \frac{r}{a} = \frac{1}{2} \frac{r}{a} Re$$

At position near the sphere the solution is indeed self-consistent with the approximation made to derive it, when $Re \ll 1$, but the inertia forces corresponding to the solution become comparable with viscous forces at distances from the sphere of order a/Re . At these large distances, the solution and the Stokes' law are therefore not valid, although this by itself may not be of consequence since the fluid velocity and the inertia and viscous forces are all small there. It could in fact be seen [19] that it is possible to find a velocity distribution which is a valid approximation to the solution of the complete N-S equations everywhere in the fluid when $Re \ll 1$, and which coincides with the above solution, when r/a is of order unity.

2.5 Singularity and Boundary integral solutions

To solve the creeping-flow equations (2.3), many techniques have been developed in the literature, most of them based on the representation of solutions in terms of either eigenfunction expansion and/or vector harmonic functions [9]. These methods turn out to be powerful to solve problems in which the geometry of the solid boundaries or interfaces either coincides with a coordinate surface(s) in some orthogonal coordinate system (as in the case of the Stokes' problem in Sec. 2.4) or else lies close to such a surface.

However, the linearity of the Stokes equation allows another class of solution methods that is more readily applied to problems with complicated boundary geometries. These methods for solving Stokes equations are based on *fundamental* or *Singularity solutions*, corresponding to the flow produced by point forces in a fluid.

For problems involving solid boundaries, a general solution can be obtained in integral form, corresponding to a *distribution of point forces* over all of the boundaries. Such a solution can be derived making use of the so-called *Boundary integral equations*. When a fluid interface is involved, a similar integral formulation is obtained by generalization to a distribution of singularities at the interface. The solution of a specific problem is then transformed to determining the distribution of surface forces that is necessary to satisfy boundary conditions. If the boundary shapes are simpler, an analytic approximation can sometimes be achieved by means of equivalent, internal distributions of point forces and force multipole singularities: this is the so-called *Singularity method*. In the case of complex shapes, the solution can only generally be accomplished numerically, following the so-called *Boundary integral method* [18].

2.5.1 Fundamental solution: the Stokeslet

The solution of the creeping-flow equations for a point force \mathbf{f} , closely related to the Green's functions of the Stokes flow, can be found solving the equations

$$\boxed{\mu \nabla^2 \mathbf{v} - \nabla p = \mathbf{f} \delta(\mathbf{x} - \mathbf{x}_0) \quad , \quad \nabla \cdot \mathbf{v} = 0} \quad (2.23)$$

where \mathbf{f} is an arbitrary constant, \mathbf{x}_0 an arbitrary point, and δ the three-dimensional Dirac delta function. Introducing the Green's function $\underline{\mathbf{G}}$, we write the solution in the form:

$$\boxed{v_i(\mathbf{x}) = \frac{1}{8\pi\mu} G_{ij}(\mathbf{x}, \mathbf{x}_0) f_j}$$

\mathbf{x}_0 is usually called the *source point* or *pole*, and \mathbf{x} the *observation* or *field point*. Physically, $\mathbf{v}(\mathbf{x})$ expresses the velocity field due to the concentrated point force of strength \mathbf{f} placed at the point \mathbf{x}_0 , and may be identified with the flow produced by the slow settling of a small particle.

It is convenient to classify the Green's functions into three categories depending on the topology of the domain of flow. First, we have the free-space Green's function for infinite unbounded flow; second, the Green's functions for infinite or semi-infinite flow that is bounded by a solid surface; and third, the Green's functions for internal flow that is completely confined by solid surfaces. The Green's functions in the second

and third categories are required to vanish over the internal or external boundaries of the flow. As the observation point \mathbf{x} approaches the pole \mathbf{x}_0 all Green's functions exhibit singular behaviour and, to leading order, behave like the free-space Green's function. The Green's functions for infinite unbounded or bounded flow are required to decay at infinity at a rate equal to or lower than that of the free-space Green's function. In the next sections, we will treat the Green's function for the free-space, deferring to the next chapter the discussion for the space bounded by an infinite rigid plane and by a rigid sphere [18].

The pressure and the stress fields associated with the flow may be taken in the form:

$$p(\mathbf{x}) = \frac{1}{8\pi} \mathcal{P}_j(\mathbf{x}, \mathbf{x}_0) f_j \quad , \quad \sigma_{ik}(\mathbf{x}) = \frac{1}{8\pi} T_{ijk}(\mathbf{x}, \mathbf{x}_0) f_k \quad (2.24)$$

where the stress tensor associated with the fundamental solution is defined as:

$$T_{ijk}(\mathbf{x}, \mathbf{x}_0) = -\delta_{ik} \mathcal{P}_j(\mathbf{x}, \mathbf{x}_0) + \partial_k G_{ij}(\mathbf{x}, \mathbf{x}_0) + \partial_i G_{kj}(\mathbf{x}, \mathbf{x}_0) \quad (2.25)$$

Substituting the (2.24),(2.25) in the (2.23) we obtain the equations to be satisfied to derive these tensors:

$$\begin{aligned} -\partial_k \mathcal{P}_j(\mathbf{x}, \mathbf{x}_0) + \nabla^2 G_{kj}(\mathbf{x}, \mathbf{x}_0) &= -8\pi \delta_{kj} \delta(\mathbf{x} - \mathbf{x}_0) \\ \partial_i T_{ijk}(\mathbf{x}, \mathbf{x}_0) &= \partial_i T_{jki}(\mathbf{x}, \mathbf{x}_0) = -8\pi \delta_{kj} \delta(\mathbf{x} - \mathbf{x}_0) \end{aligned}$$

The free-space Green's function

It is possible to derive the solution formally by the Fourier transform or by the method of superposition of harmonic functions [9]. Both of these methods lead to the following expression:

$$\mathbf{v}(\mathbf{x}) = \frac{1}{8\pi\mu} \underline{\mathbf{G}}^{(S)}(\mathbf{x} - \mathbf{x}_0) \cdot \mathbf{f} \quad , \quad \boxed{G_{ij}^{(S)}(\mathbf{y}) = \frac{\delta_{ij}}{|\mathbf{y}|} + \frac{y_i y_j}{|\mathbf{y}|^3}} \quad , \quad \mathbf{y} = \mathbf{x} - \mathbf{x}_0$$

where $\underline{\mathbf{G}}^{(S)}(\mathbf{y})$ is called the *Stokeslet* or the *Oseen-Burger tensor*. The velocity field generated by a stokeslet is plotted in Figure 2.5.3. The pressure and stress fields associated to the flow may be written in the forms (2.24), where:

$$\mathcal{P}_i(\mathbf{y}) = 2 \frac{y_i}{|\mathbf{y}|^3} \quad , \quad T_{ijk}(\mathbf{y}) = -6 \frac{y_i y_j y_k}{|\mathbf{y}|^5} \quad (2.26)$$

It must be noticed that $\underline{\mathcal{P}}$ and $\underline{\mathbf{T}}$ represent two fundamental solutions of Stokes flow. Specifically, $\underline{\mathcal{P}}$ represents the velocity at the point \mathbf{x} due to a point source of strength -8π with pole at \mathbf{x}_0 , or, equivalently, the velocity at \mathbf{x}_0 due to a point source of strength -8π with pole at \mathbf{x} , whereas:

$$v_i(\mathbf{x}_0) = T_{ijk}(\mathbf{x} - \mathbf{x}_0) q_{ik} = -T_{ijk}(\mathbf{x} - \mathbf{x}_0) q_{ik}$$

where $\underline{\mathbf{q}}$ is a constant matrix, represents the velocity field due to a singularity called the *Stresslet* with pole at \mathbf{x} . Moreover, can be easily shown that the divergence of the point-force $\underline{\boldsymbol{\sigma}}$ has an useful property. Integrating over a closed volume V enclosed by ∂V , we can use the fact that $\nabla \cdot \underline{\mathbf{T}} = \underline{\mathbf{0}}$ everywhere except at \mathbf{x}_0 , following

from (2.26). Therefore, choosing a sphere of radius ϵ arbitrary small, centered in \mathbf{x}_0 (so that $\mathbf{x} - \mathbf{x}_0 = -\epsilon \mathbf{n}$), :

$$\begin{aligned} \int_V (\nabla \cdot \underline{\boldsymbol{\sigma}})_j dV &= \frac{1}{8\pi} \int_V \partial_k T_{ijk} f_j dV = \frac{f_j}{8\pi} \oint_{\partial V} T_{ijk}(\mathbf{x} - \mathbf{x}_0) n_k(\mathbf{x} - \mathbf{x}_0) dS(\mathbf{x} - \mathbf{x}_0) \\ &= \frac{3f_j}{4\pi} \int_0^{2\pi} \int_0^\pi \frac{n_i n_j n_k}{\epsilon^2} n_k \epsilon^2 \sin \theta d\theta d\varphi = \frac{3f_j}{4\pi} \int_0^{2\pi} \int_0^\pi n_i n_j \sin \theta d\theta d\varphi = \delta_{ij} f_j = f_i \\ &\implies \boxed{\partial_k T_{ijk}(\mathbf{x} - \mathbf{x}_0) = 8\pi \delta_{ij} \delta(\mathbf{x} - \mathbf{x}_0)} \end{aligned} \quad (2.27)$$

An important property of the stokeslet solution, specifically for locomotion, is *directional anisotropy*. Indeed, we see from equation that if we evaluate the velocity in the direction parallel to the applied force, then in the direction perpendicular to it:

$$v_{\parallel} = f/4\pi\mu r \quad , \quad v_{\perp} = f/8\pi\mu r \quad , \quad \implies \boxed{v_{\perp} = 2v_{\parallel}} \quad \text{with } r = |\mathbf{y}|$$

For the same applied force, the flow field in the parallel direction is therefore twice that in the perpendicular direction. Alternatively, to obtain the same velocity, one would need to apply a force in the perpendicular direction twice as large as in the parallel direction ($F_{\perp} = 2F_{\parallel}$). Such anisotropy, which is reminiscent of the anisotropy in the mobility matrix for long slender bodies, is at the origin of the drag-based propulsion method employed by swimming microorganisms (see [15]).

2.5.2 The boundary integral equation

In many cases the solution of linear, elliptic, and homogeneous boundary value problems may be represented in terms of boundary integrals involving the boundary values of the unknown function and its derivatives. A convenient starting point for deriving a boundary integral equation for the Stokes' flow is the "relaxed" version of the Lorentz reciprocal identity (2.7) written identifying \mathbf{v}' and the corresponding stress tensor $\underline{\boldsymbol{\sigma}}'$ with the point-force velocity field and stresses:

$$\oint_S \mathbf{v} \cdot (\underline{\boldsymbol{\sigma}}' \cdot \mathbf{n}) dS - \int_V \mathbf{v} \cdot (\nabla \cdot \underline{\boldsymbol{\sigma}}') dV = \oint_S \mathbf{v}' \cdot (\underline{\boldsymbol{\sigma}} \cdot \mathbf{n}) dS - \int_V \mathbf{v}' \cdot (\nabla \cdot \underline{\boldsymbol{\sigma}}) dV \quad (2.28)$$

$$\text{with } v_i(\mathbf{x}) = \frac{1}{8\pi\mu} G_{ij}^{(S)}(\mathbf{x}, \boldsymbol{\xi}) f_j \quad \text{and} \quad \sigma_{ik}(\mathbf{x}) = \frac{1}{8\pi} T_{ijk}(\mathbf{x}, \boldsymbol{\xi}) f_k$$

Recalling the divergence of T_{ijk} from (2.27) and substituting in (2.28):

$$\oint_S G_{ij}^{(S)}(\mathbf{x} - \boldsymbol{\xi}) \sigma_{ij}(\boldsymbol{\xi}) n_k dS(\boldsymbol{\xi}) = -8\pi\mu \left[\oint_S v_i(\boldsymbol{\xi}) T_{ijk}(\mathbf{x} - \boldsymbol{\xi}) n_k dS(\boldsymbol{\xi}) + \int_V v_i(\boldsymbol{\xi}) \delta_{ij} \delta(\mathbf{x} - \boldsymbol{\xi}) dV(\boldsymbol{\xi}) \right]$$

where we used that our generic velocity field solves the Stokes equation ($\nabla \cdot \underline{\boldsymbol{\sigma}} = \mathbf{0}$) and we assumed the surface normal vector $\hat{\mathbf{n}}$ pointing out of the fluid region¹. Using

¹we shall distinguish in the following such surface normal vectors from the generic ones pointing inside the surface by using a "hat" $\hat{\mathbf{n}}$ symbol.

the properties of the Dirac and Kroenecker delta functions, the last integral simplify to $v_j(\mathbf{x})$ in the interior of V , and zero outside, and we obtain², if $x \in V \setminus \partial V \equiv S$:

$$\boxed{\mathbf{v}(\mathbf{x}) = -\frac{1}{8\pi\mu} \oint_S [\underline{\boldsymbol{\sigma}}(\boldsymbol{\xi}) \cdot \hat{\mathbf{n}}(\boldsymbol{\xi})] \cdot \underline{\mathbf{G}}^{(S)}(\mathbf{x} - \boldsymbol{\xi}) dS(\boldsymbol{\xi}) - \oint_S \mathbf{v}(\boldsymbol{\xi}) \cdot \underline{\mathbf{T}}(\mathbf{x} - \boldsymbol{\xi}) \cdot \hat{\mathbf{n}} dS(\boldsymbol{\xi})} \quad (2.29)$$

This is the famous integral representation for the solution of the creeping-flow equations which is usually attributed to Ladyzhenskaya [20], stating that a Stokes velocity field may be reconstructed throughout a region V using only values of the velocity and stress fields on the boundary of V .

The first integral on the right-hand side represents clearly a velocity field generated by a distribution of surface forces of strenght $\mathbf{t}dS = \underline{\boldsymbol{\sigma}} \cdot \hat{\mathbf{n}}dS$, since $\underline{\mathbf{G}}^{(S)}(\mathbf{x} - \boldsymbol{\xi})$ is the velocity field generated by a point-force in $\boldsymbol{\xi}$. By analogy with potential theory, this integral is usually termed the *single-layer potential*.

The second integral on the right-hand side is denoted as the *double-layer potential* and has a density function that is just the velocity \mathbf{v} on the boundaries S of the flow domain. This term can be interpreted as a distribution of sources or sinks of strenght $\mathbf{v} \cdot \hat{\mathbf{n}}$ and a true “double layer” of Stokeslet, indeed if we write it using the (2.25):

$$v_j T_{ijk} \hat{n}_k = -\mathcal{P}_i \mathbf{v} \cdot \hat{\mathbf{n}} + (\partial_k G_{ij}^{(S)} + \partial_i G_{kj}^{(S)}) v_j \hat{n}_k \quad \text{and} \quad \oint_S \mathcal{P}_i \hat{n}_j dS = 2 \oint_S \frac{x_i - \xi_i}{|\mathbf{x} - \boldsymbol{\xi}|^3} dS = \frac{4}{3} \pi \delta_{ij}$$

the first term is recognized to correspond to sources and sinks, whereas the second one, as we will see in the next subsection, corresponds to opposing Stokeslets of dipole strength \mathbf{v} displaced in the direction of $\hat{\mathbf{n}}$, plus opposing Stokeslets of dipole strength $|\mathbf{v}| \hat{\mathbf{n}}$ in the direction of \mathbf{v} . This symmetric placement of point forces implies that no net force or torque is exerted on the fluid.

Of course, the equation (2.29) and the corresponding form for the pressure do not provide a solution for any specific problem until the density functions \mathbf{v} and \mathbf{t} are specified on S . In fact, all that we really have done is to obtain an integral formula for \mathbf{v} that is equivalent to the differential form of the creeping-flow equation (2.3). To obtain a solution for any particular problem, we must determine the density functions so that the velocity field \mathbf{v} satisfies the boundary conditions on S . In general, this requires numerical solution of the integral equations that result from applying boundary conditions to (2.29). In fact, this is the essence of the so-called *boundary-integral method* for solution of creeping-flow equations; this technique has been used widely in research and is especially suitable for free-surface and other Stokes’ flow problems with complicated boundary geometries [18].

Flow past a Solid Body

In the case of a Stokes’ flow past a stationary solid surface, the boundary integral equation can be considerably simplified. Indeed, the no-slip condition requires $\mathbf{v}|_S = \mathbf{0}$ and the second term in (2.29), the double-layer potential, vanishes. Therefore, if we call $\mathbf{v}_\infty(\mathbf{x})$ the solution at large distance from the body (the undisturbed flow),

²This formula says nothing about the boundary points $\mathbf{x} \in \partial V$.

the boundary integral equation becomes:

$$\boxed{\mathbf{v}(\mathbf{x}) = \mathbf{v}_\infty(\mathbf{x}) - \frac{1}{8\pi\mu} \oint_S \left[\frac{\mathbb{1}}{|\mathbf{x} - \boldsymbol{\xi}|} + \frac{(\mathbf{x} - \boldsymbol{\xi})(\mathbf{x} - \boldsymbol{\xi})}{|\mathbf{x} - \boldsymbol{\xi}|^3} \right] \cdot \mathbf{t}(\boldsymbol{\xi}) dS(\boldsymbol{\xi})} \quad (2.30)$$

where \mathbf{x} is now a fixed point in the flow field and $\mathbf{t}(\boldsymbol{\xi}) = \boldsymbol{\sigma}(\boldsymbol{\xi}) \cdot \hat{\mathbf{n}}(\boldsymbol{\xi})dS$ is the distribution of surface stress on the boundary S that can be obtained solving the (2.29) on the surface of the body, by means of the no-slip condition. Therefore, a general solution of the creeping-flow equations for flow past stationary solid surfaces can be expressed completely as a superposition of surface forces (stokeslets) at the boundaries S . In fact, a solution of the creeping-flow equations can always be written solely as a distribution of stokeslets over the bounding surfaces, even if these are not solid and stationary, but the simple identity of the stokeslet density function with the actual surface stress is valid only for this special case. To retain the simple physical interpretation of the density functions for other kinds of boundaries, we must use the more general form (2.29).

2.5.3 Singularities: multipole expansion for rigid bodies

The solution for creeping flow past a body, that we write in the former section in terms of a surface distribution of point forces (stokeslets) on the surface of that body, can sometimes be replaced with an internal distribution of point forces and higher-order singularities. The principle is analogous to that of the multipole expansion of electrodynamics. Indeed, at great distances from a rigid body we cannot distinguish between the points $\boldsymbol{\xi}$ on the surface and a reference origin $\mathbf{0}$ located in a convenient point inside the body. In this way, at the first order we find that $\underline{\mathbf{G}}^{(S)}(\mathbf{x} - \boldsymbol{\xi}) \sim \underline{\mathbf{G}}^{(S)}(\mathbf{x})$, so that may be moved outside the integral in (2.30). The integral of what remains, $\boldsymbol{\sigma} \cdot \hat{\mathbf{n}}$, is simply the hydrodynamic drag \mathbf{F} on the particle, and we obtain a disturbance due to the motion of the particle which is independent on the details of the body shape:

$$\mathbf{v}^d(\mathbf{x}) = \mathbf{v}(\mathbf{x}) - \mathbf{v}_\infty(\mathbf{x}) \sim \mathbf{F} \cdot \underline{\mathbf{G}}^{(S)} / 8\pi\mu$$

In order to find the higher order correction for the disturbance field, we notice that due to the linearity of the Stokes equations (2.3), a derivative of any order of the fundamental solution is still a solution of the creeping-flow equations. Thus, if we introduce the following notation for the stokeslet solutions:

$$\mathbf{v}^{(S)}(\mathbf{x}; \mathbf{f}) = \frac{\mathbf{f}}{r} + \frac{(\mathbf{f} \cdot \mathbf{x})\mathbf{x}}{r^3} \quad , \quad p^{(S)}(\mathbf{x}; \mathbf{f}) = 2\frac{\mathbf{f} \cdot \mathbf{x}}{r^3} \quad , \quad \text{with } r = |\mathbf{x}| \quad (2.31)$$

then any derivative of $\mathbf{v}^{(S)}$ and $p^{(S)}$ is a solution of (2.3) corresponding to a point singularity that is a derivative of the same order of a point force \mathbf{f} . Now, if the point force is located at $\mathbf{x} = \boldsymbol{\xi}$, we formally set $r \gg |\boldsymbol{\xi}|$ and the stokeslet solution can be expanded in form of a generalized Taylor series about $\boldsymbol{\xi} = \mathbf{0}$:

$$\begin{aligned} \mathbf{v}^{(S)}(\mathbf{x} - \boldsymbol{\xi}) &= \sum_{n=0}^{\infty} \frac{1}{n!} (\boldsymbol{\xi} \cdot \nabla_{\boldsymbol{\xi}})^n \mathbf{v}^{(S)}(\mathbf{x} - \boldsymbol{\xi}) \Big|_{\boldsymbol{\xi}=\mathbf{0}} = \sum_{n=0}^{\infty} \frac{(-1)^n}{n!} (\boldsymbol{\xi} \cdot \nabla)^n \mathbf{v}^{(S)}(\mathbf{x}) \quad (2.32) \\ &= \sum_{n=0}^{\infty} \frac{(-1)^n}{n!} \xi_{k_1} \cdots \xi_{k_n} \partial_{k_1} \cdots \partial_{k_n} \mathbf{v}^{(S)}(\mathbf{x}) = \mathbf{v}^{(S)}(\mathbf{x}) - (\boldsymbol{\xi} \cdot \nabla) \mathbf{v}^{(S)}(\mathbf{x}) + \frac{1}{2} (\boldsymbol{\xi} \cdot \nabla)^2 \mathbf{v}^{(S)}(\mathbf{x}) + \dots \end{aligned}$$

with a similar series expression for $p^{(S)}$. Inserting the expansion into the velocity integral representation (2.30):

$$\boxed{v_i^d(\mathbf{x}) = \frac{1}{8\pi\mu} \sum_{n=0}^{\infty} \oint_{S_p} [(\underline{\boldsymbol{\sigma}} \cdot \hat{\mathbf{n}})_j \xi_{k_1} \cdots \xi_{k_n}] dS \partial_{k_1} \cdots \partial_{k_n} G_{ij}^{(S)}(\mathbf{x})} \quad (2.33)$$

$$= -\frac{1}{8\pi\mu} (F_j G_{ij}^{(S)}(\mathbf{x}) - D_{jk} G_{ijk}^{(D)}(\mathbf{x}) + \dots)$$

with $G_{ijk}^{(D)}(\mathbf{x}) = \partial_k G_{ij}^{(S)}(\mathbf{x})$, $F_j = \oint_{S_p} (\underline{\boldsymbol{\sigma}} \cdot \hat{\mathbf{n}})_j dS$, $D_{jk} = \oint_{S_p} (\underline{\boldsymbol{\sigma}} \cdot \hat{\mathbf{n}})_j \xi_k dS$

Thus, for flow past a solid body, we always can use the generalized Taylor series to replace the surface distribution of stokeslets with an equivalent internal distribution of stokeslets and higher-order singularities (inside the body). This series, takes the name of *multipole expansion*, and its terms are named *multipole moments*.

The obvious question is whether there is any advantage to be gained, especially in view of the fact that we must replace a surface distribution of stokeslets only with a whole hierarchy of higher-order singularities inside. One possibility is that we may be able to replace the surface distribution with an internal distribution of lower spatial order. Thus, for example, for axisymmetric bodies, it may be possible to express the solution in terms of a line distribution of singularities along the axis of symmetry of the body. In this case, the 2D integral equation that arises from application of boundary conditions would be replaced with a 1D, though more complicated, integral equation. Another possibility is that we may be able to replace a stokeslet distribution on a body that has a very complicated surface with an internal distribution of singularities on a nearby surface that has a much simpler geometry. In any case, however, the use of internal distributions of singularities will be an advantage only if the number of terms in the multipole expansion can be limited to a relatively small set, i.e. only if the Taylor series can be truncated after a finite number of terms. Intuitively, for an exact solution, this will require bodies of simple geometry in relatively simple flows. The criteria for recognizing problems for which internal distributions of singularities offer an advantage over the solutions in terms of a surface distribution of stokeslets is, actually, a subject of current research.

Stokeslet Dipole

Anyway, equation (2.32) shows us that in the far field, regardless of the details of the body shape, all disturbance fields exhibit certain common features. The leading term, or *monopole*, will be a Stokeslet with coefficient \mathbf{F} equal to the force exerted by the fluid on the particle. This field, decaying as r^{-1} away from the solid particle, will be present if and only if the particle and fluid exert a net force on each other.

The next effect is a force dipole of strength represented by $\underline{\mathbf{D}}$, a constant second-order tensor, and velocity field :

$$\boxed{G_{ijk}^{(SD)}(\mathbf{x}) = \frac{1}{r^3} (\delta_{ij} x_k - \delta_{ik} x_j - \delta_{jk} x_i) + 3 \frac{x_i x_j x_k}{r^5}}$$

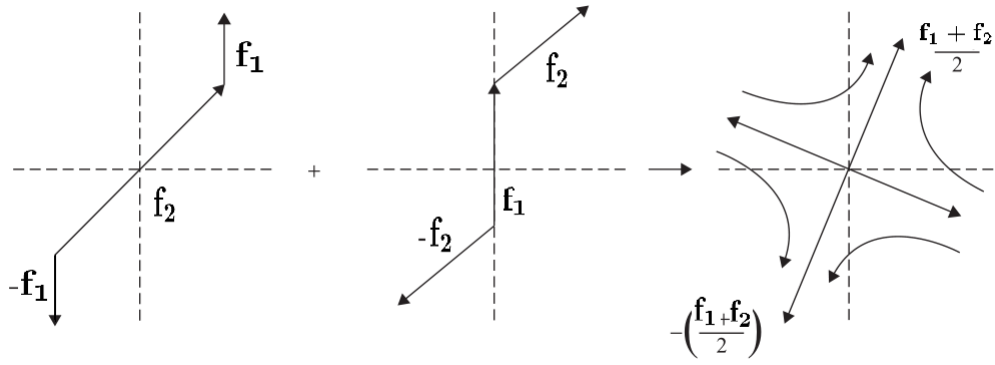


Figure 2.2: Stresslet velocity field constructed as a sum of the Stokes' dipoles.

$$\mathbf{v}^{(SD)}(\mathbf{x}; \mathbf{f}, \mathbf{b}) \equiv -(\mathbf{b} \cdot \nabla) \mathbf{v}^{(S)}(\mathbf{x}; \mathbf{f}) = \frac{(\mathbf{f} \times \mathbf{b}) \times \mathbf{x}}{r^3} - \left[\frac{(\mathbf{f} \cdot \mathbf{b})}{r^3} - \frac{3(\mathbf{f} \cdot \mathbf{x})(\mathbf{b} \cdot \mathbf{x})}{r^5} \right] \mathbf{x}$$

$$p^{(SD)}(\mathbf{x}; \mathbf{f}, \mathbf{b}) = -(\mathbf{b} \cdot \nabla) p^{(S)}(\mathbf{x}; \mathbf{f}) = 2\mu \left[-\frac{\mathbf{f}_1 \cdot \mathbf{b}}{r^3} + \frac{3(\mathbf{f}_1 \cdot \mathbf{x})(\mathbf{b} \cdot \mathbf{x})}{r^5} \right] \quad (2.34)$$

This corresponds to the velocity and pressure fields, generated by a pair of forces, one at $\mathbf{x} = \mathbf{b}/2$ with strength \mathbf{f} and the other at $\mathbf{x} = -\mathbf{b}/2$ with strength $-\mathbf{f}$, in the limit as $|\mathbf{b}| \rightarrow 0$ (see, for example, the sketch in Fig. 2.5.3). In fact, as in the electrodynamics analogous, this is suggested by the expansion $\mathbf{b} \cdot \nabla \mathbf{v}^{(S)} \simeq -\mathbf{u}^{(S)}(\mathbf{x}) + \mathbf{u}^{(S)}(\mathbf{x} + \mathbf{b})$.

Rotlet and Stresslet

It is useful to express the Stokes' dipole solution as the sum of two component parts, because each has a clear physical significance. These components are defined in a manner that is analogous to the symmetric and antisymmetric components of a second-order tensor, that is:

$$D_{jk} = s_{jk} + r_{jk} \quad , \quad \mathbf{v}^{(SD)}(\mathbf{x}; \mathbf{f}, \mathbf{b}) = \mathbf{v}^{(SS)}(\mathbf{x}; \mathbf{f}, \mathbf{b}) + \mathbf{v}^{(R)}(\mathbf{x}; \mathbf{f}, \mathbf{b})$$

$$\mathbf{v}^{(SS),(R)}(\mathbf{x}; \mathbf{f}, \mathbf{b}) = \frac{1}{2} [\mathbf{v}^{(SD)}(\mathbf{x}; \mathbf{f}, \mathbf{b}) \pm \mathbf{v}^{(SD)}(\mathbf{x}; \mathbf{f}, \mathbf{b})] \quad (2.35)$$

The symmetric part, $\mathbf{v}^{(SS)}$, is known as the *stresslet* solution, and the antisymmetric part, $\mathbf{v}^{(R)}$, is known as the *rotlet* solution. And substituting the dipole expression 2.34 in the definitions 2.35 we obtain the explicit forms:

$$\mathbf{v}^{(R)}(\mathbf{x}; \mathbf{f}, \mathbf{b}) = \frac{\mathbf{b} \times \mathbf{f} \times \mathbf{x}}{r^3} \quad \mathbf{p}^{(R)}(\mathbf{x}; \mathbf{f}, \mathbf{b}) = 0$$

The physical significance of the rotlet solution is that it is the flow that is due to a singular, point torque at the origin. Indeed, if we calculate the moment exerted

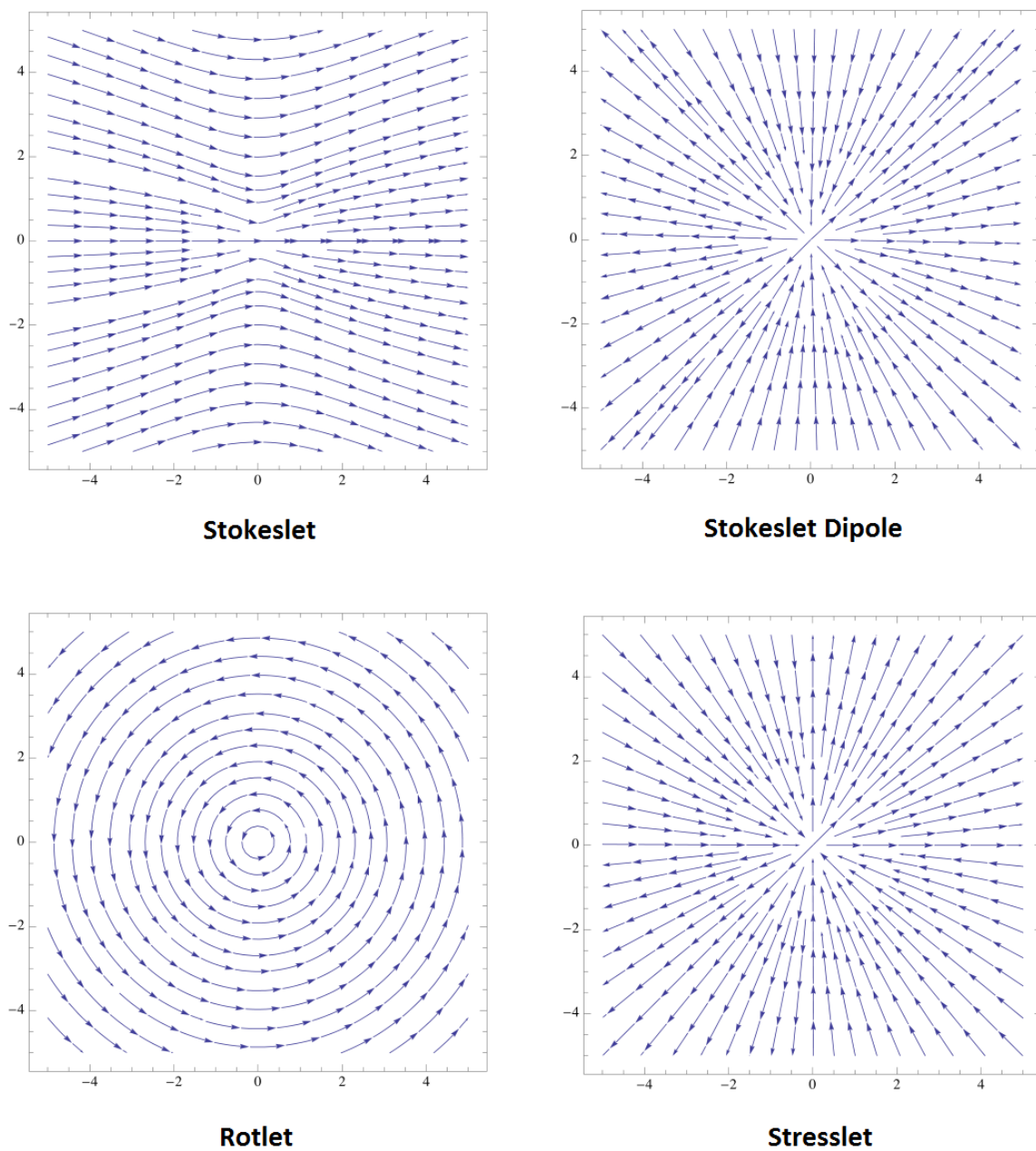


Figure 2.3: Singularities velocity fields. (Art Evans)

on the fluid outside an arbitrary control surface S centered at the origin by a rotlet of strength $\mathbf{m} = \mathbf{b} \times \mathbf{f}$, we have:

$$\mathbf{M} = \oint_S \mathbf{x} \times (\underline{\boldsymbol{\sigma}}^{(R)} \cdot \mathbf{n}) dS = 8\pi\mu\mathbf{m}$$

The stresslet solution takes the form:

$$\mathbf{v}^{(SS)}(\mathbf{x}; \mathbf{f}, \mathbf{b}) = \left[-\frac{(\mathbf{f} \cdot \mathbf{b})}{r^3} + \frac{3(\mathbf{f} \cdot \mathbf{x})(\mathbf{b} \cdot \mathbf{x})}{r^5} \right] \mathbf{x}$$

$$p^{(SS)}(\mathbf{x}; \mathbf{f}, \mathbf{b}) = 2\mu \left[-\frac{\mathbf{f} \cdot \mathbf{b}}{r^3} + \frac{3(\mathbf{f} \cdot \mathbf{x})(\mathbf{b} \cdot \mathbf{x})}{r^5} \right]$$

The stresslet exerts zero net force or torque on the fluid, that is $\mathbf{F}^{(SS)} = \mathbf{M}^{(SS)} = \mathbf{0}$, and can be thought of as a straining motion of the fluid that is symmetric about the \mathbf{f} , \mathbf{b} plane with principal axes of strain $\mathbf{f} + \mathbf{b}$, $\mathbf{f} - \mathbf{b}$, $\mathbf{f} \times \mathbf{b}$ (see Fig.2.5.3). The stresslet and rotlet velocity field have been plotted in Figure 2.5.3

Stokes Quadrupole and Potential Dipole

The Stokes' quadrupole solutions, obtained with a following derivation, are more complicated:

$$\begin{aligned} \mathbf{v}^{(S^4)}(\mathbf{x}; \mathbf{f}, \mathbf{b}, \mathbf{c}) &\equiv (\mathbf{c} \cdot \nabla)(\mathbf{b} \cdot \nabla)\mathbf{v}^{(S)}(\mathbf{x}; \mathbf{f}) \\ p^{(S^4)}(\mathbf{x}; \mathbf{f}, \mathbf{b}, \mathbf{c}) &\equiv (\mathbf{c} \cdot \nabla)(\mathbf{b} \cdot \nabla)p^{(S)}(\mathbf{x}; \mathbf{f}) \end{aligned}$$

and we will not give the explicit expression. However, one component turns out to be particularly useful in the solution of Stokes' flow problems, and that is the *potential dipole* solution, namely

$$\mathbf{v}^{(PD)}(\mathbf{x}; \mathbf{d}) \equiv -\frac{1}{2}\nabla^2\mathbf{v}^{(S)}(\mathbf{x}; \mathbf{d}) = -\frac{\mathbf{d}}{r^3} + \frac{3(\mathbf{d} \cdot \mathbf{x})\mathbf{x}}{r^5}, \quad p^{(PD)} = 0$$

The potential dipole exerts zero net force on the fluid. Physically, it corresponds to a mass dipole at the origin – that is, the flow generated by a mass source at $\mathbf{x} = \mathbf{d}/2$ and a mass sink at $\mathbf{x} = -\mathbf{d}/2$ in the limit $|\mathbf{d}| \rightarrow 0$.

General Rules for singularity solutions

Unfortunately, the use of fundamental solutions to solve Stokes' flow problems by means of internal distributions of singularities has not yet become completely systematized. Many problems involving flow in the vicinity of a solid sphere can be solved by a superposition of point-forces and/or higher-order singularities at the center of the sphere. Some problems involving prolate axisymmetric ellipsoids (spheroids) can be solved by a superposition of point-force and higher-order singularities on the symmetry axis between the two foci of the ellipse. However, general rules that are guaranteed to guide the choice of singularities or the choice of internal surface geometry for all possible situations cannot be offered.

If there is a net force on the body, the leading-order term must be a stokeslet or stokeslet distribution, and experience suggests that the stokeslet is always accompanied by the potential dipole. If there is a net torque on the body, we require a rotlet or rotlet distribution, and this will be the leading term if the net force is zero. Finally, if the net force and torque are both zero, the leading term often (though not always) involves the stresslet.

In the next section we will show how the methods is easily applied in the case of a Stokes' problem for a rigid sphere. A more extensive treatment and many example can be found in [21].

Distribution of singularities for the traslation of a sphere

As we showed in Section 2.4, the translation of a spehical particle through a quiescent fluid, problem equivalent to a stationary uniform flow past the particle, produces a net force (drag) on the sphere. Thus, to construct a solution by means of internal singularities we require a stokeslet of strength \mathbf{f} located at the sphere center. However, by itself, the stokeslet flow does not satisfy the no-slip and kinematic boundary conditions at the surface of the sphere. Taking, as in the former, the velocity of the sphere \mathbf{U} and its radius a , the no-slip condition is:

$$\mathbf{v} = \mathbf{U} \quad \text{at} \quad r = a \quad (2.36)$$

whereas the Stokeslet at $r = a$ takes the form

$$\mathbf{v}^{(S)}(\mathbf{x} = a\mathbf{e}_r, \mathbf{f}) = \frac{\mathbf{f}}{8\pi\mu a} + \frac{(\mathbf{f} \cdot \mathbf{e}_r)\mathbf{e}_r a^2}{8\pi\mu a^3} = \frac{\mathbf{f} + (\mathbf{f} \cdot \mathbf{e}_r)\mathbf{e}_r}{8\pi\mu a} \quad (2.37)$$

Hence it is clear that the stokeslet solution alone cannot satisfy the no-slip condition. However, if we add at the sphere surface a potential dipole

$$\mathbf{v}^{(PD)}(\mathbf{x} = a\mathbf{e}_r, \mathbf{d}) = -\frac{\mathbb{1}_2}{8\pi\mu a^3} + \frac{3a^2(\mathbf{d} \cdot \mathbf{e}_r)\mathbf{e}_r}{8\pi\mu a^5} = \frac{-\mathbf{d} + 3(\mathbf{d} \cdot \mathbf{e}_r)\mathbf{e}_r}{8\pi\mu a^3} \quad (2.38)$$

and comparing (2.37) and (2.38) it is obvious that a superposition $\mathbf{v}(\mathbf{x}) = \mathbf{v}^{(S)}(\mathbf{x}; \mathbf{f}) + \mathbf{v}^{(PD)}(\mathbf{x}; \mathbf{d})$ of the stokeslet and potential dipole solutions will satisfy the creeping-flow equations and also the boundary condition (2.36), if

$$\mathbf{v}^{(S)}(\mathbf{x} = a\mathbf{e}_r, \mathbf{f}) + \mathbf{v}^{(PD)}(\mathbf{x} = a\mathbf{e}_r, \mathbf{d}) = \frac{\mathbf{f} + (\mathbf{f} \cdot \mathbf{e}_r)\mathbf{e}_r}{8\pi\mu a} + \frac{-\mathbf{d} + 3(\mathbf{d} \cdot \mathbf{e}_r)\mathbf{e}_r}{8\pi\mu a^3} = \mathbf{U}$$

$$\implies a^2\mathbf{f} - \mathbf{b} = 8\pi\mu a^3\mathbf{U} \quad , \quad a^2\mathbf{f} + 3\mathbf{d} = \mathbf{0} \quad \implies \quad \mathbf{d} = -\frac{a^3\mathbf{U}}{4} \quad , \quad \mathbf{f} = 6\pi\mu a\mathbf{U}$$

Therefore, not surprisingly, we recover Stokes's law: $\mathbf{f} = \mathbf{F}_D$.

2.6 Faxen's Law for a body in an unbouded fluid

In the former, in particular in the Sections (2.4) and (2.5.3), we found through two different methods the force acting on a sphere traslating in a quiescent fluid, or

equivalently for the uniform flow past a sphere at rest. In both of the cases the force exerted by the sphere on the fluid turned out to be equal to the Stokes' law expression $\mathbf{F}_D = 6\pi\mu a\mathbf{U}$. Now, we consider a correction to this formula in the case of an undisturbed generic steady flow $\mathbf{v}_\infty(\mathbf{x})$ not necessarily uniform, using the Lorentz Reciprocal theorem (2.6). Clearly, the result we will obtain can be interpreted as the correction to an undisturbed flow due to the motion of a translating sphere, so we can find the multipole moments of (2.33) by means of this method.

To apply the Reciprocal theorem to the problem, we need a fictitious velocity field, therefore, let us suppose that we have obtained the solution of the creeping-motion equations for uniform flow \mathbf{U} past a stationary body of surface S . We denote the solution of this problem as \mathbf{v} and the corresponding surface-force vector on S as $\mathbf{t} = \underline{\boldsymbol{\sigma}} \cdot \mathbf{n}$. Then, applying the reciprocal theorem:

$$\mathbf{U} \cdot \oint_S \mathbf{t}' dS = \mathbf{U} \cdot \mathbf{F}' = \oint_S \mathbf{v}' \cdot \mathbf{t} dS \quad , \quad \mathbf{t} = \underline{\boldsymbol{\sigma}} \cdot \mathbf{n}$$

If we have actually solved the uniform-flow problem, we can immediately deduce the surface-force on the same body held fixed in any undisturbed flow $\mathbf{v}_\infty(\mathbf{x})$ that satisfies the Stokes equations. In particular, we have:

$$\boxed{\mathbf{U} \cdot \mathbf{F}' = \oint_S \mathbf{v}_\infty \cdot \mathbf{t}' dS} \quad (2.39)$$

i.e. we can obtain the surface-force \mathbf{t}' for the undisturbed flow $\mathbf{v}_\infty(\mathbf{x})$ by means of a simple integration of this formula, with \mathbf{t} known from the solution of the uniform-flow problem, but without any need to solve the actual corresponding Stokes equations.

A powerful result discovered originally by Faxén, is obtained applying the (2.39) to a stationary solid sphere of radius a . In this case, the solution for uniform flow is known from 2.22, and hence:

$$\mathbf{t}(r = a) = \frac{3}{2a}\mu\mathbf{U} \implies \mathbf{U} \cdot \mathbf{F}' = \int_S \mathbf{v}_\infty(\mathbf{x}) \cdot \left(\frac{3\mu\mathbf{U}}{2a}\right) dS$$

and since \mathbf{U} is arbitrary:

$$\mathbf{F}' = \frac{3\mu}{2a} \int_S \mathbf{v}_\infty(\mathbf{x}) dS$$

Finally, supposing the origin to be at the center of the sphere, we can expand $\mathbf{v}_\infty(\mathbf{x})$ on S in a multipole representation around $\mathbf{x} = \mathbf{0}$:

$$\mathbf{v}_\infty(\mathbf{x}) = \mathbf{v}_\infty(\mathbf{0}) + \mathbf{x} \cdot \nabla \mathbf{v}_\infty(\mathbf{0}) + \frac{\mathbf{x}\mathbf{x}}{2} : \nabla^2 \mathbf{v}_\infty(\mathbf{0}) + \dots$$

$$\mathbf{F}' = 6\pi\mu a \left[\mathbf{v}_\infty(\mathbf{0}) + \frac{a^2}{6} \nabla^2 \mathbf{v}_\infty(\mathbf{0}) + \text{const} \nabla^4 \mathbf{v}_\infty(\mathbf{0}) + \dots \right]$$

where the integrals of the odd-number terms in the expansion vanish because S is a sphere. Moreover, because of the Stokes equation $\nabla^4 \mathbf{v}_\infty(\mathbf{x}) = \nabla \nabla^2 p = \mathbf{0}$ and the same for all the terms $\nabla^{2n} \mathbf{v}_\infty(\mathbf{x})$. Thus, we obtain the exact result:

$$\boxed{\mathbf{F}' = 6\pi\mu a \left(\mathbf{v}_\infty(\mathbf{x}) + \frac{a^2}{6} \nabla^2 \mathbf{v}_\infty(\mathbf{x}) \Big|_{\mathbf{x}=\mathbf{0}} \right)} \quad (2.40)$$

In the original work of Faxén an analogous relation can be found for the torque, in the more general case where the sphere is also rotating:

$$\mathbf{M} = 8\pi\mu a^3\boldsymbol{\Omega}_\infty(\mathbf{0})$$

These important results are known as *Faxén Laws*. According to these laws, if we specify the undisturbed velocity, then the force on a sphere can be calculated directly from the formula 2.40, without any need to solve the problem corresponding to the free-stream velocity $\mathbf{v}_\infty(\mathbf{x})$. The interesting feature of this law is that the correction to the Stokes' Law required by the general ambient flow $\mathbf{v}_\infty(\mathbf{x})$ is relatively simple, being proportional to the ambient pressure gradient $\nabla\mathbf{v}_\infty^2(\mathbf{0}) = \nabla p(\mathbf{0})/\mu$ in the center of the sphere.

Moreover, we have shown what the expression for the second moment in the multipole expansion for a sphere is, and that is the higher order one. In general using the right \mathbf{t} and $\mathbf{v}_\infty(\mathbf{x})$, the higher order moments can be found for every particle shape.

Chapter 3

Hydrodynamic interactions

The mathematics is not there till we put it there.
Sir Arthur Eddington

When two particles immersed in a viscous fluid approach each other, the motion of each one is influenced by the other, even in absence of interparticle interactions, such as van der Waals and electrostatic forces. The velocity field generated by the motion of one particle is transmitted through the fluid medium and influences the motion, the force, the torque and the stresses on the other particle. This kind of interaction is called *hydrodynamic*.

We have seen in the previous chapter that the presence of a rigid body in a Stokes' flow produces a disturbance in the velocity field that decays as r^{-1} , where r is the distance from the body. The rate of decay depends on the type of disturbance: if there is a net hydrodynamic force on the body, the far-field disturbance flow is dominated by the stokeslet velocity field (2.31) with a strength \mathbf{f} that depends on the net force, and the velocity disturbance decays as r^{-1} ; if there is no net force on the body, but the undisturbed flow is linear so that the dominant disturbance mode is a rotlet or stresslet, the disturbance decays as r^{-2} , and so forth.

As a consequence of the long-range perturbation to the velocity field in such a case, we may expect significant hydrodynamic interactions when other bodies or boundaries are present, even when the separation distance is relatively large. For example, the sedimentation velocity of a solid particle is still significantly influenced by walls or other particles when separation distance is more than 10 particle radii away.

Unfortunately, most of the classical analytical techniques are very difficult (or impossible) to apply. The exceptions are two spheres, or a sphere and a plane wall, for which bispherical coordinates may be employed to obtain exact eigenfunction expansions for solution of the creeping-flow equations. But, since only a few cases can be approached with this technique, it is essential to have other solution procedures that do not rely on a specific coordinate system. One is the boundary-integral method [18], but ultimately this requires numerical methods for solving the boundary-integral equations.

The alternative methods of attack depend on the separation between the surface; in particular, if the particles are widely separated (the distance between closest points

on the surfaces is much greater than the particle size), a general asymptotic method known as the method of reflections is available. Problems near contact problems are not reviewed here, because are beyond the scopes of this work, but a complete treatment can be found in [10]. Moreover, we will only treat interaction between only two particles, indeed, because of the linearity of the Stokes equations, the general construction for a N -particle system is, with only minor changes in the notation, essentially the same as the framework for the pair interaction problem.

We divide the discussion on interactions according to particle-particle (Section 3.1) and particle-wall interactions (Section 3.2) .

3.1 The method of reflections

Two particles will be considered widely separated when $a/d \gg 1$, where a is the characteristic particle size and d is the particle-particle distance. In this approximation, a general asymptotic scheme known as *method of reflections*, valid for arbitrary shapes has been shown to be convergent [23], and its applicability relies on the possibility to express the solution analytically as a series in terms of the small parameter a/d .

The basic idea is to approximate the solution as a series of terms that satisfy the creeping-flow equations at each level, but only alternatively satisfy the boundary conditions at the solid surfaces. In the zeroeth order approximation, the solution is formed by a superposition of the field produced by the isolated particle solutions, and the hydrodynamic interactions are neglected. We have shown in Section 2.5.3 that the disturbance field of an isolated particle may be written as a multipole expansion and that such an expansion is particularly useful in the study of the far field. The construction of the series is thus based on the idea that the ambient field about each particle consists of the original ambient field plus the disturbance field produced by the other particle(s). The method is iterative, since a correction of the ambient field about a given particle generates a new disturbance solution for that particle, which in turn modifies the ambient field about another particle. The process of incorporating the effect of an ambient field (called *incident*) with a new disturbance field is called a *reflection*, hence the name of the method.

To illustrate the procedure in the case of two particles, let us suppose that the particle 1 and 2 move in an unbounded fluid with velocities \mathbf{U}_1 and \mathbf{U}_2 , with position $\mathbf{x}_{1,2} = \mathbf{x}_{1,2}(t)$, and isolated particle solutions $\mathbf{v}_{1,2}(\mathbf{x})$. On the surfaces S_1 and S_2 of each particle, the boundary conditions are

$$\mathbf{v}_{1,2}^{(0)} = \mathbf{U}_{1,2} + \boldsymbol{\omega}_{1,2} \times (\mathbf{x} - \mathbf{x}_{1,2}) - \mathbf{v}_\infty \quad \text{on } S_{1,2}$$

and so if we set $\mathbf{v}^{(0)} = \mathbf{v}_\infty + \mathbf{v}_1^{(0)} + \mathbf{v}_2^{(0)}$, we see that the errors in the boundary condition follow as $\mathbf{v}_2^{(0)}(\mathbf{x})$ for a point $\mathbf{x} \in S_1$ and $\mathbf{v}_1^{(0)}(\mathbf{x})$ for a point $\mathbf{x} \in S_2$. This error will be at least as small as a/d , since the decay in $\mathbf{v}_1^{(0)}$ and $\mathbf{v}_2^{(0)}$ is at most that of a Stokeslet. The next reflection fields, the first order ones, will reduce this error. They are formally defined as the solutions to the Stokes equations vanishing at infinity with the additional conditions

$$\begin{aligned} \mathbf{v}_1^{(1)} = \mathbf{v}_{12} &= -\mathbf{v}_2 & \text{on } S_2 \\ \mathbf{v}_2^{(1)} = \mathbf{v}_{21} &= -\mathbf{v}_1 & \text{on } S_1 \end{aligned}$$

Now the errors in the boundary condition scale as $\mathbf{v}_{12}(\mathbf{x})$ for a point \mathbf{x} on the surface of particle 1, and $\mathbf{v}_{21}(\mathbf{x})$ on particle 2. The error has been reduced, since the far field values of $\mathbf{v}_{12}(\mathbf{x})$ and $\mathbf{v}_{21}(\mathbf{x})$ are smaller (by a factor a/d) than the near field values of the same order, which are of the same order of the far field values of $\mathbf{v}_{1,2}^{(0)}(\mathbf{x})$. The higher order correction are obtained in exactly the same manner. For example, the next reflections are obtained with \mathbf{v}_{12} and \mathbf{v}_{21} playing the roles previously played by $\mathbf{v}_{1,2}^{(0)}$. The reflected field of order n will be denoted by :

$$\begin{aligned}\mathbf{v}_1^{(2)} &= \mathbf{v}_{121}(x) = -\mathbf{v}_{212}(\mathbf{x}) && \text{on } S_2 \\ \mathbf{v}_2^{(2)} &= \mathbf{v}_{212}(x) = -\mathbf{v}_{121}(\mathbf{x}) && \text{on } S_1\end{aligned}$$

In general, we will indicate with a superscript n the field taking into account all the reflection up to the n -th:

$$\begin{aligned}\mathbf{v}_1^{[n]} &= \sum_{k=1}^n \mathbf{v}_1^{(k)} = \mathbf{v}_1 + \mathbf{v}_{12} + \mathbf{v}_{121} + \mathbf{v}_{1212} + \dots \\ \mathbf{v}_2^{[n]} &= \sum_{k=1}^n \mathbf{v}_2^{(k)} = \mathbf{v}_2 + \mathbf{v}_{21} + \mathbf{v}_{212} + \mathbf{v}_{2121} + \dots\end{aligned}\tag{3.1}$$

This will give an error in the boundary condition is given by the values taken by the highest order reflected fields evaluated at the surface of the other particle, i.e. $(a/d)^n$.

The most natural form for the reflected fields is the multipole expansion (2.32), with moments determined by application of the Faxen Laws on the incident fields. For simple shapes as spheres (Section (2.6)) or ellipsoids, analytical forms of the Faxen laws are available, and so the method of reflections will yield analytical solutions.

The method of reflections works equally well for both the resistance and the mobility problems, but its main application in microhydrodynamics lies in mobility problems because they arise more frequently, and the method produces the desired solutions directly, i.e., without an inversion of the resistance problem. The second reason is that the far field forms of the mobility problems consist of dipole-dipole interactions, which are much weaker than the monopole-monopole interactions usually encountered in resistance problems. Nevertheless, in the following, we will make use of the method in a particular resistance problem (Chapter 5), so we start for explaining this case.

3.1.1 Resistance problems

As we saw in Chapter 2, in the resistance problems particle motions and the ambient field are prescribed and the force, torque and higher order moments have to be determined. Also, the zeroeth order fields v_1 and v_2 produce exactly the prescribed particle motions. In subsequent reflections, the reflected fields satisfy the no-slip condition. Thus at each reflection, the multipole expansion for the reflected field always leads off with a Stokeslet. The strength of the Stokeslet \mathbf{f} , i.e., the hydrodynamic force on the particle, from (2.33) always scales as the difference between the ambient velocity and the particle velocity. Since the latter is zero at the higher order reflections, \mathbf{f} will be equal to the magnitude of the incident field, which in turn is simply

the far field limit of the previous reflection. Thus in resistance problems we typically have the following behaviour:

$$\mathbf{F}_\alpha^{(n+1)} \sim \mathcal{O}\left(\frac{a}{d}\right) \mathbf{F}_\beta^{(n)}$$

the $(n+1)$ -th reflection's contribution to the hydrodynamic force on the particle α will be a/d times smaller than n -th reflection's contribution to particle β . In particular, for flow past two stationary bodies, we have:

$$F^{(N)} \sim \mathcal{O}\left(\frac{a}{d}\right)^N$$

The scale for other moments, such as the torque and stresslet, may be obtained by reference to the Faxén relations; the end result is that for a given reflection, the n -th moment is $\mathcal{O}(a/d)$ smaller than the $(n-1)$ -th order moment.

3.1.2 Mobility problems

In mobility problems, particle motions in a specified ambient field are to be determined. The motions arise from prescribed forces and torques on each particle. As in the resistance case, we must start with the single-particle solutions \mathbf{v}_1 and \mathbf{v}_2 , but in the reflection procedure some differences have to be considered. In fact, the zeroth order fields produce exactly the prescribed forces and torques. Therefore, in subsequent reflections the particle motions must be such that the reflected fields are force-free and torque-free. These translational and rotational velocities will scale as the ambient velocity and velocity gradient. Furthermore, the multipole expansion for the reflected fields will lead off with a stresslet of strength \mathbf{S} of the same order as the ambient velocity gradient. Thus, in mobility problems we typically have a behaviour as:

$$\mathbf{U}_\alpha^{(n+1)} = \mathcal{O}\left(\frac{a}{d}\right)^3 \mathbf{U}_\beta^{(n)}$$

where two powers in a/d are due to the far field decay of the stresslet field, while the additional factor is due to the relative magnitudes of $\mathbf{U}_\beta^{(n)}$ and $\mathbf{S}_\beta^{(n)}$

And given the same amount of information concerning the Faxén relations for the moments, and after the same number of reflections, the results for the mobility functions will be accurate to higher order in a/d than the result for the resistance functions. Thus, usually, is convenient to solve the entire collection of mobility problems and then invert these if the resistance solutions are also required.

3.2 Particle-Wall interactions

In many aspects, the analysis for particle-wall interactions is similar to that for particle-particle interactions. Here again, we will only treat the case of the particle far away from the wall, with a small a/R , where R is the distance from the wall. Under these circumstances a suitably modified form of the method of reflections is appropriate, with the reflections off the wall conveniently represented by image singularities. This approach has been used since for a long time, and started with the works of Lorentz [24], Faxén [25] and Blake [26].

3.2.1 Stokeslet near a wall

We need to construct the Greens functions $\underline{\mathbf{G}}^W(\mathbf{x}, \mathbf{x}_0)$ and $\mathcal{P}^W(\mathbf{x}, \mathbf{x}_0)$, for the velocity and pressure fields associated with a unit point force acting in the \mathbf{e}_k direction direction at $\mathbf{x} = \mathbf{x}_0$ and satisfying the no-slip condition on the plane boundary. The no-slip condition is applied only on the plane boundary (not on a body near the boundary, so that a surface or line distribution of singularities in the body can be used to satisfy the no-slip condition). Assumed that the wall is located in $z = 0$, we must impose that:

$$\underline{\mathbf{G}}^W(x, y, z = 0; \mathbf{x}_0) = 0$$

A first approach, proposed by Lorentz, used the reciprocal theorem to obtain an image system for the wall. An alternative way is to follow Blake, taking a point force of equal magnitude but opposite sign at the image point inside the wall $\mathbf{x}_0^{\text{im}} = (x_0, y_0, -z_0)$ to write the boundary condition on the wall in a more convenient way, and solving the Creeping Flow equations for a velocity field

$$\mathbf{v} = \frac{1}{8\pi\mu}(\underline{\mathbf{G}}^{(S)}(\mathbf{x}, \mathbf{x}_0) + \underline{\mathbf{G}}^{wd}(\mathbf{x}, \mathbf{x}_0)) \cdot \mathbf{f} \quad , \quad \underline{\mathbf{G}}^W = \underline{\mathbf{G}}^{(S)} + \underline{\mathbf{G}}^{wd}$$

by means of the two dimensional Fourier transform. In this way, Blake showed that $\underline{\mathbf{G}}$ may be constructed from a Stokeslet and a few image singularities including a Stokeslet, a potential dipole, and a Stokeslet doublet

$$\underline{\mathbf{G}}^W(\mathbf{x}, \mathbf{x}_0) = \underline{\mathbf{G}}^{(S)}(\mathbf{x} - \mathbf{x}_0) - \underline{\mathbf{G}}^{(S)}(\mathbf{x} - \mathbf{x}_0^{\text{im}}) + 2z_0^2 \underline{\mathbf{G}}^{(D)}(\mathbf{x} - \mathbf{x}_0^{\text{im}}) - 2z_0 \underline{\mathbf{G}}^{(SD)}(\mathbf{x} - \mathbf{x}_0^{\text{im}}) \quad (3.2)$$

where $\hat{\mathbf{x}} = \mathbf{x} - \mathbf{x}_0$, and \mathbf{x}_0^{im} is the image of \mathbf{x}_0 respect to the wall. And:

$$\begin{aligned} G_{ij}^{(S)}(\mathbf{x}) &= \frac{1}{|\mathbf{x}|} + \frac{x_i x_j}{|\mathbf{x}|^3} \\ G_{ij}^{(D)}(\mathbf{x}) &= \pm \frac{\partial}{\partial x_j} \left(\frac{x_i}{|\mathbf{x}|^3} \right) = \pm \left(\frac{\delta_{ij}}{|\mathbf{x}|^3} - 3 \frac{x_i x_j}{|\mathbf{x}|^5} \right) \\ G_{ij}^{(SD)}(\mathbf{x}) &= \pm \frac{\partial S_{i1}}{\partial x_j} = x_1 G_{ij}^{(D)}(\mathbf{x}) \pm \frac{\delta_{j1} x_i - \delta_{i1} x_j}{|\mathbf{x}|^3} \end{aligned}$$

3.2.2 Stokeslet near a big sphere

An interaction similar to the wall-particle one, is that between large and small particles, which although involve multiple length scales. Let a and b denote the size of the large and small particles, respectively, and let d denote a measure of the gap between them. In the case $a \ll d \ll b$, whereas the larger particle is in the far field of the smaller one, the smaller particle is in the near field of the larger one, whence a special form of the method of reflections is required. The key idea is that over length scales associated with the larger particle, the disturbance fields produced by the smaller one may be approximated by fields produced by equivalent a small number of Stokes singularities, remembering that the higher order ones diminish in influence as powes of a/d .

So, for the reflections at the larger particle, the entire multipole solution has to be retained, or equivalently we must use the exact result for the image singularities induced by Stokes singularities near the particle. Such information is available only for simple shapes - such as spheres, cylinder, and plane wall - so there is a restriction on the shape of the large particle or wall.

The simplest case is that of a big sphere, and the first singularity, the Stokeslet, can be calculated with two different analysis for the axisymmetric part (Stokeslet directed along the line of centers) and the trasverse case. The calculation can be found in [10], and was firstly performed by Oseen; the resulting Green's function of the flow is:

$$\begin{aligned} \underline{\mathbf{G}}^{\text{RS}}_{ij}(\mathbf{x}, \mathbf{X}) = & \underline{\mathbf{G}}^{(S)}(\hat{\mathbf{x}}) - \frac{R\delta_{ij}}{r^*|\mathbf{X}|} - \frac{R^3}{|\mathbf{X}^3|} \frac{\hat{x}_i^* \hat{x}_j^*}{r^{*3}} - \frac{|\mathbf{X}|^2 - R^2}{|\mathbf{X}|} \left(\frac{X_i^* X_j^*}{R^3 r^*} - \frac{R}{|\mathbf{X}|^2 r^{*3}} (X_i^* \hat{x}_j^* + X_j^* \hat{x}_i^*) + \right. \\ & \left. + \frac{2X_i^* X_i^* X_n^* \hat{x}_n^*}{R^3 r^{*3}} \right) - (|\mathbf{x}|^2 - R^2) \Phi_{ij} \end{aligned} \quad (3.3)$$

$$\begin{aligned} \Phi_{ij} = & \frac{|\mathbf{X}|^2 - R^2}{2|\mathbf{X}|^3} \left[-\frac{3\hat{x}_i^* X_j}{R r^{*3}} + \frac{R\delta_{ij}}{r^{*3}} - 3R \frac{\hat{x}_i^* \hat{x}_j^*}{r^{*5}} - \frac{2X_i^* X_j}{R r^{*3}} + \frac{6X_j \hat{x}_i^* \hat{X}_k^* \hat{x}_k^*}{R r^{*5}} \right. \\ & + \frac{3R}{|\mathbf{X}^*|} \frac{\hat{x}_i^* X_j^* r^{*2} + \hat{x}_j^* X_i^* |\mathbf{X}^*|^2 + (r^* - |\mathbf{X}^*|) r^{*2} |\mathbf{X}^*| \delta_{ij}}{r^{*3} |\mathbf{X}^*| (r^* |\mathbf{X}^*| + x_k X_k^* - |\mathbf{X}^*|^2)} \\ & - \frac{3R}{|\mathbf{X}^*|} \frac{(|\mathbf{X}^*| \hat{x}_i + r^* X_i^*) (X_j^* r^{*2} - |\mathbf{X}^*|^2 \hat{x}_j^* + (x_j - 2X_j^*) r^* |\mathbf{X}^*|)}{r^{*2} |\mathbf{X}^*| (r^* |\mathbf{X}^*| + x_k X_k^* - |\mathbf{X}^*|^2)^2} \\ & \left. - \frac{3R}{|\mathbf{X}^*|} \frac{x_i X_j^* + |\mathbf{x}| |\mathbf{X}^*| \delta_{ij}}{|\mathbf{x}| |\mathbf{X}^*| (|\mathbf{x}| |\mathbf{X}^*| + x_k X_k^*)} + \frac{3R}{|\mathbf{X}^*|} \frac{(|\mathbf{X}^*| x_i + |\mathbf{x}| X_i^*) (|\mathbf{X}^*| x_j + |\mathbf{x}| X_j^*)}{|\mathbf{x}| |\mathbf{X}^*| (|\mathbf{x}| |\mathbf{X}^*| + x_k X_k^*)^2} \right] \end{aligned}$$

where R is the radius of the big sphere, $\mathbf{X} = \mathbf{x}_0$ is the position of the Stokeslet, $\mathbf{X}^* = \mathbf{X}/|\mathbf{X}|^2$ is the image point inside the sphere, $\hat{\mathbf{x}} = \mathbf{x} - \mathbf{X}$, $\hat{\mathbf{x}}^* = \mathbf{x} - \mathbf{X}^*$, and $r^* = |\hat{\mathbf{x}}^*|$.

Higdon [27] observed that this formula may be interpreted as a line distribution of singularities with poles in the interior of the sphere. Specifically, they found that the radial component of the image system may be resolved into a Stokeslet, a potential dipole, and a stresslet with poles at the inverse point \mathbf{X}^* . The corresponding transverse component may be resolved into a line distribution of Stokeslets, potential dipoles, and Stokeslet doublets extending from the origin up to the inverse point.

Chapter 4

Cilia dynamics

In the matter of physics, the first lessons should contain nothing but what is experimental and interesting to see.

A pretty experiment is in itself often more valuable than twenty formulae extracted from our minds.

Albert Einstein

Cilia and flagella are two different names that are often used interchangeably for the same structure of eukaryotic cells. As suggested by the meaning of the words (lat. cilia “eyelashes”, flagellum “whip”) the term cilia tends to be used when the cellular appendages are short and abound on a single cell, whereas the term flagellum is used for longer filaments, of which only one or two are usually found per cell. Their inner structure is characterised by a cylindrical core called the axoneme, which is a cylindrical arrangement of elastic filaments (microtubules) and force generating molecular motors (dynein).

In this chapter we will give a synthetic overview of the problem arising in the study of the cilia mechanics in the first section, then we will show the characteristic of the single cilium structure and dynamics in the second section, and at last we will discuss the self-synchronization effects on cilia arrays due to hydrodynamics interactions. A complete treatment of the subject can be found in [28], which we shall follow closely in the first sections of the chapter.

4.1 Principal issues

Although it is well established that flagellar and ciliary movements are based on active sliding similar to the well-known mechanism in muscle, the flagellar system seems to be more complicated. This is because the muscle system shows only one-dimensional contraction, due to active sliding occurring homogeneously along the muscle filaments, whereas the flagellar system gives rise to rhythmic initiation and propagation of two- or three-dimensional bends, due to a time- and space-dependent pattern of active sliding within the flagellum. In this work we will focus only on the ciliary structure and motion. One challenging problem that immediately arises is how bending waves are self-organized in cilia and flagella. Structural and functional considerations of cilia and flagella are necessary in solving this problem.

If many such flagella or cilia are close together, they exhibit on a large scale propagating waves known as metachronal waves. In ciliated surfaces of protozoa, for example, where beating cilia occur in large numbers, the activity of adjacent cilia is coordinated via hydrodynamic interactions to produce metachronal waves passing over the surface. Another interesting problem then arising is how metachronal waves are self-organized in the ciliated surface. In attempting to solve this problem, it is important to consider the advantage of these wave phenomena from a functional point of view. Through the metachronal coordination of ciliary activity, ciliated systems seem to achieve higher efficiency for the propulsion of fluids than could be achieved by random movement of the cilia.

Of particular interest is the presence of the two self-organizational phenomena on quite different levels. On one hand, the coordination in time and space of mechanochemical processes at the molecular level produces bending waves at the level of an individual cilium. On the other hand, the metachronal coordination of such activity in individual cilia in turn generates wave phenomena at the level of a ciliated system. This suggests that regardless of the system level, universal principles may apply to the coordination in time and space of the 'active' processes at the lower level leading to self-organization of temporal, spatial and functional orders at the upper level. Cilia and flagella, thus, provide a good example for studying functional and structural hierarchy. In spite of many studies of the structure, biochemistry and motility of individual organelles, few attempts have been made to identify the universal principles.

Like other nonlinear distributed systems, these motile systems exhibit a large repertoire of self-organizational phenomena at each level. At the individual organelle level, flagella and cilia show regular beating patterns such as oscillations and excitability, with or without the absolute and relative refractory period. They also show irregular patterns such as reversal of the direction of wave propagation and intermittent beating caused by spontaneous stopping and starting transients. At the ciliated-system level, groups of cilia show at least four types of regular metachronal waves depending on the relationship between the beat direction of individual organelles and the propagating direction of the metachronal waves (see section 4.4). They often show irregular patterns due to a weak metachronism, e.g. sometimes two oppositely propagated metachronal waves collide to disappear (annihilating waves) or sometimes they collide to evoke a new metachronal wave (non-annihilating wave or soliton). Irregular patterns of this kind have been studied less intensively than regular patterns. Recently the presence and role of irregularity, or chaos, have been pointed out in various biological systems. This suggests that rather than considering them separately, we should consider both regular and irregular patterns as general phenomena characterized by their degree of order (or the degree of disorder).

4.2 Structure of a cilium

Flagella and cilia are living motile organelles projecting from the surface of eukaryotic cells. They produce bending waves to propel single cells in a medium or to move fluid over the fixed cell surface. Most of them beat at $\sim 10 - 40$ Hz, but the form of the beat is quite variable. Their length ranges from $2 \mu m$ to several millimetres and

the diameter is about $0.2 \mu\text{m}$. Therefore, the typical Reynolds number is $Re \sim 10^{-3}$ and the Creeping Flow approximation can be applied.

Strictly speaking, flagella and cilia have very diverse ultrastructures depending on the species from which they come, but they are generally similar to one another and have a basic structure of microtubules in arrangements called axonemes[36]. So these different names are merely a matter of definition and the experimental results of one system can be assumed to apply to the other. In most cases, therefore, it is not necessary to distinguish between the two systems.

As pointed out before, many flagella and cilia possess an identical axoneme structure in spite of their various beating patterns. Throughout the length of the cilium, nine microtubules are arranged to form a basic structure of the axoneme though its cross-sectional patterns vary with the distance from the tip.

To emphasize this *structural asymmetry* one of the ciliary axonemes, seen in a longitudinal section, and a series of base-to-tip cross-sections at different levels are illustrated in Figure 4.1:

- At level (1) , nine singlet microtubules and a central pair of singlet microtubules are arranged. No other specific structures can be seen.
- At level (2), instead of singlet microtubules, nine outer doublet microtubules are arranged around the central pair. This microtubule arrangement is known as the **9 + 2 axoneme** [34].
- Level (3) is the transition zone where the central pair terminates.
- At level (4), instead of doublet microtubules, nine triplet microtubules are arranged to form a basal body.

The intact ciliary or flagellar axoneme is surrounded by an extension of the cell membrane and bathed in cytoplasm. This cytoplasmic communication with the cell body, where ATP is produced by mitochondria, provides the necessary channel for supplying the ATP to the motile system of the axoneme. The transport process of the ATP along the flagellum is simple diffusion. A function of the membrane is thus to maintain the proper concentration of ATP and essential ions (e.g. Mg^{2+}) around the axoneme.

4.3 Kinematics and dynamics of the single cilium

For its structure and its typical behaviour a cilium can be treated as a typical device for low-Reynolds swimmer, also because of its characteristic function of pushing and displacing a flow with an effective net force. As anticipated, cilia generally show asymmetric beating in a cycle that can be separated into two phases: the effective stroke and the recovery stroke (Fig.4.3). This non-reciprocal motion allows an effective push on the fluid, according to the scallop theorem (see section 2.2.7).

During the effective stroke the cilium only bends a little, except near its base, and then swings rapidly around the basal region more or less in one plane. This is followed by the recovery stroke in which a bend is initiated at the base and propagates to the tip of the cilium. As a result, the cilium moves more slowly back to the starting point

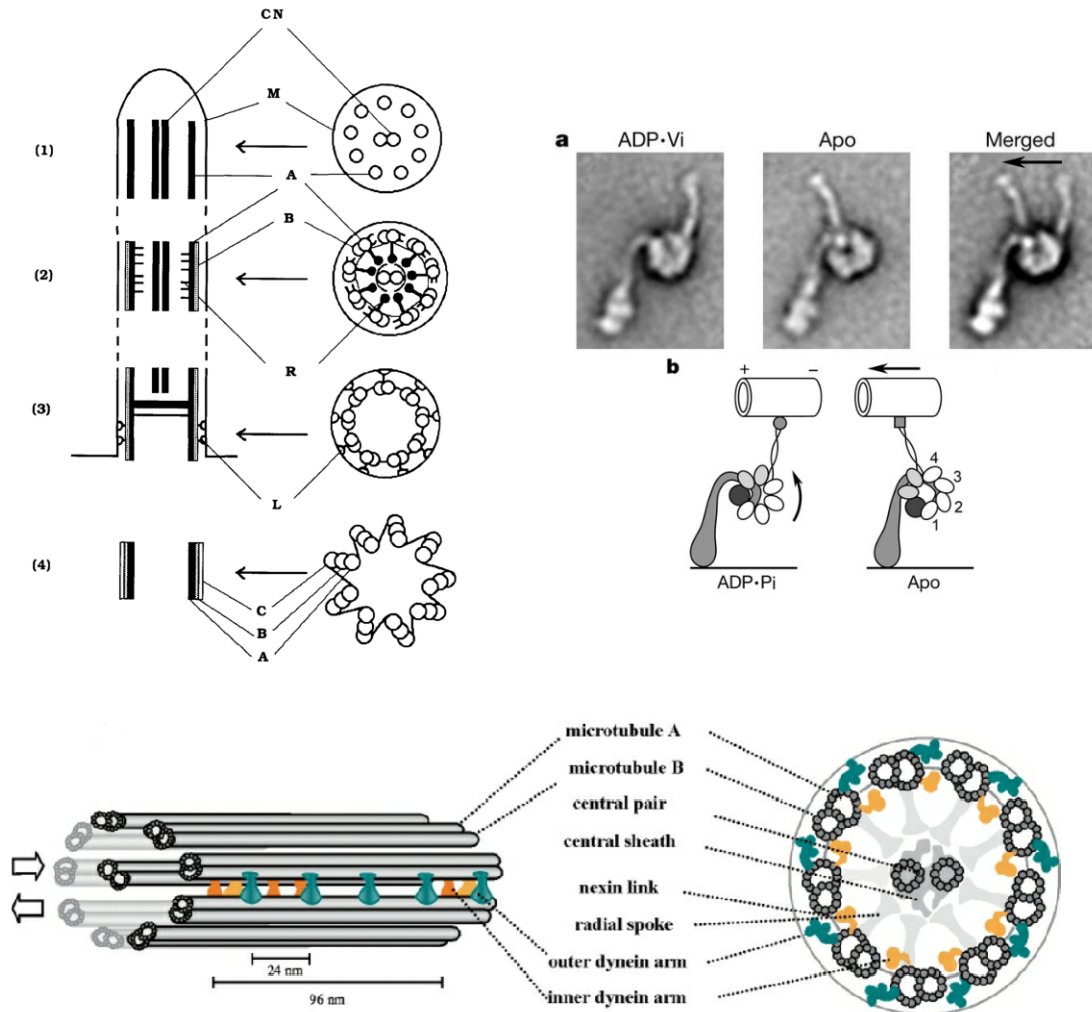


Figure 4.1: **On the top (left)**: Schematic drawing of a median longitudinal section of an axoneme (left), and the cross-section as viewed from base to tip (right) at each level as indicated: A, B and C, are the A-, B- and C-subtubules; CN, the central pair of singlet microtubules; M, the cell membrane; R, radial spokes; L, the cilial neck. (1): At the tip, the B-subtubules disappear, but the A-subtubules remain in the axoneme. (2): The '9 + 2' axonemal structure is retained along most of the length of the flagellum. (3): The transition zone is described as the interval between termination of the central tubules and origin of the C-subtubules. (4): The basal body is composed of nine sets of triplet microtubules, each triplet containing the A-, B- and C-subtubules.

On the top (right): Electron micrographs (a) depicting the structure and speculative power stroke of a single headed dynein molecule, as schematically illustrated in (b). Apo refers to the nucleotide free dynein structure and corresponds to the post-power stroke conformation, whereas ADP·Vi refers to the ADP with vanadate construct that is thought to mimic the pre-power stroke conformation corresponding to the ADP·Pi state. The arrow indicates 15nm.

Below: 3D drawing of the axoneme structure. Modified from [28].

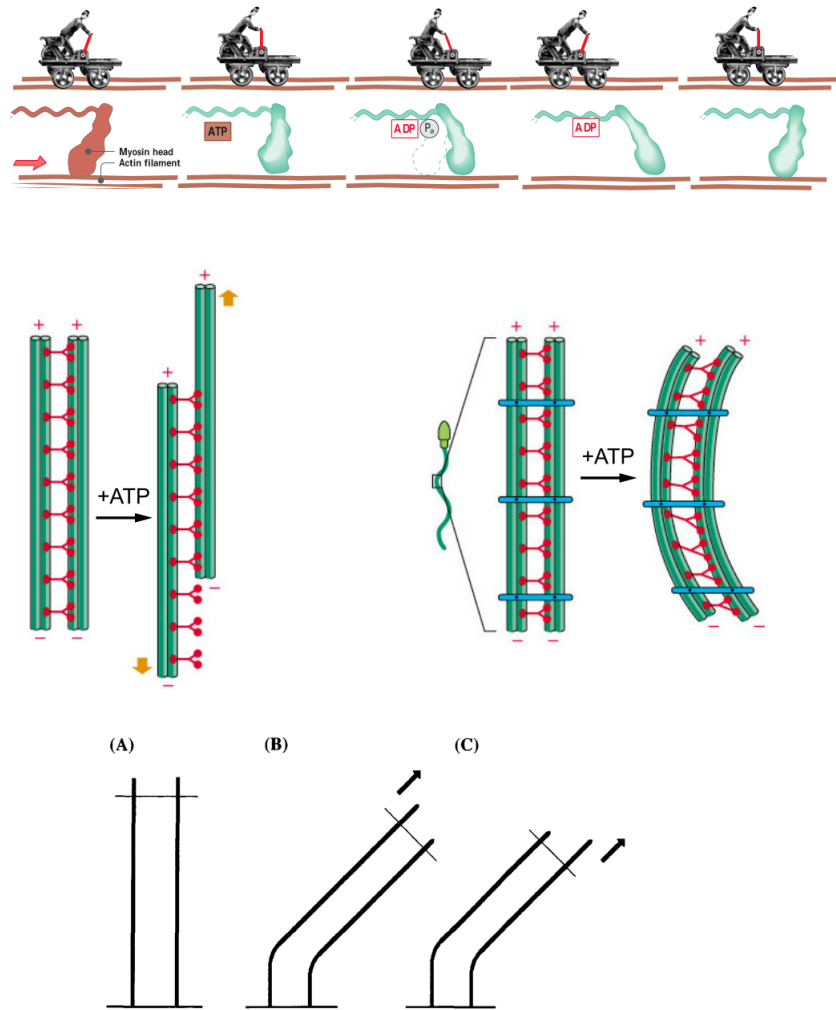


Figure 4.2: **On the top:** Schematic illustration of a processive molecular motor (in this case myosin) moving along a polar filament (in this case actin) as observed experimentally in [29]. Taken from [30, 31].

In the middle: Schematic illustration of dynein induced microtubule sliding with and without geometric constraints. The case of freely sliding microtubules is realised in axonemes whose nexin links are broken, which disintegrate upon activation of dynein [30, 31]. Taken from [28].

Below: Comparison of a typical relationship between microtubule position and bending pattern: (A) straight up; (B) bent by the *contractile microtubule mechanism*; and (C) bent by the 'sliding microtubule mechanism'. The contractile microtubule mechanism suggests that the microtubule on the outer side of a bend will change its position tipward relative to that on the inner side (shown by the arrow). The outer side of the microtubule will stretch and the inner side will relatively contract, to cause a bend. In contrast the sliding microtubule mechanism predicts that the microtubule on the inner side of a bend will slide tipward (shown by the arrow) to form the bend.

of the effective stroke. The resultant beat cycle is either planar or three-dimensional depending on whether the cilium recovers in the same plane as the effective stroke.

Thus, the study of the cilium kinematics is centered on finding which solution of the creeping flow equation with specific boundary conditions, is such that the observed motion is achieved, and which structural and physical characteristics of the cilium influence this solution. Recently, some authors [35] showed how this kinematics could derive entirely by an efficiency reasoning. They determined numerically the kinematics and energetics of the most efficient cilium, by computing the time-periodic deformation of a wall-bound elastic filament leading to transport of a surrounding fluid at minimum energetic cost, where the cost is taken to be the positive work done by all internal molecular motors. The optimal kinematics are found to strongly depend on the cilium bending rigidity through a single dimensionless number, called the Sperm number (which measures the ratio between the cilium length and the elasto-viscous penetration length) and closely resemble the two-stroke ciliary beating pattern observed experimentally.

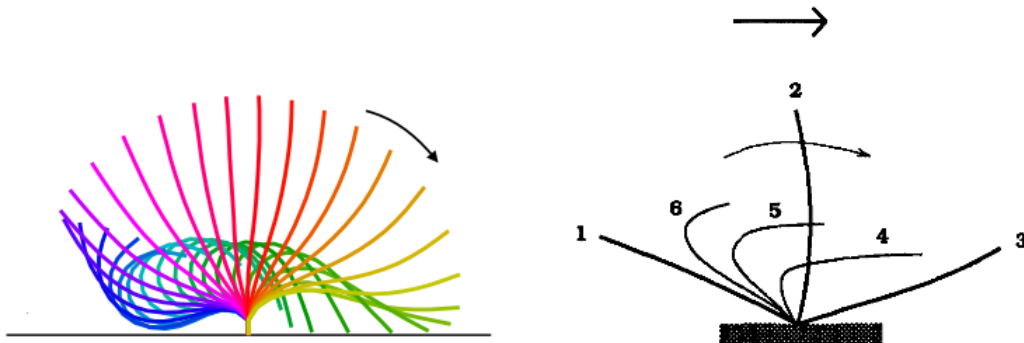


Figure 4.3: The beating cycle of a cilium consists of the effective stroke (1 - 3) in which the extended cilium moves rapidly toward one side by making an 'oar-like' movement, and the recovery stroke (4 - 6) in which the cilium moves more slowly back by propagating a bend from the base to the tip. The effective stroke occurs more or less in one plane. The recovery stroke swings either in the same plane or out of the plane. The arrows indicate the water flow caused by activity of the organelles.

Dinamical Models

The principal question that arises is thus: how can bending waves be generated by the action of molecular motors within the axoneme? The 9+2 axoneme is inherently active. A large number of dynein molecular motors are located in two rows between neighbouring microtubules. In the presence of ATP, which is a chemical fuel, these motors can generate forces and thus induce local displacements between adjacent microtubules. Dyneins induce relative forces between neighbouring microtubules. As a result of these forces, the filaments have the tendency to slide with respect to each other (see Fig. 4.2). If such a sliding is permitted globally, the filaments simply separate but no bending occurs. Bending results if the global sliding is suppressed by

rigidly connecting the filament pair in the region close to one of the two ends. In this situation, sliding is still possible locally, however, but only if the filaments undergo a bending deformation. This coupling of axonemal bending to local microtubules sliding has *been* demonstrated experimentally. In situations where the axoneme is cut at its basal end, filaments slide and in the presence of ATP separate without bending [36]. Small gold-beads specifically attached to microtubules in fully functioning flagella can be used to directly visualize the local relative sliding during beating [37].

The dynamics of axonemal bending and wave patterns have been addressed theoretically by several authors[28]. One can distinguish two principally different mechanisms to generate oscillatory deformation patterns of the axoneme.

- (i) Deterministic forcing: a chemical oscillator could regulate the dynein motors to be activated and deactivated periodically. In this case, the internal active system creates a dynamical force pattern, which drives the system in a deterministic way [39].
- (ii) Self-organized beating: the axoneme oscillates spontaneously as a result of the interplay of force-generating elements and the elastic filaments. Machin [40] and Brokaw [41] suggested the possibility of self-organized beating assuming a force-generating system capable of oscillations.

Patterns of beating have been studied using numerical simulations of a variety of different models [40, 43]. The effect of a coupling of the motor activity to the sliding displacement as well as to curvature were discussed in order to find specific situations where simulated and observed bending waves could be matched qualitatively and quantitatively. Other authors [45], instead of looking for specific models characterized the general properties of the class of systems which can be called *internally driven filaments* and for which the axoneme is an example, focusing on an oscillating instability of the motor–filament system.

In this systems, in general, spontaneous oscillations occur via a so-called Hopf bifurcation [44], where an initially stable quiescent state becomes unstable and starts to oscillate. The parameter governing the instability is the concentration of ATP C_{ATP} : and in the vicinity of the bifurcation, the behaviour of the system is governed by linear terms which are generic and do not depend on the microscopic details, and the general behaviours of the system are characterized from a few assumptions [45].

4.4 Collective cilia dynamics: Metachronal Waves

As we mentioned in the first part of this Chapter, synchronism and metachronism are widely found in populations of cilia. Cilia are generally arranged in rows across and along the cell surface of protozoa and on respiratory-tract epithelia. The movements of adjacent cilia are synchronized to beat in phase along one direction, but out of phase along another direction which is at right angles (often perpendicular) to the lines of synchronism. Waves of ciliary movements, known as metachronal waves, propagate along this out-of-phase direction.

The metachronal waves passing across the ciliated surface would look something like the waves of motion of wheat when the wind blows over a field. The advantages of the metachronal coordination of cilia are to increase the amount of fluid propelled

and to maintain continuity of flow [46]. Individual ciliary movement takes a different form depending on the ciliary system (e.g. planar, helical, oscillatory, or excitable beating). Thus, as shown in Figure 4.4, at least four main patterns of metachronism have been recognized according to the relationship between the direction of the effective stroke of the ciliary beat and the direction of propagation of the metachronal waves [47]

When metachronal waves travel in the same direction as the effective stroke, this is called a *symplectic* metachronism. The coordination is called *antiplectic* when metachronal waves and the effective stroke point in opposite directions. When an observer, looking in the direction of metachronal wave transmission, observes an effective stroke toward the right perpendicular to the wave direction, it is called a *dexioplectic* metachronism. The mirror-image of this configuration is called *laeoplectic*. The latter two types of metachronism are due to the three-dimensional beat cycle of the cilium.

In dexioplectic and laeoplectic metachronism, the ciliary beat cycle consists of a relatively faster effective stroke, in which the cilium is extended and rotates in a vertical plane about its base, and a relatively slower recovery stroke, in which the cilium bends closer to the cell surface and rotates in a horizontal plane, either anti-clockwise or clockwise as viewed from above the plane. This sideways recovery stroke is of great advantage in reducing the resistive forces which may interfere with the continuity of the forward flow generated by the effective strokes.

Figure 4.5 illustrates the fluid volume influenced by the movement of a cilium (termed 'envelope of flow') exhibiting a beat cycle typical of the lateral cilia of *Mytilus* gill and the corresponding laeoplectic metachronal wave. Strong viscous coupling takes place between cilia in the plane of the effective stroke, as the envelope of flow of the effective stroke is more extensive than that of the recovery stroke (producing faster fluid flows during the effective stroke than during the recovery stroke).

Moving cilia in this plane synchronize when the large envelopes of the effective strokes overlap extensively in the plane of beat. Perpendicular to the plane of the effective stroke, relatively weak coupling takes place between adjacent motile cilia because the cilia move to one side in their recovery stroke and the envelope of flow in the recovery stroke will be asymmetrical with respect to the plane of the synchronism.

Through this asymmetrical viscous coupling, the lateral movement of one cilium in its recovery stroke can interact with the lateral movement of the adjacent cilium in the direction of the sideways recovery stroke. Consequently, adjacent cilia will be out of phase with one another, hence the metachronism [46].

Dynamical models

The observation of the metachronal self-organized behaviour of cilia, generates a natural question: why would these appendages phase lock in such a manner?

The internal actuation of each cilium is independent from that of its neighbors, and they do not communicate with each other except through the fluid. However, when they are closely packed on surfaces, cilia arrays display the collective behavior described in the former. Naturally, the physical origin of this kind of coordinated beating is the central question of ciliary dynamics, which a number of theoretical

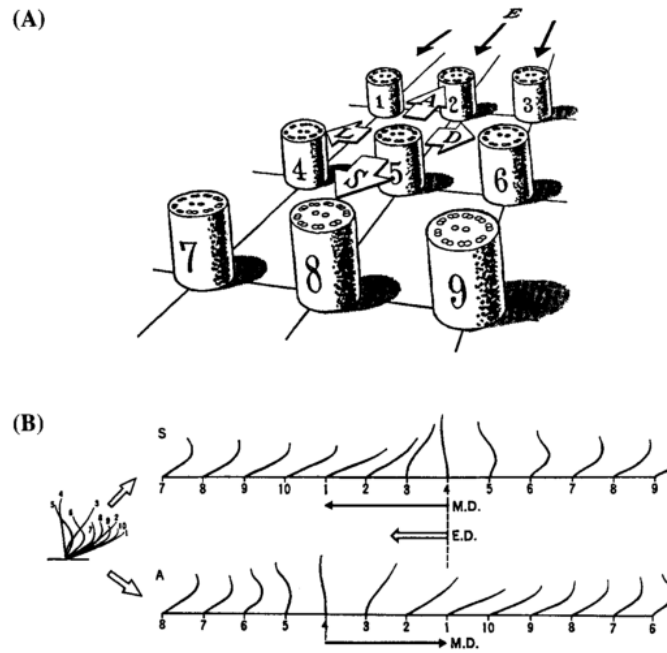


Figure 4.4: Diagram showing metachronal waves. **(A)**: Cilia are arranged in rows across and along the cell surface. The arrow E shows the direction of the effective stroke. The arrows S , A , L and D represent the directions of symplectic, antiplectic, laeoplectic and dexioplectic metachronal waves. In the case of symplectic or antiplectic metachronism, cilia in lines (1,2,3), (4,5,6) and (7,8,9) beat synchronously. In the case of laeoplectic or dexioplectic metachronal waves, cilia in lines (1,4,7), (2,5,8) and (3,6,9) beat synchronously. **(B)**: The full cycle of a typical ciliary beating position at equal intervals in time (left) and the position of an array of cilia at a given time (right). The upper array (denoted by S) and lower array (denoted by A) represent symplectic metachronism and antiplectic metachronism, respectively. $M.D.$ and $E.D.$ represent the direction of metachronal waves and the effective stroke, respectively. Each cilium has the same number assigned to the identical bending position during a cycle. From [48].

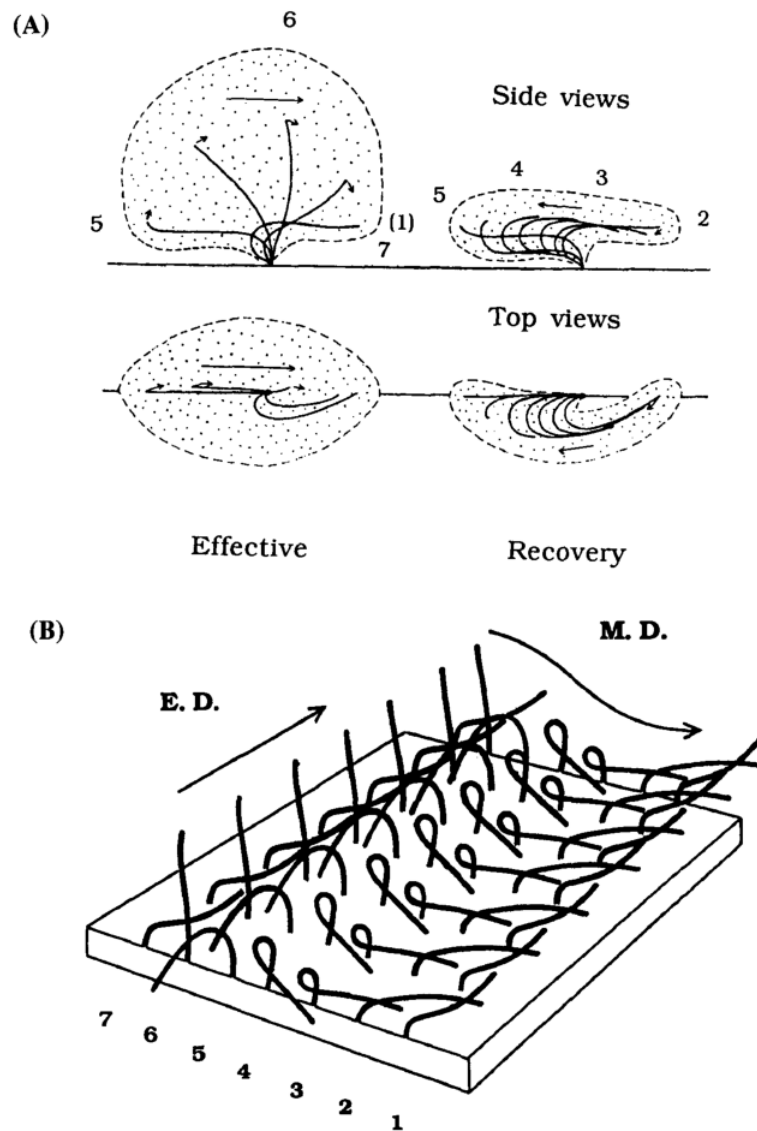


Figure 4.5: (A): The shape and relative size of the 'envelopes of flow' formed by the effective and recovery strokes of a ciliary beat. The dotted area is a rough image of the extent of the envelope. During the recovery stroke the cilium moves back in a clockwise direction (as shown in the view from above), causing asymmetry in the recovery stroke. The resulting asymmetry provides viscous coupling between adjacent motile cilia, perpendicular to the plane of the effective stroke. Every other stage in the beat cycle is numbered. The recovery stroke starts at stage 2 and ends at stage 5, followed by the effective stroke which starts at stage 5 and ends at stage 7 (or 1). From [46].

(B): Laeoplectic metachronal waves. The cilia in row 1 (identical to row 7) are at the end of their effective stroke. The numbers assigned to the various stages of the beat cycle are the same for Fig. 4.26A and B. E.D. and M.D. indicate the direction of the effective stroke and that of the propagation of the metachronal wave, respectively. From [49].

studies have attempted to answer [6, 7, 22, 50]. Two different approaches have been proposed.

In the first one, the mechanics of each cilium is modeled as accurately as possible, and numerical simulations are used to compute the collective beating [6]. The crucial ingredient in that approach is to correctly model the internal load-dependent force generation in the axoneme (without load dependence, or feedback, there is no phase locking as can be expected [22]). With that approach, it is found that two cilia starting randomly end up beating in perfect synchrony within two beating cycles [6]. If instead there are a large number of cilia, waves arise naturally as a result of hydrodynamic interactions. Subsequent work showed that as the waves develop from arbitrary initial conditions the rate of work done by the cilia as they are beating is decreasing [6]. Physically, because of viscous drag, it is energetically advantageous for one cilium to beat in the presence of a neighboring cilium with a similar phase.

The second approach considers simplified models for the dynamics of the cilia, providing analytical insight into the necessary conditions for phase locking [22, 7, 50]. An early study considered a regular lattice of cilia, where the direction of the beating plane is assumed to obey a balance between rotational Brownian motion and rotation induced by the flow created by all other cilia. For small enough temperature, a transition is observed between a state with no average net flow, and a state where all cilia point in the same direction and drive a net flow [50]. Further modeling is provided by considering a simplified load-dependent internal molecular engine. In that case, metachronal waves arise only if a constant phase shift is assumed to exist between each cilium and its neighbor [50].

Motivated by nodal flows in development [51], a second study considered cilia whose tips perform three-dimensional trajectories over a surface. Each cilium is modeled by a sphere subject to an active load-dependent force, and interacting hydrodynamically with a second cilium. Depending on the relative position and orientation of the two cilia models, in-phase ($\phi = 0$) or out-of-phase locking ($\phi = \pi$) arise from random initial conditions [7]. A similar model with two sphere-like cilia rotating due to an applied torque near a wall was recently proposed. In that case, in-phase locking is obtained provided that the circular trajectory of each cilium is allowed to vary in response to hydrodynamic interactions [22].

A recent table-top experiment has been used to examine the physics of hydrodynamic synchronization [52]. In this work, a pair of centimeter-sized rectangular paddles are immersed in silicone oil with a viscosity 10^5 times that of water. The paddles are rotated by motors that deliver constant torque. In accord with the theoretical results of [22], a small compliance was required for phase locking. The time scale for synchronization was long compared with the paddle rotation period, and is governed by the strength of the hydrodynamic interaction between the paddles. To achieve steady phase locking, the driving torques had to be closely matched.

Chapter 5

Optimal cilia kinematics Numerical results

If we knew what it was we were doing,
it would not be called research, would it?

Albert Einstein

In this chapter we build some simple models which allow us to study in more detail the kinematics of arrays of cilia. We focus on the total force exerted by the cilia on the fluid they are immersed in, which because of the property of Low-Reynolds numbers flows, can be calculated simply by the kinematics of the single cilia. Throughout the chapter we ask the fundamental question of which is the best kinematics to exert a maximal net force on the surrounding fluid. In the case of an array of cilia attached to a rigid sphere, this is the same force that the motion of cilia causes on the sphere, allowing for instance the motion of microorganisms like the Paramecium.

In the first section, we discuss the approximation made to model the complex geometry of the single cilium and to simplify the problem of the hydrodynamical interactions between cilia. In the second section we show the numerical methods and the results obtained with the first simplest problem of the interaction of two ideal cilia near a rigid plane wall. Then, we generalize the results to the case of N -cilia arrays. The third section is devoted to the more complex problem of the motion near a rigid sphere. At last, in Section 5.5 we analyze the case of an infinite array near a plane wall.

5.1 Ideal cilia: approximations and kinematics

We start considering a cilium to be an appendage of length L , bounded to a solid generic surface, that could be plane, spherical or of any shape. The system is immersed in a fluid of viscosity μ , density ρ , and the motion will be supposed to be always with $Re/S \ll 1$, where in this case $S = U/L\omega$ and ω is the typical frequency of stroke of a cilium.

In order to simplify the geometry of the problem, we want to model the force exerted by the moving cilium on the fluid with that exerted by a more handable

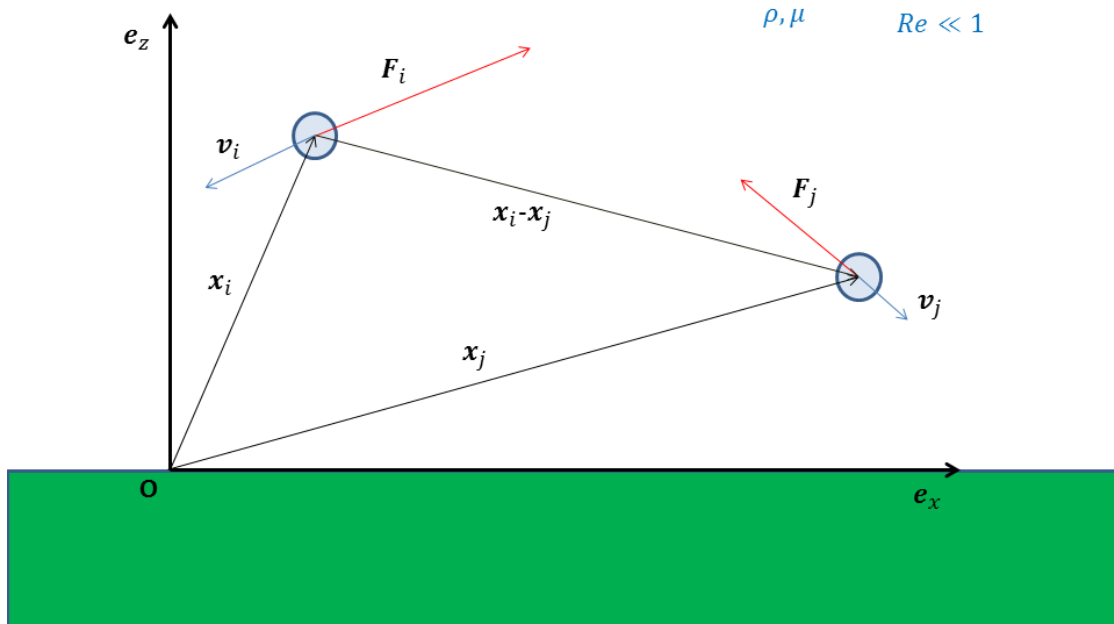


Figure 5.1:

rigid particle. Obviously, the simplest shape we can consider, for both symmetry and analytical reasons, is the spherical one. Therefore, we will approximate the effect of each cilium's motion on the fluid with that of a sphere of radius $a \lesssim L$, centered at the mass center (or an effective point of application) of the cilium, distant d from the wall. The sphere will exert a force \mathbf{F} on the fluid during the motion, and will experience viscous drag friction.

Now we have to model the effect of the motion of a generic other cilium (particle) on our ideal spherical one (particle 1). Due to the motion of a particle, the velocity field of the fluid will change in a complex fashion. As we saw in the previous chapters, the simplest way to model the effect of an obstacle's motion on a fluid, is to consider the action of a point force centered on the mass center (or an effective point of application) of the cilium structure. This minimal approximation represents the first order disturbance in the multipole expansion 2.32, and is largely used in literature for objects even more complex than cilia, and in this specific case has allowed to show, in the interaction dynamics of 1D and 2D array of cilia, the arising of metachronal waves [22].

We restrict ourselves to the case of a far-field interaction, justified by opportune geometric condition guaranteeing the distance between the particles to be such that $|\mathbf{x}_2 - \mathbf{x}_1| \gg a$. In this approximation, we can consider the effects of each particle as a point-force acting on the fluid instantaneously with velocity \mathbf{v}_1 and \mathbf{v}_2 , respectively. Therefore, we shall consider the one-to-one interaction between two cilia and the wall as an interaction between a Stokeslet with strenght equal to the drag force \mathbf{F}_1 , centered at the center of mass the particle 1, and a sphere centered in the center of mass of the second one. (see Fig. 5.1)

Clearly, to know the force on the particle 1 due to the motion of the particle 2, the force on particle 2 due to the motion of the particle 1 has to be taken into

account. Thus we will use the so-called *reflection method* analysed in Section 3.1, which consists in considering the influence of one particle as it was moving alone in the fluid, on the other. Then, reflecting the found field for the second particle to calculate the correction to the motion of the one supposed isolated. Indicating with r_{ij} the distance between the particles, the field calculated taking into account the n -th reflection gives:

$$\mathbf{F}^{[n]} = \sum_{i=0}^n \mathbf{F}^{(i)} \quad , \quad \mathbf{F}_{j \rightarrow i}^{[n]} = -a \underline{\mathbf{G}}_j \cdot [6\pi\mu a \mathbf{v}_j - a \underline{\mathbf{G}}_i \mathbf{F}_{i \rightarrow j}^{[n-1]}] \quad \Rightarrow \quad |\mathbf{F}_{j \rightarrow i}^{(n)}| \sim \left(\frac{a}{r_{ij}} \right)^n$$

$$\mathbf{F}_i^{(0)} = 6\pi\mu a \mathbf{v}_i \quad , \quad \mathbf{F}_i^{(n)} = 6\pi\mu a \mathbf{v}_i + \mathbf{F}_{j \rightarrow i}^{(n)} \quad , \quad i, j = 1, 2; \quad i \neq j$$

where $\underline{\mathbf{G}}_j = \underline{\mathbf{G}}(\mathbf{x}_i, \mathbf{x}_j)$ is the Green function corresponding to a Stokeslet with the particular boundary conditions considered. At the first order, we shall write, instantaneously:

$$\begin{cases} \mathbf{F}_1 \simeq \mathbf{F}_1^{[1]} = 6\pi\mu a [\mathbf{v}_1 - a \underline{\mathbf{G}}(\mathbf{x}_1, \mathbf{x}_2) \cdot \mathbf{v}_2] \\ \mathbf{F}_2 \simeq \mathbf{F}_2^{[1]} = 6\pi\mu a [\mathbf{v}_2 - a \underline{\mathbf{G}}(\mathbf{x}_2, \mathbf{x}_1) \cdot \mathbf{v}_1] \end{cases} \quad (5.1)$$

where should be evident that the first term is of order a/r_{ij} and the second of order $(a/r_{ij})^2$. We underline that (5.1) does not give exactly the first order reflection in the meaning of equation (3.1), because we are neglecting the second term in the Faxén expansion (2.40), considering that the particle i only sees a point force flow coming from particle j . Clearly, the term $\nabla^2 \underline{\mathbf{G}}_j$ would be small near particle i , and our approximation is meaningful, but does not give a zero-velocity field at the first order in a/r_{ij} on the surface of particle j , where the laplacian term becomes important. Therefore, for our purpose we shall consider the force to be:

$$\mathbf{F}_{1,2} = 6\pi\mu a \left(\mathbf{v}_{1,2} - \frac{\underline{\mathbf{G}}(\mathbf{x}_1, \mathbf{x}_2) \cdot \mathbf{F}_{2 \rightarrow 1}}{6\pi\mu} \right)$$

This reasoning can directly generalized for the case of the interaction among N particle. Indeed, thanks to the linearity of the Stokes flow, we can decompose the fluid disturbed field acting on the i -th particle as the sum of the $N - 1$ disturbance field induced by the other particles motion.

$$\begin{cases} \mathbf{F}_1(t) = 6\pi\mu a \left[\mathbf{v}_1(t) - a \sum_{i=2}^N \underline{\mathbf{G}}(\mathbf{x}_1(t), \mathbf{x}_i(t)) \cdot \mathbf{v}_i(t) \right] \\ \vdots \\ \mathbf{F}_j(t) = 6\pi\mu a \left[\mathbf{v}_j(t) - a \sum_{i \neq j}^N \underline{\mathbf{G}}(\mathbf{x}_j(t), \mathbf{x}_i(t)) \cdot \mathbf{v}_i(t) \right] \\ \vdots \\ \mathbf{F}_N(t) = 6\pi\mu a \left[\mathbf{v}_N(t) - a \sum_{i \neq N}^N \underline{\mathbf{G}}(\mathbf{x}_N(t), \mathbf{x}_i(t)) \cdot \mathbf{v}_i(t) \right] \end{cases} \quad (5.2)$$

$$\mathbf{F}(t) = - \sum_{i=1}^N \mathbf{F}_i(t)$$

5.2 Numerical approach

In all the cases we will consider, the Green function $\underline{\mathbf{G}}(\mathbf{x}_i, \mathbf{x}_j)$ is a nonlinear function, and it's quite prohibitive to find an analytic solution to the systems (5.1) or (5.2). Therefore, we shall proceed numerically, and this is the approach we will follow:

- We first fix the motion of the cilia that are in the system under attention, trying to catch the most simple and important physical features of their strokes. We impose the position $\mathbf{x}_i(t)$ and the velocity $\mathbf{v}_i(t)$ for every cilium and for every time t . Clearly, for the reason we explained in the previous chapters (section (2.2.7)) the motion has to be periodic and not reciprocal, to be efficient at low Reynolds numbers. Therefore we impose a typical constant frequency ω for the motion of the sphere, and the initial conditions $\mathbf{x}_i(0)$, $\mathbf{v}_i(0)$ can be more suitably considered in terms of the phase differences ϕ_i respect to a reference cilium with $i = 1$, the frequency ω , the separation between two cilia δ , the amplitude A and the distance from the wall d ;
- We use the physical and geometrical parameters of the problem to write a dimensionless version of (5.2) and (5.1);
- For every time t we calculate the total force $\mathbf{F}(t)$ on the system, summing the different contributes in the interactions;
- We take the average on one period of \mathbf{F} . We call this net average force

$$\bar{\mathbf{F}}(\{x_i(0), v_i(0)\}_{i=1}^N, \omega, A) \equiv \bar{\mathbf{F}}(\omega, \{\phi_i\}_{i=2}^N, \delta, d, A) = \frac{\omega}{2\pi} \int_0^{2\pi/\omega} \mathbf{F}(t) dt$$

- We optimize on all the possible values of the phase differences $\{\phi_i(0)\}_{i=2}^N$ for a fixed ω , looking on the discrete distribution which maximizes the value of $\bar{\mathbf{F}}$, for different configurations of the parameter δ and A .

5.3 Interaction among cilia near a rigid plane

We start considering the simple geometry of spheres moving near a rigid plane wall. In this case, the Green Function is the (3.2),

We rewrite $\underline{\mathbf{G}}^W$ as:

$$\begin{aligned} \underline{\mathbf{G}}^W(\mathbf{x}, \mathbf{x}_0) &= \underline{\mathbf{G}}^W(\hat{\mathbf{x}}, \hat{\mathbf{X}}) = \frac{1}{|\hat{\mathbf{x}}|} + \frac{\hat{x}_i \hat{x}_j}{|\hat{\mathbf{x}}|^3} - \frac{1}{|\hat{\mathbf{X}}|} - \frac{\hat{x}_i \hat{x}_j}{|\hat{\mathbf{X}}|^3} + \\ &\quad - 2d(1 \mp d) \left(\frac{\delta_{ij}}{|\hat{\mathbf{X}}|^3} - 3 \frac{\hat{X}_i \hat{X}_j}{|\hat{\mathbf{X}}|^5} \right) \mp 2d \frac{\delta_{j1} \hat{X}_i - \delta_{i1} \hat{X}_j}{|\hat{\mathbf{X}}|^3} \end{aligned}$$

where $\hat{\mathbf{x}} = \mathbf{x} - \mathbf{x}_0$, $\hat{\mathbf{X}} = \mathbf{x} - \mathbf{x}_0^{(im)}$, and $\mathbf{x}_0^{(im)} = (x_0, y_0, -z_0)$. The function $\underline{\mathbf{G}}^W(\mathbf{x}, \mathbf{x}_0)$ is, as anticipated, highly non linear.

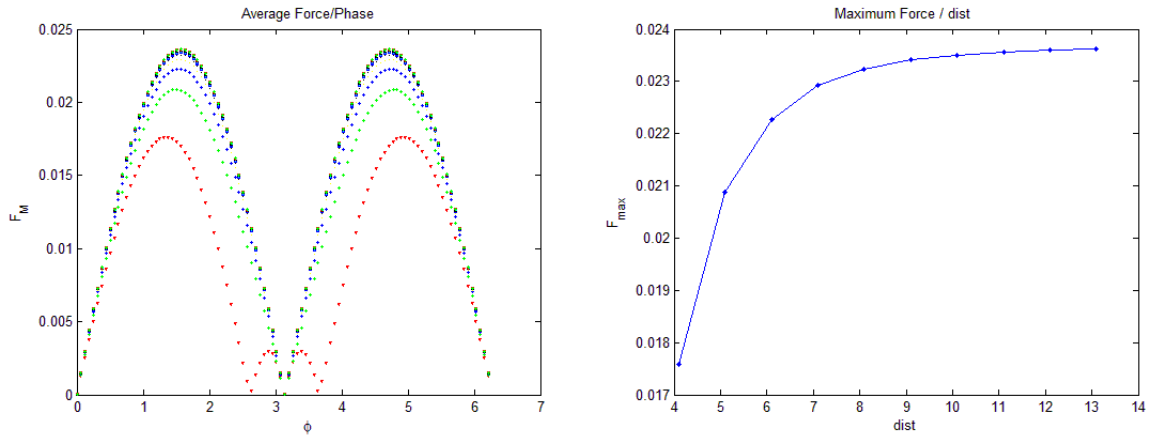


Figure 5.3: Maximum average force in function of the phase difference (on the left), and the reciprocal distance (on the right), for two cilia moving on a segment near a wall. $\phi_{eff} = \pi/2$, $d = 1$

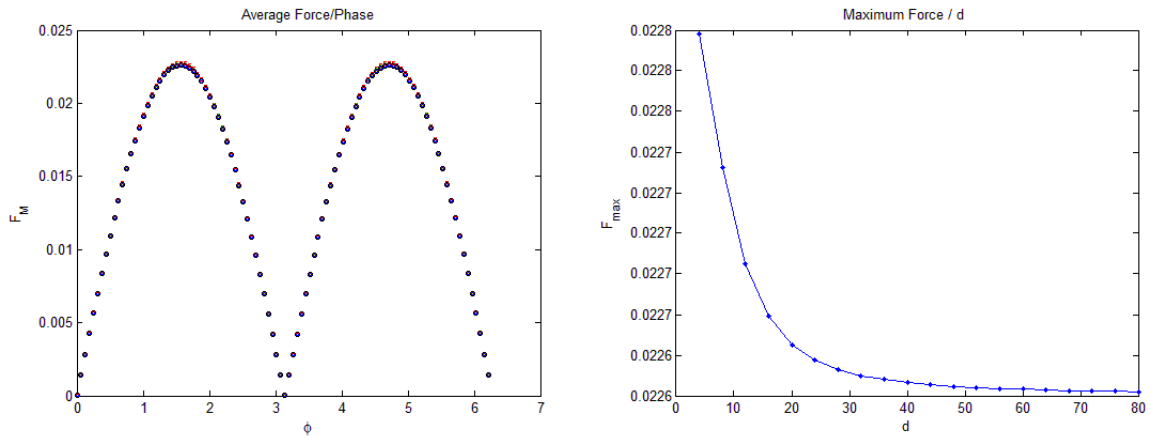


Figure 5.4: Maximum average force in function of the phase difference (on the left), and the distance from the wall (on the right), for two cilia moving on a segment near a plane wall. $\phi_{eff} = \pi/2$, $d = 1$

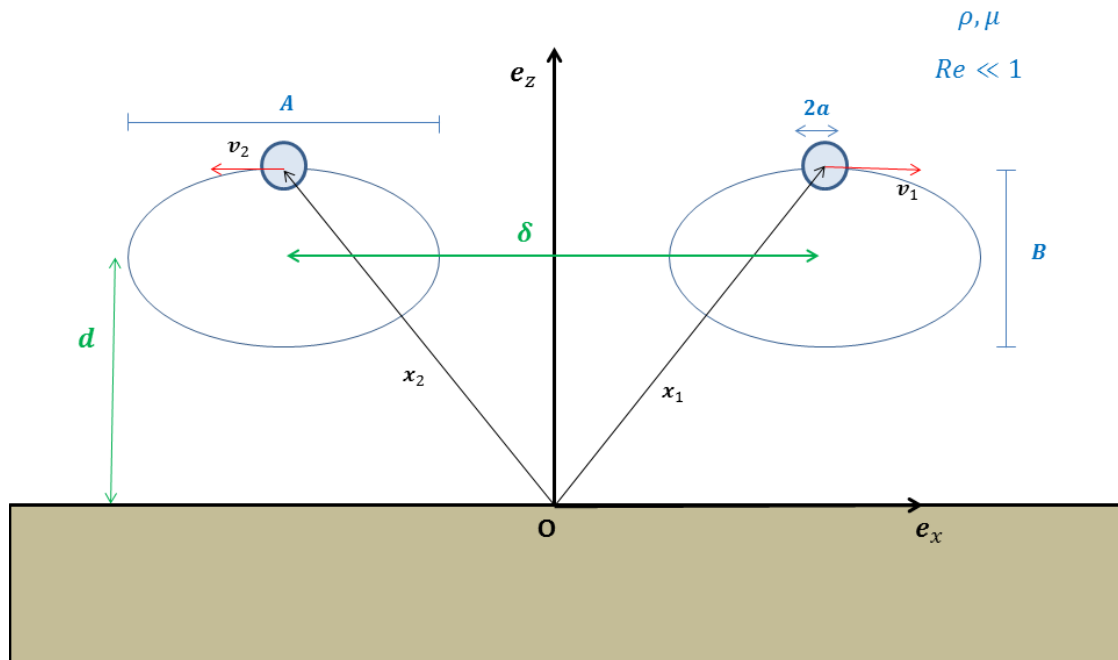


Figure 5.5: 2 cilia elliptical motion near a plane wall.

5.3.2 2 cilia: Elliptical motion

The first complication we can add to the problem, is to consider an elliptical motion of the spheres. This configuration is closer to the effective physics of the cilia's strokes, indeed, when one sphere moves on the upper half of the ellipse its force transfers to the fluid models the effective stroke of the cilium, on the other hand, when the sphere runs over the half of the ellipse closer to the wall it models the recovery stroke. The kinematics is given by:

$$\begin{aligned}\mathbf{x}_1(t) &= (-\delta/2 + A \cos(2\pi t), 0, d + B \sin(2\pi t)) \\ \mathbf{x}_2(t) &= (\delta/2 + A \cos(2\pi t + \phi), 0, d + B \sin(2\pi t + \phi))\end{aligned}$$

In this geometry (sketched in Fig. 5.5), we observe at first a remarkable difference with the previous one: the average force for a zero phase difference does not vanish. Then, we plotted the usual graph showing the average force as function of ϕ , for different values of the geometrical parameters of the problem.

Varying distance from the wall

The first behaviour we can check is a decreasing maximal force with an increasing distance from the wall, where the two Stokeslets become more isolated and the interaction with the wall becomes weaker. This is shown in Fig. 5.6 for a circular trajectory with distant cilia, but works equally in all the possible configurations.

Varying axis ratio

Putting $d = 1$, we can now explore the changing of the phase and the maximal force behaviour in function of the geometry of the ellipse, i.e. the ratio between the length

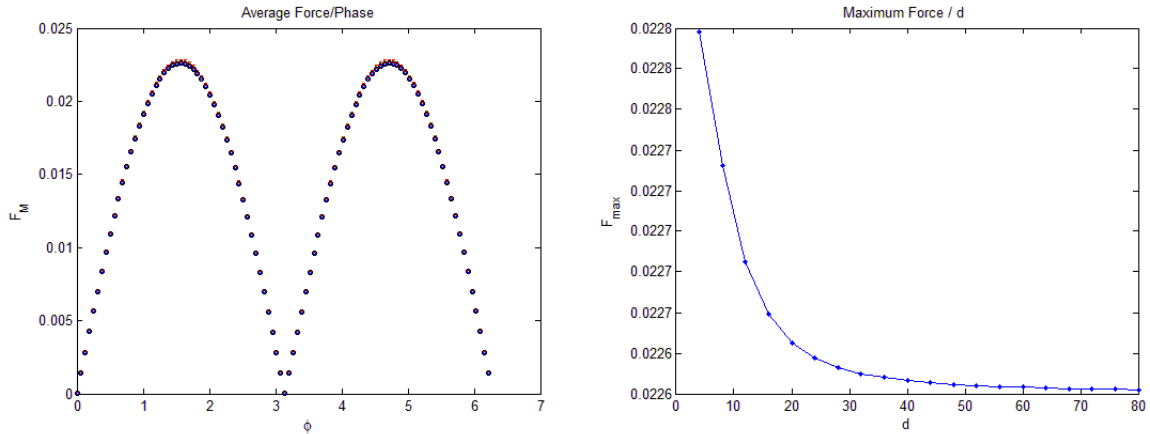


Figure 5.6:

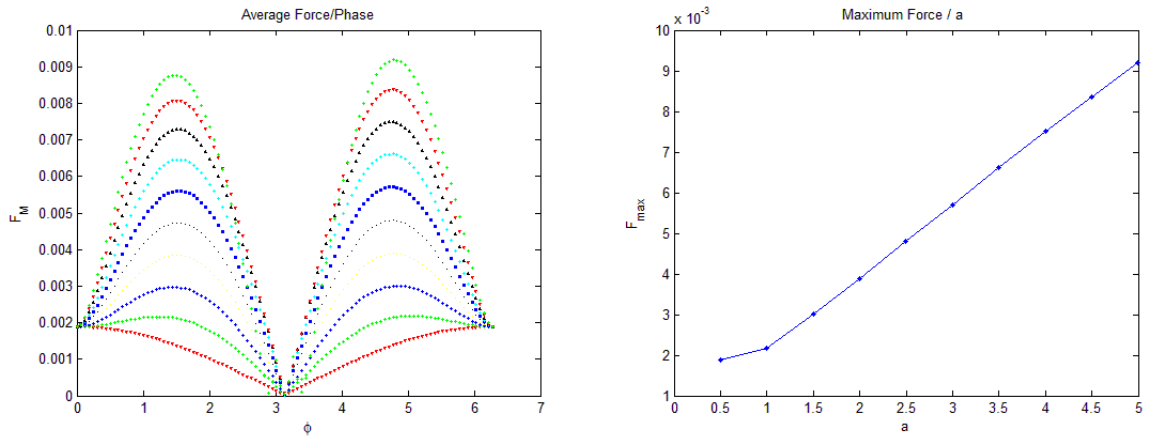


Figure 5.7: \bar{F} in function of ϕ with $d = b = 1$, varying A in the range 0.5 to 5. On the right: \bar{F}_M in function of A .

of its axes. In Figg. 5.7, 5.8 we see how the different values of the force depends on the phase for different ratio between the axes.

We see that in the circular case, the best phase difference is 0 or 2π , such that the cilia prefer to be in perfect synchronization, and increasing both the transverse and the parallel axis' length, the force increases because of the more intense interaction with the wall in the first case, and between the cilia in the second case. The phases become quickly close to the value $\pi/2$, as soon as we turn from the circular trajectory towards a less interactive configuration. At last, it shifts back slowly towards the synchronized configuration, as we increase again the interaction.

Varying reciprocal distance - circular trajectory

The most interesting result arises from the analysis of the behaviour of the maximal force for different reciprocal distances between the two cilia. In Figg. 5.10, 5.11, 5.12 we show, as in the former, the variation of the force in function of the phase, and the maximal value for different distance, in three different circular configurations, with increasing radius.

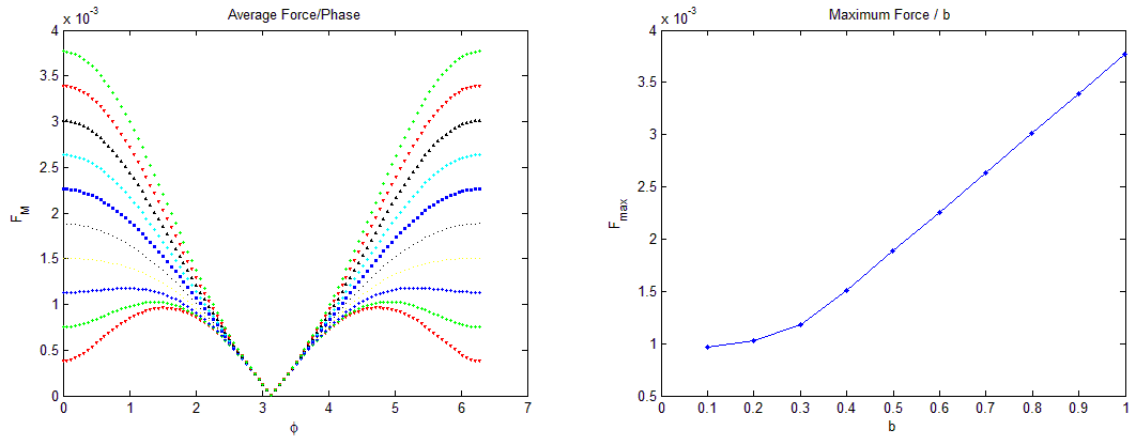


Figure 5.8: \bar{F} in function of ϕ with $d = b = 1$, varying B in the range 0.1 to 1. On the right: \bar{F}_M in function of B .

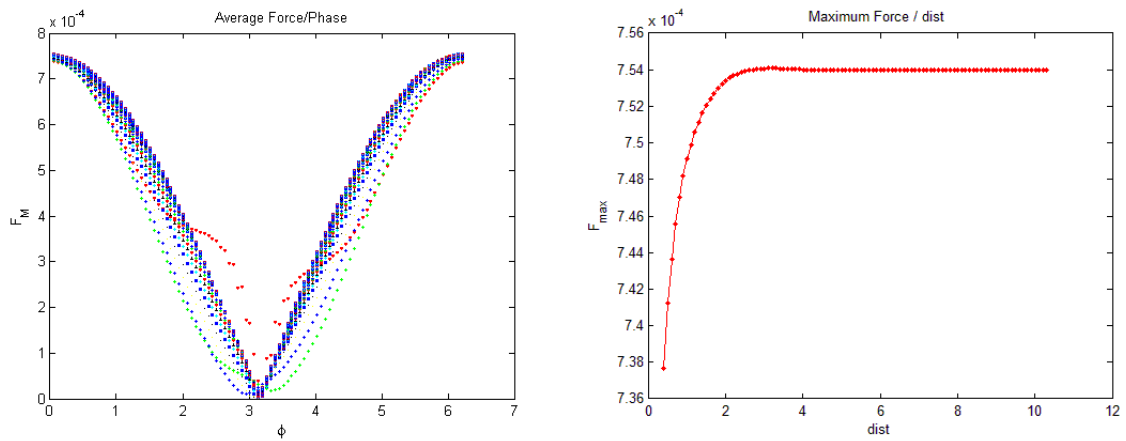


Figure 5.10: $a = b = 0.2$

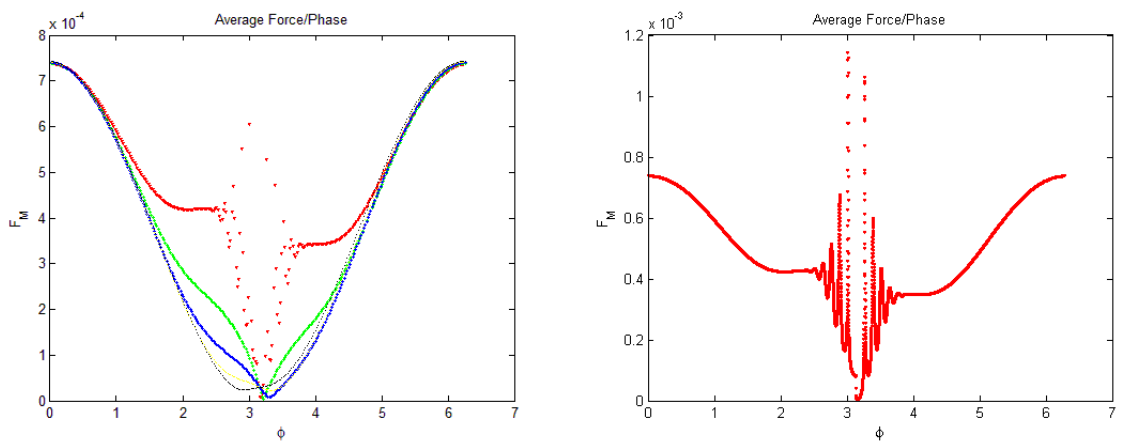


Figure 5.9: Highly irregular behaviour of the force in function of the phase difference, for $a = b = 0.2$, $d = 1$, $\delta = 0.40 \rightarrow 0.42$. On the right an enlargement of the red curve.

When the distance between the cilia is small and the radius is big, i.e. when they

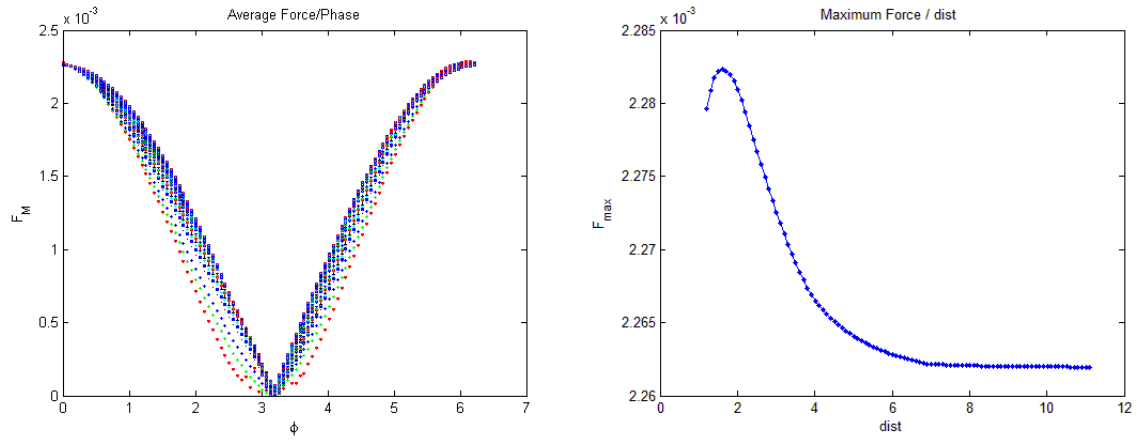


Figure 5.11: $a = b = 0.6$

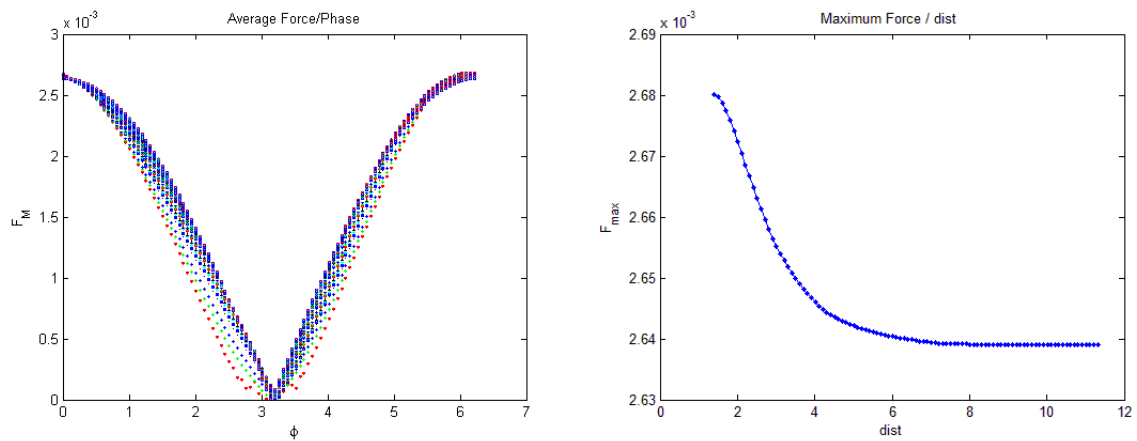


Figure 5.12: $a = b = 0.8$

get really close during the motion, the non linearity of the system and gives a highly irregular behaviour (shown in Fig. 5.9), and since the far-field approximation is not valid for this small distances, we can't extract any physical information from this. We thus performed the analysis for distance big enough to stay away from this highly non linear regime.

We see that for small values of the radius, thus when we have a weaker interaction, the system tends to reach a minimum value very quickly. For intermediate radius, it shows an efficient distance for which the force is maximal. Increasing the radius, and thus the interaction, the force decreases continuously, approaching to its minimum value without a maximum.

5.3.3 4 cilia: Linear and elliptical motion

The more interesting problem of the interaction among 4 cilia, can be easily implemented in terms of numerical "economy", and is a better candidate to see a linear organisation of the best phase difference distribution. Nevertheless, despite our expectations, the best phase distribution in the case of linear and elliptical motions are:

$\#_d$	A	δ	$\phi_{eff}^{(4,lin)}$
20	1	2.1	(0 2.9845 1.5708 1.0996)
20	1	2.3	(0 1.7279 1.5708 1.2566)
20	1	2.5	(0 1.7279 1.5708 1.2566)
20	1	3	(0 1.7279 1.5708 1.4137)
20	1	3.5	(0 1.7279 1.5708 1.4137)
20	1	4	(0 1.5708 1.5708 1.4137)
20	1	5	(0 1.5708 1.5708 1.5708)
20	1	10	(0 1.5708 1.5708 1.5708)
20	1	10^2	(0 1.5708 1.5708 1.5708)
20	1	10^3	(0 1.5708 1.5708 1.5708)

Table 5.1: Best phase distribution of 4 spheres in rectilinear motion, for different values of the distance between them. $\#_d$ is the number of ϕ scanned within $[0, 2\pi]$, everywhere the distance from the wall is $d = 1$.

$\#_d$	$a = b$	δ	$\phi_{eff}^{(4,ell)}$
20	0.5	1.1	(0 , 5.655 , 5.655 , 5.969)
20	0.5	1.3	(0 , 5.655 , 5.655 , 5.969)
20	0.5	2	(0 , 5.655 , 5.655 , 5.655)
20	0.5	5	(0 , 5.969 , 5.969 , 5.969)
20	0.5	6	(0, 0, 0, 0)
20	0.5	10	(0, 0, 0, 0)
20	0.5	10^2	(0, 0, 0, 0)

Table 5.2: Best phase distribution of 4 spheres in elliptical motion, for different distances between them.

Thus, no metachronal behaviour is observed. We can argue that the border effects, due to the low number of cilia, are important in such a geometrical configuration, clearly different from an infinite array of cilia.

Unfortunately, the algorithm for a simulation with more than 8 cilia is hugely expensive in computational terms, and our study can be just, at a present stage, lead up to this relatively small N . Therefore, we report the distribution for 6 and 8 cilia only after an improvement of the numerical approach, in order to reduce the border effects, explained in the next subsection.

5.3.4 Periodic boundary conditions

A simple extension of our model, which allows us to cancel the border effects due to the finite number of cilia, can be made imposing the interaction among the cilia to be a “first neighbors” interaction with periodic boundary conditions. Each cilium interacts only with his first neighbors on the right and on the left, the N -th one interact with the first, and the *vice versa*. This generalization has both advantages and disadvantages. Indeed, even if extended for the external cilia, the interaction is strongly limited for the internal ones.

We performed the calculation for 4, 6 and 8 spheres moving on a segment and on an ellipse, obtaining:

$\#_d$	A	δ	$\phi_{eff}^{(4,lin)}$
20	1	2.1	(0, 3.7699, 1.5708, 5.6549)
20	1	10	(0, 1.5708, 1.5708, 0)
20	1	50	(0, 1.5708, 1.5708, 5.9690)
20	1	100	(0, 1.5708, 1.5708, 5.6549)
20	1	200	(0, 1.5708, 1.5708, 5.3407)
20	1	10^3	(0, 1.5708, 1.5708, 4.7124)
20	1	$2 \cdot 10^3$	(0, 4.7124, 4.7124, 1.5708)
20	1	10^4	(0, 4.7124, 4.7124, 1.5708)
20	1	$2 \cdot 10^4$	(0, 4.7124, 4.7124, 1.8850)
20	1	10^5	(0, 4.7124, 4.7124, 5.3407)

Table 5.3: $\#_d$ is the number of ϕ scanned within $[0, 2\pi]$, everywhere the distance is $d = 1$

$\#_d$	$a = b$	δ	$\phi_{eff}^{(4,ell)}$
20	0.5	1.1	(0, 3.142, 3.456, 3.456)
20	0.5	1.5	(0 3.1416 3.4558 3.4558)
20	0.5	1.8	(0 3.1416 3.1416 3.1416)
20	0.5	2	(0, 3.142, 3.142, 2.827)
20	0.5	2.5	(0 3.4558 3.4558 3.4558)
20	0.5	3	(0, 5.341, 5.341, 0)
20	0.5	5	(0, 5.027, 5.027, 5.341)
20	0.5	10	(0, 5.027, 5.027, 5.027)
20	0.5	10^2	(0, 5.027, 5.027, 5.027)
20	0.5	10^3	(0, 5.027, 5.027, 5.027)

Table 5.4: $\#_d$ is the number of ϕ scanned within $[0, 2\pi]$, everywhere the distance is $d = 1$

$$\phi_{eff}^{(4,lin)} \simeq (0, 4.71, 4.71, 1.57) \sim (0, 3\pi/2, 3\pi/2, \pi/2) \quad , \quad \phi_{eff}^{(4,ell)} \simeq (0, 0, 0, 2.36)$$

$$\phi_{eff}^{(8,lin)} \simeq (0, 1.05, 1.05, 1.05, 1.05, 5.24)$$

Therefore, also in this better approximation, no particular patterns are observed. Although for the solution with the bigger N , a slight tendency to the monotony seems to appear. Anyway, this results doesn't confirm the hypothesis of metachronal effective motion.

5.4 Interaction among cilia near a rigid sphere

Another interesting situation, in which cilia interaction has a propelling function, is the case of a spheric object moving with the help of attached cilia on its surface. We start modeling this system as previously done, considering a sphere of radius R with other smaller spheres moving near its surface.

We start again with the 2-cilia configuration, whose effect on the fluid is represented here by the motion of two spherical particles of radius $a \ll R$, placed at an effective distance d from the surface of the microorganism (see Fig. (5.13)). Let us call \mathbf{x}_1 and \mathbf{x}_2 the position vectors of the two particles in a cartesian reference frame, with the origin placed in the center of the big sphere.

We restrict ourselves to the case of a far-field interaction, justified by the condition $a \ll d \ll R$. In this approximation, we can consider the effects of each particle as a point-force acting on the fluid instantaneously with velocity \mathbf{v}_1 and \mathbf{v}_2 , respectively. In this case the force between the sphere is

$$\mathbf{F}_{1,2} = 6\pi\mu a \left(\mathbf{v}_{1,2} - \frac{\mathbf{G}^{RS}(\mathbf{x}_1, \mathbf{x}_2) \cdot \mathbf{F}_{2 \rightarrow 1}}{6\pi\mu} \right)$$

where $\mathbf{G}^{RS}(\mathbf{x}, \mathbf{X})$ is a two-order tensor, representing the Green's function (3.3) for an infinite flow that is bounded internally by a solid sphere at rest in the origin with a stokeslet in \mathbf{X} , and is, as known, of the order $\sim 1/R$.

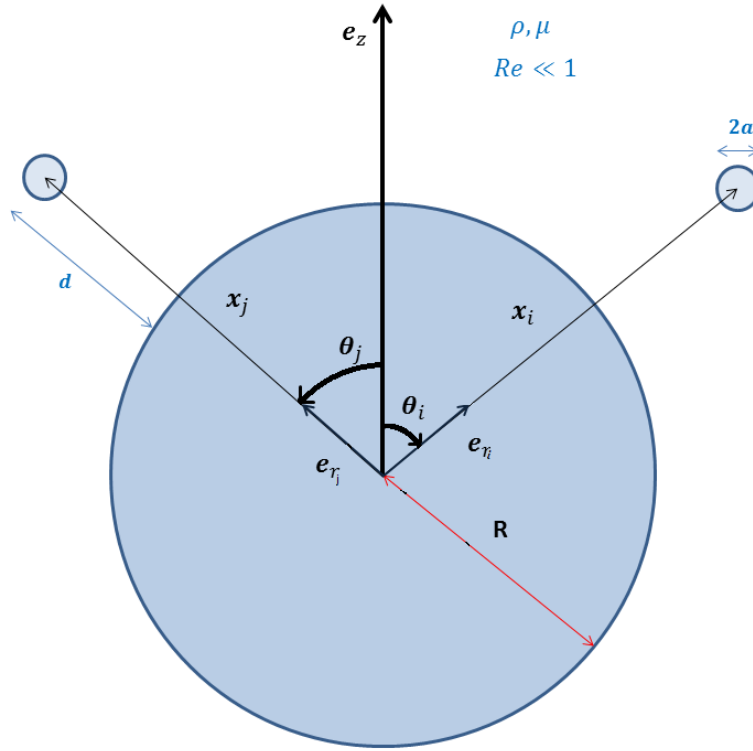


Figure 5.13: 2 cilia elliptical motion near a big rigid sphere.

As before, we want to calculate the force acting on the sphere when the motion of the two particles is fixed, e.g. we will consider $\mathbf{F}_{1,2}(\mathbf{x}_1(t), \mathbf{x}_2(t))$ as unknowns and $\mathbf{v}_{1,2}(t)$ as given data of our problem. More specifically, let us restrict to the case axisymmetric. In spherical coordinates:

$$\mathbf{x} \longrightarrow (r, \theta, \phi) \quad , \quad \mathbf{x} = (r \cos \varphi \sin \theta, r \sin \varphi \sin \theta, r \cos \theta) \quad , \quad \mathbf{v} = \dot{r} \mathbf{e}_r + r \dot{\theta} \mathbf{e}_\theta + r \dot{\varphi} \mathbf{e}_\varphi$$

$$\mathbf{e}_r = (\cos \varphi \sin \theta, \sin \varphi \sin \theta, \cos \theta), \quad \mathbf{e}_\varphi = (-\sin \varphi, \cos \varphi, 0)$$

$$\mathbf{e}_\theta = (\cos \varphi \cos \theta, \sin \varphi \cos \theta, -\sin \theta)$$

We impose the position and the velocity to be of the form:

$$\mathbf{x}_{1,2}(t) = (R + d) \mathbf{e}_{r_{1,2}} + \theta_{1,2}(t) \mathbf{e}_{\theta_{1,2}} + \varphi_{1,2} \mathbf{e}_{\varphi_{1,2}} \quad , \quad \mathbf{v}_{1,2} = (R + d) \dot{\theta}_{1,2} \mathbf{e}_{\theta_{1,2}}$$

and adimensionalizing using the physical parameters we have:

$$t' = \omega t \quad , \quad F' = F / \mu a^2 \omega \quad , \quad v' = v / a \omega \quad , \quad G' = a G \quad , \quad d / R = \text{const}$$

where ω is the typical frequency of the cilium's stroke. So, renaming all the variables $x' \rightarrow x$, the equations become:

$$\mathbf{F}_1(t) = 6\pi[\mathbf{v}_1(t) - \mathbf{G}^S(\theta_1(t), \theta_2(t), \varphi_1, \varphi_2) \cdot \mathbf{v}_2(t)]$$

$$\mathbf{F}_2(t) = 6\pi[\mathbf{v}_2(t) - \mathbf{G}^S(\theta_2(t), \theta_1(t), \varphi_2, \varphi_1) \cdot \mathbf{v}_1(t)]$$

and, from 2.8, the total force acting on the big sphere at the time t is equal to

$$\mathbf{F}^S(t) = -\mathbf{F}_1(t) - \mathbf{F}_2(t)$$

5.4.1 2 cilia: angular motion

We thus consider a modelisation of the cilium's stroke as generalisation of the linear one near a rigid plane, taking an angular trajectory along \mathbf{e}_θ , and a periodic motion with the same frequency and a phase difference ϕ :

$$\theta_1(t) = \theta_1(0) + \delta\theta_1 \sin(2\pi t) \quad , \quad \theta_2(t) = \theta_2(0) + \delta\theta_2 \sin(2\pi t + \phi) \quad (5.3)$$

Our first goal is to find the effective phase that maximize the average total force over a period. To prevent superpositions and to preserve the symmetry, we choose initial conditions such that $\theta_0 = \theta_1(0) = -\theta_2(0)$, $\delta\theta \equiv \delta\theta_1 = \delta\theta_2$, $\varphi_1 = \varphi_2 = 0$ and $2|\theta_2(0) - \theta_1(0)| > \delta\theta_1 + \delta\theta_2$:

$$\theta_1(t) = \theta_0 + \delta\theta \sin(2\pi t) \quad , \quad \theta_2(t) = -\theta_0 + \delta\theta \sin(2\pi t + \phi)$$

Numerically, we find that $\bar{F} = \langle |\mathbf{F}^S| \rangle$ has the shape in Fig.1 with two peaks for $\phi_{eff}^{(2,ang)}$. This result is in total agreement with the one obtained in the case of two sphere near a plane, but the force is bigger, due to the geometry of the configuration. The best phase is again

$$\boxed{\phi_{eff}^{(2,ang)} = \pi/2}$$

showing a recurrence of the symmetry in the interactions.

A question with no analogous in the plane geometry case arises, i.e. for which separation the maximum average force \bar{F}_M^S , corresponding to the most efficient phase difference, assumes the higher value?

In Fig.1 the initial conditions are a fixed $\delta\theta_{1,2}$ and different $\theta_{1,2}(0)$, in a range that prevents superpositions. In Fig.2, we see the value of ϕ_M , phase difference that maximize the force \bar{F} for different $\theta_{1,2}(0)$ and $\delta\theta_{1,2}$. In Fig.3 we have \bar{F} for various $\theta_{1,2}(0)$ and amplitudes.

As expected after the analysis of Section (5.3.1), the system receives a best push for cilia as close as possible.

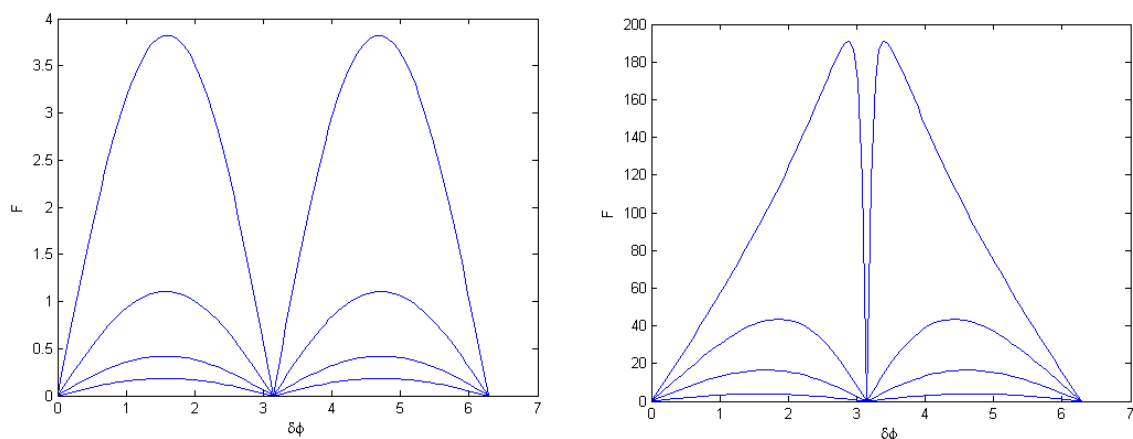


Figure 5.14: Average force on the sphere in function of the phase difference between the two cilia. On the left: the plot shows \bar{F} for 4 different values of θ_0 , with an amplitude of $\delta\theta \simeq 0.313$. The two peaks occurs for $\delta\phi \simeq \pi/2$ and $\delta\phi \simeq 3\pi/2$. On the right $\theta_0 \simeq 0.79$ is fixed and the various graphs show four different amplitude $0.20 \leq \delta\theta \leq 0.79$.

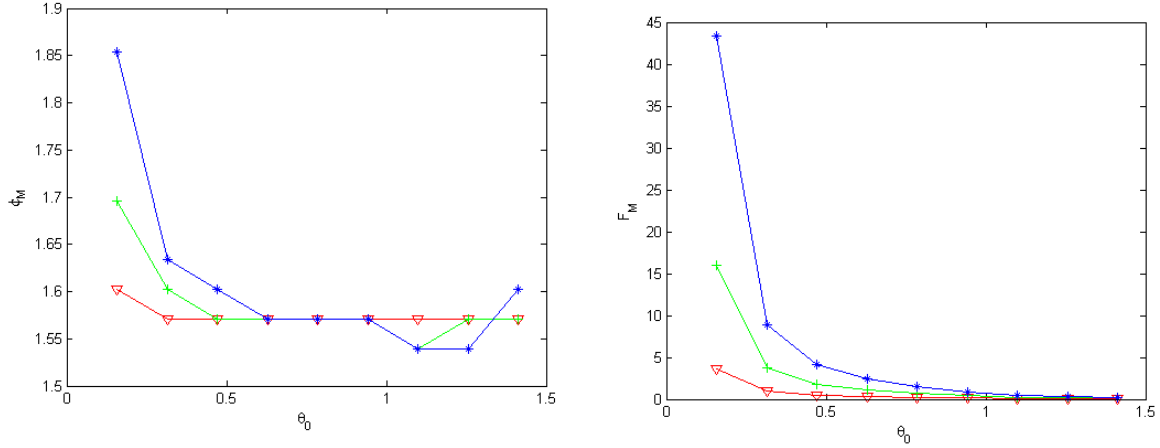


Figure 5.15: Phase difference and Maximal Force vs initial angle, for various amplitudes.

5.4.2 4 cilia: angular and elliptical motion

If we consider a sphere with more than two cilia, we will have, due to the linearity of the Stokes' equations:

$$\begin{cases} \mathbf{F}_1(t) = 6\pi \left[\mathbf{v}_1(t) - \sum_{i=2}^N \underline{\mathbf{G}}^{RS}(\theta_1(t), \theta_i(t)) \cdot \mathbf{v}_i(t) \right] \\ \vdots \\ \mathbf{F}_j(t) = 6\pi \left[\mathbf{v}_j(t) - \sum_{i \neq j}^N \underline{\mathbf{G}}^{RS}(\theta_j(t), \theta_i(t)) \cdot \mathbf{v}_i(t) \right] \\ \vdots \\ \mathbf{F}_N(t) = 6\pi \left[\mathbf{v}_N(t) - \underline{\mathbf{G}}^{RS}(\theta_N(t), \theta_i(t)) \cdot \mathbf{v}_i(t) \right] \end{cases} \quad (5.4)$$

$$\mathbf{F}^S(t) = - \sum_{i=1}^N \mathbf{F}_i(t)$$

If we consider a configuration where every cilium is performing an oscillatory motion with frequency ω and amplitude $\delta\theta$, and preserving the symmetry such that

$$\theta_1(t) = \theta_{01} + \delta\theta \sin(2\pi t) \quad , \quad \theta_2(t) = \theta_{02} + \delta\theta \sin(2\pi t + \phi_2) \quad , \quad \dots \quad , \quad \theta_N(t) = \theta_{0N} + \delta\theta \sin(2\pi t + \phi_N)$$

every equation of the nonlinear system (5.4) becomes:

$$\mathbf{F}_j(t) = 6\pi \left[\mathbf{v}_j(t) - \sum_{i \neq j}^N \mathbf{G}^S(\{\theta_i(0)\}_{1,N}, \{\theta_i(0)\}_{2,N}, \delta\theta) \cdot \mathbf{v}_i(t) \right] \quad , \quad i = 1, \dots, N \quad (5.5)$$

The code was modified to perform the calculation with N cilia, but the huge time required still prevents us to extend this method to more than 4 cilia. In the case

$N = 4$ we performed numerical calculation to find which is the best distribution of phase differences ϕ . The best result we found shows an increasing phase difference:

$$\phi_{eff}^{(4,angl)} = (0, 2.51, 3.77, 2\pi)$$

In this configuration we notice an increasing distribution of phase difference, but we don't see any constant difference, which would mean the arising of a metachronal wave.

5.5 Infinite array of cilia

In the previous sections, we considered only a finite number of interacting ideal cilia. Another possible extension of the plane geometry problem, studied in Section (5.3.1), is to consider an infinite array of sphere as sum of infinite copies of N cilia. This system has shown [22] the arising of metachronal waves as result of the phase dynamics of cilia in interaction.

Fixed a kinematics for N cilia, every one will interact not only with the other $N - 1$, but with infinite copies of them equally spaced (see Fig. 5.16). Therefore, the force on each sphere will be

$$\mathbf{F}_i(t) = 6\pi \sum_{i \neq j}^N \left[\mathbf{v}_i(t) - \sum_{k=-\infty}^{\infty} \mathbf{G}^W(\mathbf{x}_i(t), \mathbf{x}_j(t) - kx_0) \cdot \mathbf{v}_j(t) \right], \quad x_0 = N\delta \quad (5.6)$$

where δ is the distance between two adjacent cilia, and so x_0 the size of the ideal box of N cilia. Hence, we have to calculate the sum in (5.6).

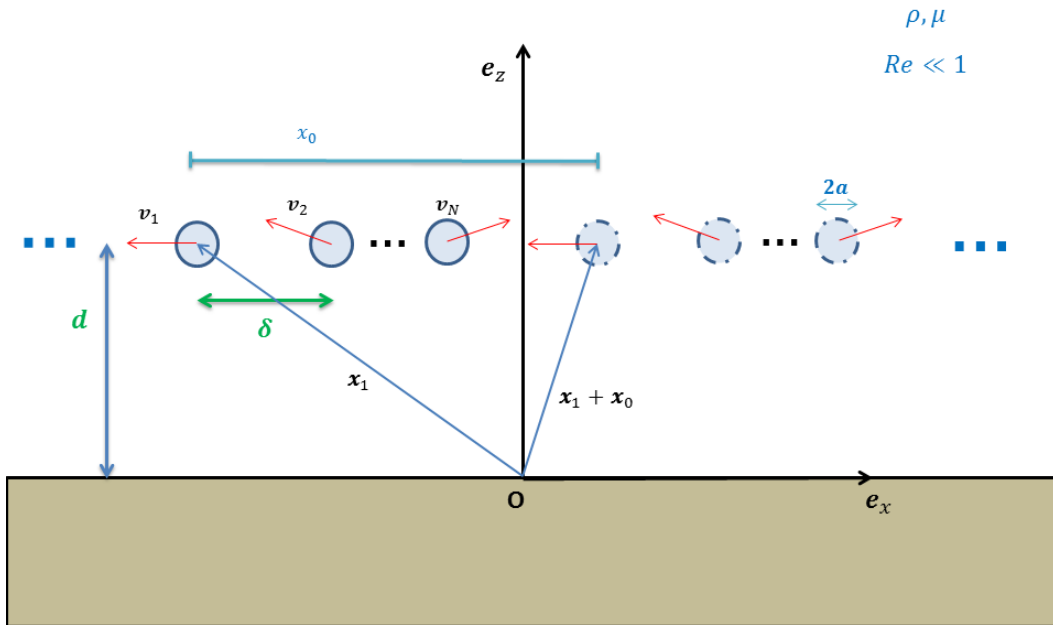


Figure 5.16: Infinite array of Spheres: configuration and variables.

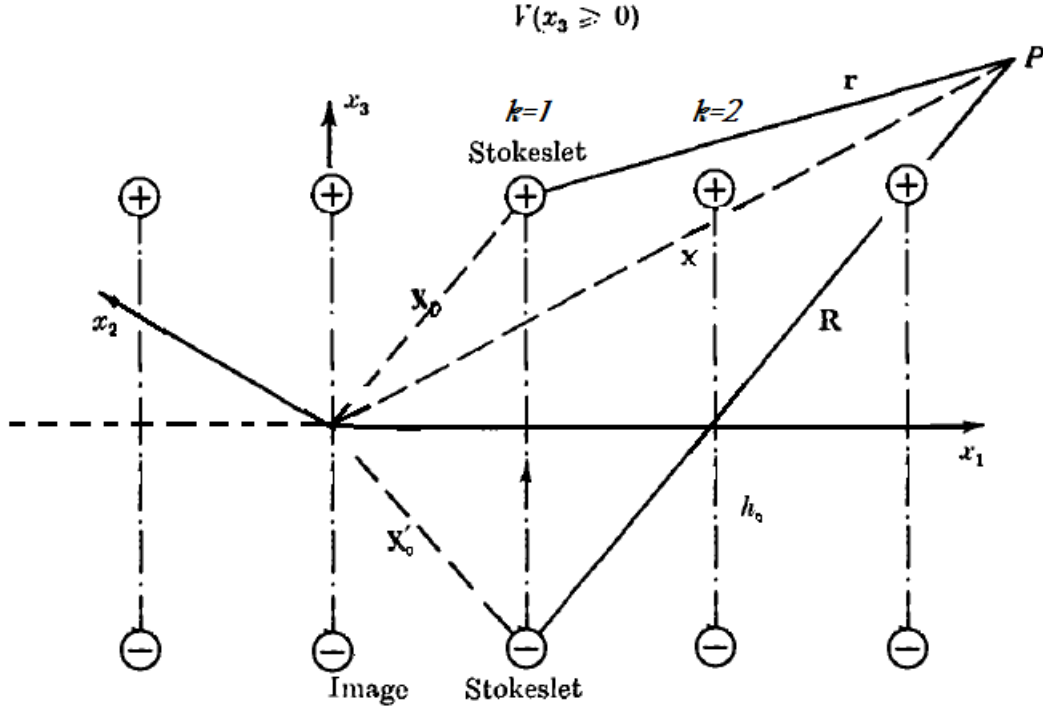


Figure 5.17: Infinite array of Stokeslet: configuration.

Recalling the variables with reference to Fig. 5.17:

$$\hat{x}_1 = x - kx_0 = x - kx_0^{im} = \hat{X}_1 \quad , \quad r = |x - kx_0| \quad , \quad R \equiv |\hat{\mathbf{X}}| = \sqrt{(x - kx_0)^2 + h_0^2}$$

$$\begin{aligned} \mathbf{G}_{11}^{\mathbf{W}}(\mathbf{x}, kx_0) &= \frac{1}{r} + \frac{\hat{x}_1^2}{r^3} - \frac{1}{R} - \frac{\hat{X}_1^2}{R^3} - (2h_0^2 - 2h_0\hat{X}_1) \left(\frac{1}{R^3} + 3\frac{\hat{X}_1^2}{R^5} \right) \\ &= \frac{2(R^3 + r^3)(x - kx_0)^2 - r^3h_0^2}{r^3R^3} - 2h_0(x - kx_0 - h_0) \frac{R^2 + 3(x - kx_0)^2}{R^5} \end{aligned}$$

$$\mathbf{G}_{11}^{\mathbf{W}}(\mathbf{x}, x_0) = \sum_{k=-\infty}^{\infty} \mathbf{G}_{11}^{\mathbf{W}}(\mathbf{x}, kx_0)$$

In the limit of great distance ($h \ll r$), $R \rightarrow r = |x - kx_0|$, thus:

$$\begin{aligned} \mathbf{G}_{11}^{\mathbf{W}}(\mathbf{x}, kx_0) &\simeq \frac{4|x - kx_0|^3(x - kx_0)^2}{|x - kx_0|^6} - \frac{2h_0(x - kx_0) \cdot 4(x - kx_0)^2}{|x - kx_0|^5} \\ &= \frac{4(x - kx_0)^2 - 8h_0(x - kx_0)}{|x - kx_0|^3} = \frac{4(x - kx_0)(x - kx_0 - 2h_0)}{|x - kx_0|^3} \end{aligned}$$

$$\mathbf{G}_{11}^{\mathbf{W}}(\mathbf{x}, x_0) \simeq \sum_{k=-\infty}^{\infty} \frac{4(x - kx_0)(x - kx_0 - 2h_0)}{|x - kx_0|^3}$$

The velocity field corresponding to this Green function is plotted in Fig. 5.18. Numerically, this sum has been implemented for $N = 3, 5$, with result:

$$\phi_{eff}^{(3\infty, lin)} = (0, 4.71, 4.40) \quad , \quad \phi_{eff}^{(5\infty, lin)} = (0, 4.40, 4.71, 4.71, 4.71)$$

$\#_{disc}$	A	δ	$\phi_{eff}^{(3\infty,lin)}$
20	1	2.1	(0, 1.2566, 2.5133)
20	1	10	(0, 4.7124, 4.7124)
20	1	50	(0, 1.5708, 1.5708)
20	1	100	(0, 4.7124, 4.7124)
20	1	200	(0, 4.7124, 4.7124)
20	1	10^3	(0, 1.5708, 1.5708)
20	1	$5 \cdot 10^3$	(0, 4.7124, 4.7124)
20	1	10^4	(0, 1.5708, 1.5708)
20	1	10^5	(0, 1.5708, 1.5708)

Table 5.5: $\#_d$ is the number of ϕ scanned within $[0, 2\pi]$, everywhere the distance is $d = 1$

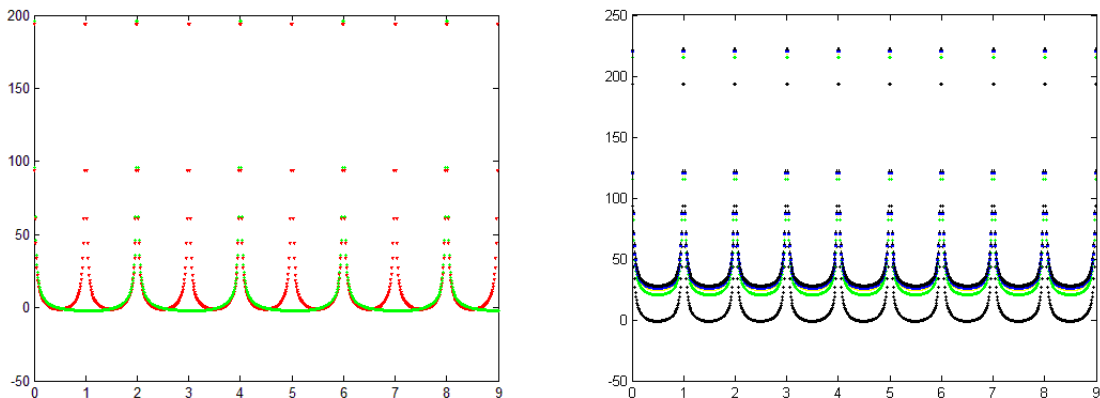


Figure 5.18: Sum on k in the Green function for an infinite array. $k_{max} = 1000$: on the left varying x_0 , on the right h

5.6 Conclusions

In conclusion, in this work we explored, from a new point of view, the issue of optimal coordination of moving bodies as a model for cilia anchored on a surface. Cilia are known to deform as so-called metachronal waves, and the hypothesis in the literature is that these waves somehow correspond to optimal modes of deformation of the surface. Assuming this optimality to correspond to a maximum force exerted on the fluid with given kinematic constraints, we asked in a simplified setting whether this was actually the case.

We studied the cases of a plane and a spherical surface, with different constraints on the trajectories of the *ideal* cilia. Definitely, from all our work the arising of metachronal waves does not appear in any of the configuration considered. This can be ascribed to different causes:

- First of all, we assumed that cilia deform with given kinematics and maximize the “push” force, but it could be the case that they maintain a constant force and vary kinematics, being the flexibility of their bodies a main characteristic of the motion.

- Moreover, for the usual configurations of cilia near a wall, as for the Paramecium or the transport of mucus layers, the number of cilia $N \gg 1$, but due to the numerical limits we encountered we could only put ourselves in the case $N \sim O(1)$.
- The approximation that we used, only made use of the with the long-range hydrodynamics and the first reflection for the no-slip condition on the moving spheres. In the case of cilia attached to a plane, we went as far as to maximize the interaction, realizing an infinite array of spheres, but even in this case the interaction was limited to the first reflection.

However, the importance of this work lies in the fact that within the constraints of the numerics and the limits of our approximations, we answered for the first time the tricky question about the kinematic optimality of the metachronal solution for cilia arrays.

Acknowledgements

Think you're escaping and run into yourself.
Longest way round is the shortest way home.
James Joyce, Ulysses

This thesis symbolically traces the end of a personal, 5-years long, amazing adventure. Therefore I want to say thank you to all the fellows, friends, places that have been changing me during this time.

First of all, I wish to express my most sincere gratitude to my family, both small and large, that has given me material and moral support, and like glue stretched to fill the holes I always create in my life.

Then, I thank my friends and University mates, all over the world.

In Rome: Ambra, who's been the perfect travel mate for a long part of my bulging and intense Roman adventure; my *occult advisor* Andrea P. without whose support I would have never work out a way through the intricacy of bureaucracy; my healthy conscience Giorgio; the ever-present Arkadij; and Andrea V., David, Francesca, Giacomo, Leonardo, Simone.

In Lyon: Domiziana, Julien, Massimiliano and Natalia, who really enriched me as a person, and made my French experience unforgettable.

In San Diego: my *older bro* Rodrigo; On Shun and Gwynn, who showed me what and how research can be done, passing on their enthusiasm and work spirit to me.

In Sicily: all my long-standing friends, who I will be missing everywhere and forever.

A big thank you is due also to my official and non-official advisors: Prof. Eric Lauga, for his emotional and scientific enthusiasm; Dr. Roberto Di Leonardo for his patience, kindness and collaboration, and Prof. Andrea Giansanti, who made possible my istitutional research project abroad.

At last, as always, I am grateful to the gorgeous living prayer of Nature all around me, and to every occasional Master the road gave me as unexpected present.

Bibliography

- [1] M.G. Nielsen and E.C. Raff. *The best of all worlds or the best possible world? Developmental constraint in the evolution of beta-tubulin and the sperm tail axoneme.* Evolution & Development, **4**(4), pp.303–15 (2002) [5](#)
- [2] S. Nonaka et al. *Randomization of left-right asymmetry due to loss of nodal cilia generating leftward flow of extraembryonic fluid in mice lacking KIF3B motor protein.* Cell, **95**(6), p.829 (1998) [5](#)
- [3] Y. Okada et al. *Mechanism of nodal flow: A conserved symmetry breaking event in left-right axis determination* Cell, **121**(4), p.633 (2005) [5](#)
- [4] C. Brennen and H. Winnet. *Fluid mechanics of propulsion by cilia and flagella* Annu. Rev. Fluid Mech. **9**, p.339 (1977) [5](#), [6](#)
- [5] J. R. Blake and M. A. Sleight. *Mechanics of ciliary locomotion* Biol. Rev. Cambridge Philos. Soc. **49**, p.85. (1974) [6](#)
- [6] S. Gueron, K. Levit-Gurevich, N. Liron, J. J. Blum. *Cilia internal mechanism and metachronal coordination as a result of hydrodynamic coupling.* Proc. Natl. Acad. Sci. U.S.A. **94**, 6001 (1997) [6](#), [59](#)
- [7] A. Vilfan, F. Julicher. *Hydrodynamic flow patterns and synchronization of beating cilia* Phys. Rev. Lett. **96**, 058102 (2006) [59](#)
- [8] McDonough. *Lectures in elementary fluid dynamics: Physics, Mathematics and Applications* <http://www.engr.uky.edu/~acfd/me330-lctrs.pdf> (2009) [16](#)
- [9] Gary Leal. *Advanced Transport Phenomena, Fluid Mechanics and Convective Transport Processes.* Cambridge University Press, New York (2010) [11](#), [21](#), [31](#), [32](#)
- [10] S.Kim, S.J.Karilla. *Microhydrodynamics: Principles and Selected Applications* Dover Publications, New York (2005) [11](#), [21](#), [22](#), [27](#), [44](#), [48](#)

- [11] R.Aris. *Vectors, Tensors, and the Basic Equations of Fluid Mechanics*.
Dover publications, New York (1962) 11
- [12] D.J.Tritton. *Physical Fluid Dynamics*
Clarendon Press (1988) 11
- [13] Guyon, Hulin, Petit, Mitescu. *Physical Hydrodynamics*
Oxford University Press, New York (2011) 11, 14, 21, 22, 27
- [14] E.M. Purcell. *Life at low Reynolds number*
American Journal of Physics, **45**, p.1 (1977) 18, 24
- [15] E.Lauga, T.R.Powers. *The hydrodynamics of swimming microorganisms*
Reports on Progress in Physics, **72** 096601 (2009) 18, 24, 33
- [16] Hilfinger. *Dynamics of Cilia and Flagella*
PhD thesis (2005)
<http://www.mpipks-dresden.mpg.de/mpi-doc/julichergruppe/webseite/Dissertations/AndreasHilfinger2006.pdf>
7
- [17] J.Happel, H.Brenner. *Low Reynolds number hydrodynamics: with special applications to particulate media*
M.Nijhoff Publishers, The Hague (1983) 27
- [18] C.Pozrikidis. *Boundary integral and singularity methods for linearized viscous flow*
Cambridge University Press (1992) 31, 32, 34, 43
- [19] L.D.Landau, E.M.Lifshits, E.M.Lifšic. *Fluid Mechanics, Volume 6*
Butterworth-Heinemann (1987) 30
- [20] O. A. , *The Mathematical Theory of Viscous Incompressible Flow*
Gordon & Breach, New York (1963) 34
- [21] A.T. Chwang, T.Y.Wu. *Hydromechanics of low-Reynolds-number flow. Part 2. Singularity method for Stokes flows*
J. Fluid Mech., vol. **67**, part 4, pp. 787-815 (1975) 40
- [22] Thomas Niedermayer, Bruno Eckhardt, and Peter Lenz. *Synchronization, phase locking, and metachronal wave formation in ciliary chains*
Chaos **18**, 037128 (2008)
<http://dx.doi.org/10.1063/1.2956984> 59, 62, 77
- [23] J.H.C. Luke. *Convergence of a multiple reflection method for calculating Stokes flow in a suspension*.
SIAM J.Appl. Math., 49:1635-1651 (1989) 44
- [24] H.A. Lorentz. *A general theorem concerning the motion of viscous fluid and a few applications from it*.
Collected Papers, 4:7-14, Martinus Nijhoff, Le Hague (1937) 46

- [25] H. Faxén. *The resistance against the movement of a rigid sphere in a viscous fluid enclosed between two parallel planes.*
Arkiv fur Matematik, Astonomi och Fysik, 18(29):1-52 (1924) [46](#)
- [26] J.R. Blake. *A note on the image system for a stokeslet in a no-slip boundary*
Proc. Camb. Phil. Soc. **70**, 303 (1971) [46](#)
- [27] J.J.L. Higdon. *A hydrodynamic analysis of flagellar propulsion*
Journal of Fluid Mechanics **90** : 685-711 (1979) [48](#)
- [28] M.Murase. *The Dynamics of Cellular Motility*
New York: Wiley, 1992. [49](#), [52](#), [53](#), [55](#)
- [29] J. Howard, A.J. Hudspeth, R.D. Vale. *Movement of microtubules by single kinesin molecules*
Nature, **342(6246)**: pp.154–8 (1989) [53](#)
- [30] S. Ray et al. *Kinesin follows the microtubule's protofilament axis*
J Cell Biol, **121(5)**: pp.1083–93 (1993) [53](#)
- [31] B. Rothlein. *Kollektivarbeit im Nanokosmos*
MaxPlanckForschung, **03**: pp.28–31 (2004) [53](#)
- [32] R.N. Seetharam and P. Satir. *High speed sliding of axonemal microtubules produced by outer arm dynein*
Cell Motil Cytoskeleton, 60(2):96–103, 2005.
- [33] B. Alberts et al. *Molecular Biology of the Cell*
Garland Science, New York, 4th edition, 2002.
- [34] K.E.Summers. *The role of flagellar structures in motility*
Biochim. Biophys. Ada **416**, pp. 153-168 (1975). [51](#)
- [35] C.Eloy, E. Lauga. *Kinematics of the most ecient cilium*
<http://arxiv.org/pdf/1204.6097v1.pdf> (2012) [54](#)
- [36] F.D.Warner and D.R.Mitchell
J. Cell Biol. **89** p.35 (1981) [51](#), [55](#)
- [37] C.J.Brokaw
J. Cell Biol. **114**, p.1201 (1991) [55](#)
- [38] R.Rikmenspoel.
Biophys. J. **43**, p. 177 (1978)
- [39] K.Sugino, Y.Naitoh
Nature **295** 609 (1982) [55](#)
- [40] K.E.Machin.
Proc. R. Soc. B **158** p.88 (1963) [55](#)

- [41] C.J.Brokaw.
Proc. Natl Acad. Sci., USA, 72 p.3102 (1975) 55
- [42] C.J.Brokaw
Cell. Mot. Cytoskel. **42** p.134 (1999)
- [43] C.B.Lindemann, K.S.Kanous
Cell. Mot. Cytoskel. **31** p.1 (1995) 55
- [44] S.H.Strogatz. *Nonlinear Dynamics and Chaos*
Reading, MA: Addison-Wesley (1994) 55
- [45] S. Camalet, F. Jülicher. *Generic Aspects of Axonemal Beating*
New J. Phys. **2**, p.24 (2000) 55
- [46] Sleight, M. A. *Fluid propulsion by cilia and the physiology of ciliary systems*
Perspectives in Experimental Biology. Vol. 1, ed. P. S. Davies, pp. 125-134, Pergamon Press, Oxford (1976) 56, 58
- [47] Knight-Jones, E. W. *Relations between metachronism and the direction of ciliary beat in Metazoa*
Quart. J. Microscop. Sci. 95, 503-521 (1954) 56
- [48] Murakami, A. *Ciliary and flagellar movement: control mechanism*
Cell Motility, pp. 131-156, University of Tokyo Press, Tokyo (1974) 57
- [49] Satir, P. *How cilia move*
Sci. Amer. **231**, 44-52 (1974) 58
- [50] Guirao B and Joanny J F 2007 Spontaneous creation of macroscopic flow and metachronal waves in an array of cilia Biophys. J. 92 1900–17 59
- [51] Smith D J, Blake J R and Gaffney E A 2008 Fluid mechanics of nodal flow due to embryonic primary cilia J. R. Soc. Interface 5 567–73 59
- [52] Qian B, Jiang H, Gagnon D A, Powers T R and Breuer K S 2009 Minimal model for hydrodynamic synchronization <http://arxiv.org/abs/0904.2347>